NOVEL APPROACHES TO MODULATE ENDOTHELIAL CELL MIGRATION AND ANGIOGENESIS

by

David Gau

B.S., University of Pittsburgh 2011

Submitted to the Graduate Faculty of

Swanson School of Engineering in partial fulfillment

of the requirements for the degree of

Doctor of Philosophy

University of Pittsburgh

2018

UNIVERSITY OF PITTSBURGH

SWANSON SCHOOL OF ENGINEERING

This dissertation was presented

by

David Gau

It was defended on

February 28, 2018

and approved by

Ipsita Banerjee, Ph.D., Associate Professor, Department of Chemical and Petroleum Engineering

Kenneth Hallows, M.D., Ph.D., Professor, Division of Nephrology

Alan Wells, M.D., DMSc., Professor, Department of Pathology

Dissertation Director: Partha Roy, Ph.D., Associate Professor, Department of Bioengineering

NOVEL APPROACHES TO MODULATE ENDOTHELIAL CELL MIGRATION AND ANGIOGENESIS

David Gau, Ph.D.

University of Pittsburgh, 2018

Angiogenesis, the process of neovascularization from pre-existing vasculature, is fundamental to development and tissue repair. However, aberrant angiogenesis exacerbates progression of a number of diseases including but not limited to cancer and diabetic retinopathy. Endothelial cell (EC) migration, a key event for angiogenesis, is a highly regulated process that critically relies on the dynamic remodeling of the actin cytoskeleton via orchestrated actions of various actin-binding proteins. An important aspect of the dynamic remodeling of the actin cytoskeleton, cell migration, and angiogenesis is stimulus-induced regulation of *de novo* synthesis of many important molecular components of the actin cytoskeleton by MKL (Megakaryoblastic Leukemia)–SRF (Serum-Response Factor) transcriptional machineries. Given the previous genetic evidence for the importance of MKL/SRF signaling in EC migration and angiogenesis, we first set out to explore whether angiogenesis is susceptible to small molecule-mediated inhibition of the MKL/SRF pathway. Our studies showed that CCG-1423, a small molecule inhibitor of MKL, causes a prominent defect in EC migration and angiogenesis *in vitro, ex vivo,* and *in vivo*. Inhibition of MKL led to prominent depletion of actin-binding protein Profilin-1

(Pfn1), an important molecular player of membrane protrusion and EC migration/angiogenesis, but through an unconventional indirect mechanism that involves a cellular externalization control [*Angiogenesis (2017) 20(4):663-672; J. Biol Chem. (2017) 292(28):11777-11791*]. Next, guided by computational-based rational design, we identified the first-generation small molecule inhibitors of the Pfn1:actin interaction, and further demonstrated the ability of these small molecules to inhibit EC migration, proliferation, and angiogenesis *in vitro* and *ex vivo* [*J Biol Chem (2017) Dec 27, epub*]. Finally, to gain new insights on the regulation of Pfn1, we identified and explored the consequence of novel phosphorylation event which caused insoluble aggregation of Pfn1 and actin molecules [*PLoS One (2016) 26;11(5):e0156313*].

TABLE OF CONTENTS

LIST OF FIGURES

ABBREVIATIONS AND ACRONYMS

2D: Two-dimensional

3D: Three-dimensional

ABPs: Actin-binding proteins

ADP: Adenosine-5'-diphosphate

ALS: Amyotrophic lateral sclerosis

ATP: Adenosine-5'-triphosphate

EC: Endothelial cell

ECM: Extracellular matrix

FBS: Fetal bovine serum

HEK-293: Human embryonic kidney 293

HUVEC: Human umbilical vein endothelial cells

HmVEC: Human dermal microvascular endothelial cells

MKL1: Megakaryoblastic leukemia 1

MMP: Matrix metalloproteinases

MRTF-A: Myocardin related transcription factor A

Pfn: Profilin

Pfn1: Profilin-1

PI(4,5)P_2: Phosphatidylinositol-4,5-biphosphate

PKA: Protein kinase A

PKCζ: Protein kinase C-ζ

PLP: Poly-L-proline

PPI: Phosphoinositide

RhoA: Ras homology family member A

ROCK1: Rho-associated coiled-coil kinase-1

RTKs: Receptor tyrosine kinases

SAP: SAF-A/B, Acinus and PIAS

SDS-PAGE: Sodium dodecyl sulfate polyacrylamide gel electrophoresis

siRNA: Small interfering RNA

SRF: Serum response factor

STAT: Signal transducer and activator of transcription

VASP: Vasodilator-stimulated phosphoprotein

VEGF: Vascular endothelial growth factor

WASP: Wiskott-aldrich syndrome protein

PREFACE

First and foremost, thank you to my family, friends, and most importantly my wife, Amanda Gau, for supporting me through my decade-long academic journey. I would also like to thank Dr. Partha Roy for his mentorship and support since my undergraduate days at the University of Pittsburgh. Without his support and in particular, letting me work in his lab as an undergrad, none of this would have been accomplished! Also, without the years of mentorship, motivation, and reference letters from Drs. Harvey Borovetz and Sanjeev Shroff, I would not be where I am today.

Thank you as well to my committee members Drs. Ipsita Banerjee, Ken Hallows, and Alan Wells, for the years of support and feedback on my dissertation project, especially to Dr. Alan Wells and his lab for also providing feedback on my work since my undergraduate years.

I would also like to thank others from the Roy lab and collaborators that have helped me throughout the years: Roy lab - Drs. Yongho Bae, Souvik Chakraborty, Tuhin Das, Zhijie Ding, Chang Jiang, Marion Joy, and William Veon. Collaborators – Drs. Catherine Baty, David Koes, Lee McDermott, Beth Roman, and Peter Wipf.

1.0 INTRODUCTION

Angiogenesis is the process where new blood vessels are formed from pre-existing vasculature networks and an important aspect of many pathological and physiological events such as wound healing and tumor progression (1). Most late development and post birth vascular remodeling and repair are dependent on the angiogenesis cascade whereas early development is regulated by vasculogenesis (the initial formation of the vasculature) (2). Under basal conditions, endothelial cells (ECs) are inhibited from leaving their position by basement membrane and surrounding mural cells. Angiogenesis begins when pro-angiogenic factors, such as VEGF-A (Vascular Endothelial Growth Factor-A), is released by surrounding cells and activate the ECs which causes dramatic reduction of cell-cell interaction between ECs with each other and with pericytes. Macrophages have been shown to play a major role in secretion of pro- and anti-angiogenic growth factors during the angiogenic cascade (3). Secretion of VEGF-A by macrophages has been demonstrated to be important for initiation of angiogenesis during tissue repair (4). In addition to activation of ECs, MMPs (matrix metalloproteinases) are activated which as well allows for degradation of underlying basement membrane and ECM (extracellular matrix) which provides a path for EC migration. Deattachment of the mural cells is also facilitated by angiopoietin-2 which is released by ECs. Activated ECs, known as tip cells, then invade and migrate following a cytokine gradient while leading other ECs behind, called stalk cells, which proliferate and extend the vascular network, producing immature/leaky vessels.

Delta-like-4-Notch1 signaling prevents tip cell activation of adjacent endothelial cells to control vessel sprouting (5). Finally, pericytes are recruited to the new vessels and mature the vessels by promoting stabilization and reformation of EC barrier function (6-8). The process of angiogenesis is depicted in Figure 1.

For much of the angiogenic cascade, proper cell migration and morphogenesis is required. Pro-angiogenic factors like VEGF-A are known to promote EC migration/invasion (9). On the other hand, anti-angiogenic factors typically function by at least partially inhibiting cell migration (10-12). Rho GTPase activity resulting from chemical cue by activation of VEGF receptors leads to chemotactic migration of endothelial cells. As such, inhibition of Rho GTPases has been shown to inhibit angiogenesis (13,14). Furthermore, tip cell migration requires filopodia formation which is regulated by cdc42 (15). Rac1 is also important for EC migration by controlling lamellipodial formation which in turn affects directed migration (16). RhoA plays a role in activation of PI3K in ECs which causes changes to membrane phosphoinositide levels, which in turn affect key regulators of the actin cytoskeleton and cell polarization (17). Not surprisingly, EC migration and morphogenesis requires SRF and endothelial cell knockout of SRF was demonstrated to be embryonic lethal due to hemorrhaging from defective EC migration (note that EC differentiation was not affected nor was early vascular morphogenesis) (18). SRF is also important for tip cell filopodia formation and loss of SRF leads to defective vessel connection, all of which demonstrates the importance of regulation of the actin cytoskeleton throughout the whole angiogenic cascade (18).

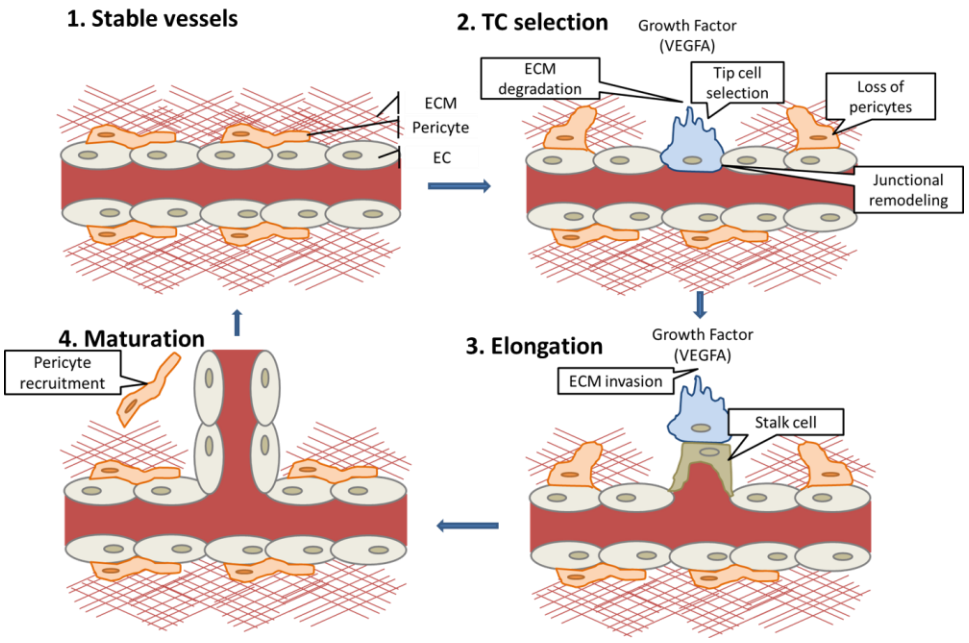

Figure 1. The angiogenic cascade illustrating the steps taken to form new vessels from existing networks adapted from (19).

1.1 CELL MIGRATION AND THE ACTIN CYTOSKELETON

Cell migration is a highly regulated cellular event that plays an important role in both physiological and pathological processes ranging from embryonic development to angiogenesis and tumor metastasis (20). Directed cell motility can be summarized as a cycle of four fundamental steps that are orchestrated in a precise spatiotemporal fashion. These steps are: 1) membrane protrusion at the leading edge driven by actin polymerization, 2) stabilization of membrane protrusion via integrin-mediated cell-matrix adhesions, 3) forward translocation of the cell body powered by actomyosin-based contractile forces, and finally, 4) release of the rear of the cell as a consequence of the mechanical action of the contractile force (i.e. when the force exceeds the adhesion strength) and/or proteolysis of cell-matrix adhesion components (21).

Dynamic remodeling of actin cytoskeleton is an essential feature for motile phenotype of all cells. Sensing various micro-environmental cues (chemical gradients, haptotatic cues etc.), cells are able to translate these signals and establish a "front end" or "leading edge" where membrane protrusions are initiated through *de novo* nucleation of actin followed by actin filament elongation and/or elongation of existing actin filaments proximal to the leading edge (22). Actin dynamics at the leading edge is controlled by the concerted actions of an ensemble of actin-binding proteins (ABPs). For example, Arp2/3 complex activated by WASP (Wiskott Aldrich Syndrome Protein) and formins are the key initiators of the nucleation process while elongation of the actin filaments at the barbed ends is aided by Ena (enabled) /VASP (vasodilator stimulated phosphoprotein) and formins in cooperation with profilin (Pfn - a prominent nucleotide exchange factor for actin) family of ABPs. The growth of actin filaments is also balanced and spatially restricted by disassembly of actin filaments by the actions of actin depolymerizing and severing factors (e.g. cofilin, gelsolin) and capping proteins, respectively. Functionalities of these ABPs are dynamically regulated by various intracellular signaling mechanisms that include interaction with Rho-family GTPases, reversible phosphorylation/ dephosphorylation and membrane phosphoinositide binding or metabolism (23) (an illustration of actin binding proteins in the remodeling process of the actin cytoskeleton is shown in Figure 2).

Another essential feature for the remodeling of actin cytoskeleton during cell motility is the regulation of *de novo* synthesis of ABPs and other actin cytoskeleton-associated proteins in response to motility cues. Serum-response factor (SRF), a ubiquitously expressed and highly conserved transcription factor, is a critical player in this process. SRF binds to the CArG consensus sequence [$CC(AT)_6GG$) – originally discovered in the transcription-regulatory sequences of serum-inducible genes including c-fos and egr-1 (24,25)] located on a variety of

genes including SRF itself and many of those involved with the actin cytoskeleton, cell-matrix as well as cell-cell adhesion, and cellular contractility such as actin, cofilin, Arp2, myosin, vinculin, cadherin and integrin to name a few (26) (27). SRF-mediated gene expression is promoted by two broad classes of transcriptional coactivators including those belonging to the myocardin and TCF (ternary complex factors: Ets1, SAP-1, Net or SAP-2) family of proteins (28,29). Note that SRF can be also regulated by the members of zinc-finger [e.g. GATA] and homeobox-domain (e.g. Nkx2-5) transcription factors. Because of competition for binding sites on SRF, myocardin and TCF families of co-activators interact with SRF in a mutually exclusive manner and activate different sets of SRF-target gene expression (30,31). Myocardin-family transcriptional co-activators consists of three members: the founding member myocardin (its expression is restricted to cardiac and smooth muscle cells) and the two widely expressed myocardin-related transcription factors (MRTF), namely MRTF-A (also known as MAL or MKL1 [*Megakaryoblastic leukemia-1*: named after its genetic rearrangement associated with acute megakaryoblastic leukemia in children (32)]), and MRTF-B (also known as MKL2). Depending on the nature of the transcriptional co-activators, SRF-mediated gene expression is sensitive to different types of upstream signaling pathways. For example, TCF-dependent SRF's gene expression program is modulated by Ras/MAPK (mitogen activated protein kinase) signaling pathway while MKL/SRF signaling is responsive to modulation of Rho-family GTPase activity (26,29,33). In this dissertation which will primarily focus on MKL, we will first provide an overview of MKL structure and regulation (the readers are encouraged to refer to several excellent reviews on MKL/SRF signaling (26,34-38), and then discuss its role in cell motility emphasizing its canonical SRF-dependent and SRF-independent functions in both physiological and pathological contexts.

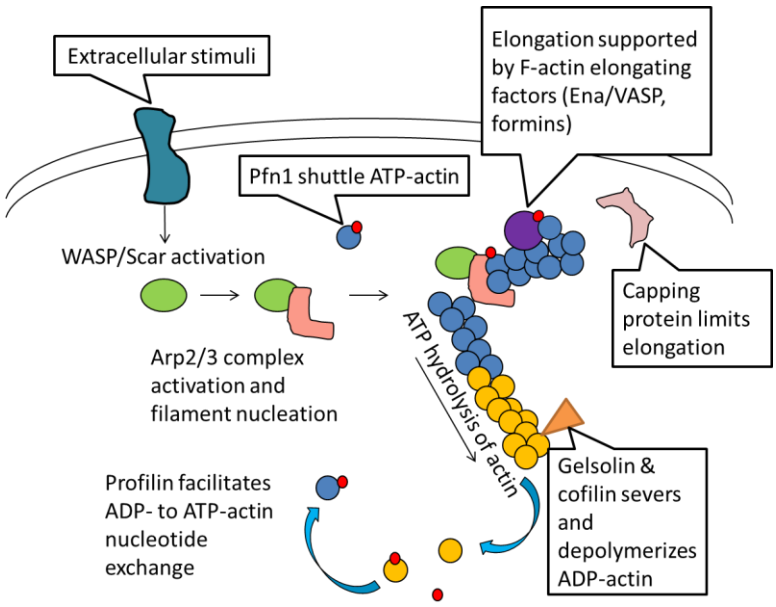

Figure 2. Process of actin polymerization illustrating the involvement of various actin-binding proteins adapted from (39).

1.2 PROTEIN STRUCTURE AND REGULATION OF MKL

Although myocardin family proteins are encoded by genes located at different chromosomal loci (human myocardin 17p11.2, MKL1: 22q13.2, MKL2 16p13.12), they share common structural motifs (see Figure 3 for structural schematics of myocardin and MKL). The three RPEL motifs at the N-terminus allow these proteins to interact with G-actin. The first basic region (denoted as B2) is located within the RPEL motifs and contains a nuclear localization signal (NLS) sequence. The second basic region (denoted as B1) harbors an additional NLS sequence and the SRF-binding site. The other domains are a glutamine-rich Q domain (also important for the regulation of nuclear localization and SRF interaction of MKL), the SAP domain (a putative DNA binding-domain that MKL can utilize to transcribe genes in an SRF-independent manner), a leucine zipper (LZ) domain (responsible for homo- and hetero-

dimerization) and a transcriptional activation domain (TAD) located at the C-terminus of the proteins (40). Note that myocardin family proteins can bind SRF and activate SRF-mediated gene expression without making specific DNA contacts (35). Although MKL is only ~35% identical to myocardin, the conserved functional domains have >60% amino acid identity between myocardin and MKL. Myocardin has two alternatively spliced forms that utilize two different initiation codons (and therefore leads to N-terminal truncation) with the longer and the shorter forms expressed predominantly in heart and smooth muscle cells, respectively (41) (42). Similarly, MKL1 can utilize two distinct initiation codons and at least in mouse fibroblasts, the N-terminal truncated form (lacks the first RPEL motif because of the location of the alternative initiation codon in between the first two RPEL motifs) appears to be the predominantly expressed form of MKL1 (30).

Despite the overall similarity in the structural domains between myocardin and MKL, unlike myocardin (which is generally constitutively localized in the nucleus and therefore active), cellular localization and activation of MKL are tightly regulated in response to intracellular signals. Under basal conditions (serum-starved), MKL shuttles between the nucleus and the cytoplasm, a process that can be halted with serum-stimulation thus allowing nuclear accumulation of MKL (43). Nuclear localization of MKL is strongly inhibited by its interaction with G-actin via the action of its RPEL motifs since binding to G-actin prevents MKL from interacting with the importin family of nuclear import factors. Cellular depletion of G-actin as a result of actin polymerization by activated Rho GTPases (stimulated in response to serum and various growth factors) leads to dissociation of MKL from G-actin allowing MKL to accumulate in the nucleus and co-activate SRF. The foundation of this model of MKL regulation is substantiated by a number of experimental findings. For example, either inhibition of Rho (either

directly by C3-tranferase or indirectly via forskolin-induced activation of cAMP/PKA pathway) or latrunculin-induced actin depolymerization leads to cytoplasmic retention of MKL and inhibition of serum-induced SRF activation. Conversely, either constitutive activation of Rho or deletion of the actin-binding RPEL domain of MKL or F-actin stabilization by jasplakilonide promotes nuclear accumulation of MKL and SRF activation (30,43-48) (49) (50). Although myocardin also possesses actin-binding capability, it has a much lower affinity for G-actin compared to MKL, and is therefore less efficiently inhibited by G-actin (51,52). Even in the absence of G-actin, myocardin also has a much stronger affinity for importin (53) and a weaker affinity for CRM1 (a key nuclear export factor) than MKL (54). Collectively, these biochemical differences potentially explain why myocardin is much less likely to be retained in the cytoplasm than MKL and therefore, its constitutively active nature. Several findings suggest that MKL-mediated SRF activation is also regulated by the state of nuclear actin polymerization. For example, mutants of actin that are artificially restrained in the nucleus and resistant to depolymerization enhance nuclear F-actin content and SRF activation (55). Formin-mediated polymerization of nuclear actin promotes nuclear localization of MKL1 and SRF activation (56) (57). Furthermore, depletion of nuclear G-actin by MICAL2 in a redox-sensitive manner promotes MKL1-SRF activity (58).

While the above studies establish that MKL-SRF activation is critically dependent on the state of actin polymerization in both cytosolic and nuclear compartments, interestingly few studies have revealed that modulation of MKL activation upon perturbations of actin-monomer sequestering or barbed-end binding proteins can occur independent of the changes in G-actin level (30,43,44,49). Molecular insights into how actin-regulatory proteins can impact MKL localization/function without affecting the actin dynamics came from a recent study that

demonstrated competition for actin-binding between MKL and various WH2-domain containing actin-polymerizing factors (N-WASP, WAVE2, Spire and Cobl) (59). These findings have led to an alternative mechanism of MKL:actin dissociation (thus enabling nuclear translocation of MKL and SRF activation) through competitive inhibition by various actin-regulatory factors.

MKL function is also regulated by post-translational modification. Although MAPK signaling is associated with TCF activation, there is evidence that MKL function can be negatively regulated by MAPK signaling. Specifically, Erk1/2, when activated, phosphorylates MKL1 in the nucleus promoting its binding to the nuclear pool of G-actin and as a result, facilitates the export of MKL from the nucleus and attenuation of SRF activity (46). Consistent with phosphorylation being a pre-requisite for formation of the repressive MKL-G-actin complex, a recent study has shown that actin-binding protein filamin interacts with MKL1 and this interaction prevents MKL1 phosphorylation switching MKL from its repressive G-actin bound state to an activated state leading to SRF activation (60). These findings open a new level of control of MKL1 function in cells.

Several knockdown and overexpression studies by a number of groups including ours have shown the basal expression level of SRF (it is also an indirect indicator of the transcriptional activity of SRF) is highly sensitive to the perturbations of MKL (26,30,61). Although MKL1 promoter also has SRF-binding sites, interestingly, our studies showed that SRF depletion does not lead to any noticeable reduction in the basal expression level of MKL1 suggesting that at its endogenous level of activation, SRF could be dispensable for regulating the basal expression level of MKL1 (61). However, overexpression of SRF causes a prominent increase in the cellular level of at least MKL1 suggesting that SRF hyperactivation can stimulate MKL expression. Therefore, MKL and SRF can regulate each other's expression. Given that SRF is a key player in

transcriptional regulation of many important elements of actin cytoskeletal system, MKL/SRF pathway therefore appears to be a crucial signaling axis that connects dynamic actin organization and transcriptional control of factors that can impact actin cytoskeleton in a complex feedback manner.

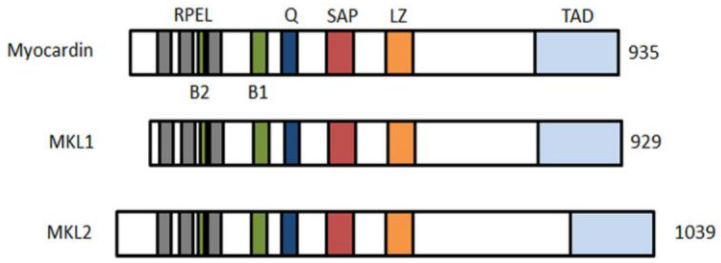

Figure 3. Structural schematic of myocardin, MKL1, and MKL2. The structure of the MKL family proteins structurally similar. The RPEL motifs (designated in grey) is the G-actin binding site. The first basic region, B2 (in green), is located between RPEL motifs and facilitates nuclear import of MKL via NLS. The next basic region, B1, facilitates MKL binding to SRF in addition to another NLS. The Q domain (designated in navy blue) is a glutamine-rich domain and involved in regulation of MKL nuclear localization and SRF interaction. The SAP domain (in red) is a DNA-binding site which allows MKL to transcribe genes in an SRF-independent manner. The LZ (leucine zipper) domain (in orange) facilitates homo- and hetero-dimerization of MKL. Finally, the TAD (transcriptional activation domain; in light blue) is located on the C-terminal end of MKL.

1.3 MKL/SRF SIGNALING IN NORMAL CELL MIGRATION

Due to its nature of the transcriptional targets, it is not surprising MKL/SRF signaling axis plays a prominent role in actin-based cellular activities such as cell migration. Some of the earlier evidence of MKL's importance in cell migration came from genetic studies performed in *Drosophila Melanogaster*. For example, one study showed that either genetic disruption of *mal-*

d, the only member of the myocardin gene encoded by drosophila and a homolog of MRTF (also referred to as DMRTF] or mutagenesis-directed introduction of premature stop codons in the *mal-d* gene (essentially truncating the C-terminal portion of MAL which has a dominant negative effect) leads to marked decrease in F-actin content and defects in migration of border cells in the ovaries during oogenesis (62,63). These defects are phenocopied by loss-of-function of DSRF (the drosophila homolog of SRF) further suggesting that MKL and SRF function together in the process of border cell migration. This study provided further evidence of mechanical tension-induced nuclear translocation of MKL in migrating cells. Similarly, Olson group showed defects in mesodermal cell and tracheal branch migration in drosophila upon either loss-of expression of DMRTF or overexpression of dominant negative mutant of DMRTF lacking its C-terminal transcriptional activation domain (62,63). Although overexpression of a constitutively active form of DMRTF (this active form harbors a deletion of the inhibitory N-terminal RPEL domains) produced the opposite phenotype, normal tissue patterning was still negatively affected likely owing to uncoordinated and accelerated cell migration as result of hyperactivation of DMRTF. These findings not only underscored the importance of nuclear localization of DMRTF for cell migration, but also implied DMRTF function must be properly regulated for normal tissue development. This study also provided genetic interaction between DMRTF and DSRF via demonstration of phenotypic similarities in wing vein formation between flies carrying hypomorphic allele of DSRF and those expressing dominant negative forms of DMRTF. Phenotypic similarities were also noted in the gain-of-function settings of DMRTF and DSRF, and the phenotypes were aggravated when DMRTF and DSRF were simultaneously overexpressed thus implying interdependence of these two factors.

The importance of MKL/SRF signaling in cell migration have been established in the mammalian contexts through various loss-of-function (gene knockout (KO), gene silencing and more recently by pharmacological inhibition) strategies. Since SRF knockout mice are embryonic lethal (embryos that are homozygous for SRF deletion exhibit defects in mesoderm and die at gastrulation (64)), various tissue-specific conditional SRF knockout mice have been developed over the years and depending on the cell/tissue-specificity of gene disruption, SRF ablation has led to developmental defects in various organs (example: liver, heart, muscle, brain) (65-68). In general, defects associated with disruption of the SRF gene are recapitulated when genes encoding both MKL isoforms (MKL1 and MKL2) are simultaneously deleted but not when only a single member of the MKL gene family is selectively deleted. Note that MKL1 KO mice in most part are viable and exhibit defects in myoepithelial differentiation of mammary epithelial cells and lactation (48,69); however, global KO of MKL2 alone is embryonic lethal (die between 13.5 and 14.5) because of defects in cardiac neural crest cell migration, vascular patterning, cardiac outflow tract and smooth muscle differentiation (70). The requirement for co-ablation of MKL isoforms to phenocopy SRF deletion in most contexts indicate functional redundancy between the two MKL isoforms and compensatory action by one isoform when function of the other is lost. Relevant to the topic of this review, brain-specific deletion of SRF causes defects in neurite outgrowth, axon guidance and neuronal migration in mice (71,72), which are also mimicked upon conditional co-ablation of MKL isoforms as found in a later study (73). The latter study discovered reduction in the expression of actin-severing proteins gelsolin and cofilin, and a dramatic upregulation of the inhibitory phosphorylation of cofilin as a result of inhibition of Cdk5 kinase and in turn activation of PAK (p21 activated kinase and a phosphorylation substrate of Cdk5)/LIMK (a PAK-activated kinase that directly phosphorylates

cofilin) signaling axis. MKL-KO-induced suppression of Cdk5 activity was further linked to diminished expression of Pctaire1, an MKL/SRF target gene and an upstream regulator of Cdk5. While identification of this signaling pathway provided a possible mechanistic avenue for MKL-dependent regulation of cell migration, a definitive causal link between MKL-dependent suppression of Pctaire1 and defect in neuronal cell migration was not directly examined in that study.

A number of studies have previously examined the role of MKL/SRF signaling in wound healing and various cardiovascular-related contexts. For example, activation of MKL/SRF signaling by isoxazole-ring containing small molecule promoted myofibroblast differentiation and wound healing in mouse model. (74). Epithelial-to-mesenchymal transformation and migration of epicardial cells were shown to rely to MKL/SRF signaling (75). Although the two MKL isoforms generally display functional redundancy, MKL2 depletion alone is sufficient to impair cardiac neural crest migration during development in mouse (76), suggesting certain functional aspects of MKL may be isoform-specific. Another report showed that CTRP6 (C1q/tumor necrosis factor-related protein-6) inhibits TGF-beta promotion of cardiac fibroblast migration and myofibroblast differentiation by targeting RhoA/MKL1 pathway (77). Rat aortic vascular smooth muscle cells (RAVSMC) also required MKL1 for migration and proliferation, both of which are important for RAVSMC to assist in remodeling vasculature in mice (78). Another recent study has shown that loss of SMAD3 can enhance proliferation and migration of human pulmonary arterial smooth muscle cells and endothelial cells (EC) by disinhibiting MKL1 and promoting its localization into the nucleus thus allowing MKL/SRF binding (79). Loss of function of MKL1 has been also shown to cause actin cytoskeletal dysfunction, impaired migration and phagocytic ability of myeloid lineage-immune cells (neutrophils, primary

dendritic cells) leading to immunodeficiency in mice. Actin cytoskeletal disturbance and defect in contractile function of MKL1-deficient neutrophils were correlated with reduced expressions of several actin regulators and actin-cytoskeleton related proteins including CDC42-binding protein, cortactin, formin-binding protein 1L (it is also known as TOCA – a positive regulator of Cdc42/N-WASP-dependent actin polymerization) and myosin-light chain 9 (Myl9 – a component of myosin II complex) (80).

Angiogenesis is another prominent vascular-related area in which MKL-dependency has been examined in a number of studies. EC migration plays a crucial role in angiogenesis. During angiogenesis, a selective population of EC, known as *tip cells*, become activated by proangiogenic cues allowing these cells to extend F-actin-rich filopodial protrusions, migrate toward guidance cues and drive the vessel sprouting while EC trailing behind the tip cells (known as *stalk cells*) proliferate to elongate the sprouts (81). MKL/SRF signaling is activated in EC in response to pro-angiogenic growth factors (*e.g.* VEGF, FGF). EC-selective disruption of either SRF or both MKL genes (MKL1 and MKL2), when conditionally induced in neonatal and adult mice, causes prominent reduction in developmental angiogenesis in the retina and heart. MKL or SRF ablation was associated with a significant reduction in the filopodial abundance and tip cell invasion during angiogenic expansion of retinal vasculature in neonatal mice. In line with these *in vivo* findings, knockdown of either SRF or MKL causes defects in migration and angiogenic ability of both human and rodent EC *in vitro* (18,75,82-85). Consistent with these genetic proof-of-principle findings, our group has recently reported that pharmacological inhibition of MKL/SRF signaling by CCG-1423 (a small molecule that binds to and inhibits nuclear localization of MKL (86,87) suppresses migration of human dermal microvascular EC *in vitro* and inhibits angiogenic ability of human and mouse EC *in vitro*, *ex vivo* and developmental

angiogenesis in zebrafish embryos *in vivo* (88). While these findings provide compelling evidence of an essential role of MKL/SRF signaling in EC migration and angiogenesis, the key drivers of EC migration and angiogenesis downstream of MKL are yet to be comprehensively identified. Several MKL/SRF-regulated genes which have been identified as pro-angiogenic (e.g. integrin, VE-cadherin and Myl9) are also required for homeostatic functions of EC and vascular integrity. Those studies, however, either lacked detailed phenotypic comparisons between LOF (loss-of-function) of MKL and the putative downstream genes, or in some cases, knockdown of those genes failed to recapitulate MKL-associated tip cell phenotypes, or the role of those genes as mediators of MKL-directed angiogenesis was not conclusively proven (18,82,89-91). Although one study has linked MKL1 and its transcriptional targets CCN1 and CCN2 (cell-secreted proteins) to angiogenesis-promoting effect of actin-binding protein thymosin β4 (84), whether the defects in tip cell-driven angiogenesis caused by MKL deficiency is linked to alterations in CCN isoforms is not definitive.

1.4 MKL/SRF SIGNALING IN CANCER CELL MIGRATION

MKL/SRF signaling also contributes to motility, invasion and metastasis of tumor cells. For example, SCAI was discovered to be a novel suppressor of human breast cancer cell (MDA-MB-231, MDA-MB-468) invasion with its mechanism of action linked to inhibition of MKL/SRF signaling in the nucleus through formation of a ternary complex and negative regulation of the expression of β1-integrin, a crucial adhesion molecule that promotes invasive phenotype of metastatic breast cancer cells (76). Through experiments involving either co-depletion of MKL isoforms or depletion of SRF, Treisman group also demonstrated requirement for MKL/SRF

signaling for directed migration and invasion (both *in vitro* and *in vivo*), and experimental lung metastasis of metastatic human breast cancer cells (MDA-MB-231) (90). Note that somewhat inconsistent with this finding, we recently showed that partial knockdown of MKL (through silencing of MKL1 only) induces a hypermotile phenotype in MDA-MB-231 cells, albeit, in a random migration assay (61). Whether this discrepancy is due to study-specific differences in the assays and experimental conditions (random vs directed motility, partial vs near complete loss of MKL, culture condition) is yet to be determined. MKL-dependency for tumor cell migration/invasion was also true for B16 mouse melanoma cells (90). In line with these findings, pharmacological inhibition of MKL/SRF signaling by either CCG-1423 or its derivative 203971 inhibited migration/invasion of melanoma and prostate cancer cells *in vitro* and experimental lung metastasis of melanoma cells *in vivo* (92,93) (94) (95). Conversely, another group showed that overexpression of MKL1 increased motility of non-invasive MCF-7 breast cancer cell line by increasing the expression of MYL9 and CYR61 (96,97). They further demonstrated a pro-migratory role of MKL1 in MDA-MB-231 cell migration and interaction between MKL1 and STAT3 in synergistically promoting MDA-MB-231 cell migration (98-100) (101,102). Several other studies related alteration in either expression or localization of MKL to cell motility phenotype in response to various molecular and/or pharmacological perturbations. For example, Tranilast (blocks calcium permeable channels) treatment led to attenuation in the protein level of MKL1 with concomitant reduction of cell migration, proliferation, and clonogenicity of MDA-MB-231 and BT-474 breast cancer cells (103). Overexpression of microRNA-200c caused cytoplasmic localization of MKL (causing a decrease in SRF activity/level) and decreased migration/invasion of breast cancer cells (104). Similarly, microRNA-206 was linked to degradation of MKL1 and inhibition of migration and invasion of malignant thyroid cancer cells

(105). Another group showed that FHOD1, a formin family member protein, promotes nuclear localization of MKL1 and knockdown of formin increases cytoplasmic MKL1 resulting in reduced migration of melanoma cells (106). Consistent with the finding of cytoplasmic retention of MKL correlated with reduced cell migration, Asparuhova et al. demonstrated that irradiation of 4T1 mouse breast cancer cells promotes nuclear localization of MKL1 leading to transcriptional upregulation of SRF-target genes and increased cell migration, invasion, and lung metastasis (107).

1.5 CONTEXT-SPECIFIC EFFECT OF MKL IN CELL MIGRATION

Although studies described thus far indicate a pro-migratory function of MKL, Leitnar et al. showed that depending on the adhesiveness of the cell-type, MKL can be either pro- or anti-migratory (108). Specifically, this study demonstrated that weakly adhesive MDA-MB-231 breast cancer cells exhibit defect in migration upon silencing of MKL and conversely, display faster migration upon overexpression of constitutively active form of MKL (lacking the N-terminal RPEL domains). MKL-induced stimulation of MDA-MB-231 cells migration was only evident in low adhesive culture condition. In culture conditions that promote stronger adhesions, while the basal migration speed of these cells was higher, MKL was unable to stimulate the migration any further. Contrasting the effect of MKL silencing on MDA-MB-231 cells, they further demonstrated that cells that generally have stronger adhesions and are non-invasive in nature, such as mouse fibroblasts and mammary epithelial cells, become hypermotile upon loss-of-function of MKL and accordingly, their motility is suppressed upon hyperactivation of MKL. The anti-migratory effect of MKL for these cells was partially reversed upon silencing of certain

cell-cell and cell-matrix adhesion-associated molecules (plakophilin, FHL1, integrin α) which were otherwise upregulated by increased MKL activity. These findings implied that MKL-induced suppression of motility of these cells was at least partly related to overexpression of adhesion molecules from an overload of MKL activity, causing cells to become excessively "sticky" (either to the underlying substrate and/or to their neighboring cells), a condition that is known to be unconducive to efficient motility. These observations led the authors to propose a model of biphasic dependency of cell migration on MKL activity that can potentially explain a context-specific role of MKL in cell migration depending on the inherent adhesiveness of the cell-type. The importance of adhesion in determining cell motility response to perturbation of MKL activity is further underscored by recent findings that overexpression of constitutively active MKL1 suppressed migration and invasion of B16 melanoma cells through promoting FAK (focal adhesion kinase) activation and paxillin phosphorylation (via increased integrin clustering) and in turn enhancing cell adhesion (109). This observation is clearly consistent with the biphasic model postulated by the Posern group (108) suggesting that a balanced level of MKL activity is perhaps most productive for cell migration.

1.6 MKL'S FUNCTION EXTENDS BEYOND ITS CANONICAL SRF FUNCTION IN CELL MIGRATION

There is some evidence in the literature which suggests that MKL's function extends beyond and above its SRF-related activity. SRF-independent activity of MKL was proposed based on differential expression of >4000 genes and phenotypic distinctions between MKL- and SRF-knockout megakaryocytes (110). Studies in the recent past have shown that MKL can regulate

expression of genes that are important for cell motility and proliferation in an SRF-independent, SAP-domain-function dependent manner. For example, through differential gene expression analyses in non-transformed HCC1 mammary epithelial cells overexpressing either wild-type MKL1 or mutants that are selectively deficient in SAP-domain function or SRF-interaction of MKL, Gurbuz et al. identified ~200 genes that are exclusively dependent on the SAP-domain function (and independent of the SRF-function) of MKL1 with tenascin C (an ECM protein that is important cell adhesion, migration and cancer metastasis) being the most prominently regulated gene relying on the SAP-domain activity of MKL1 (107,111). Several other candidate genes that are exclusively dependent on the SAP-domain function of MKL for their transcription and potentially important for cell migration are Krt5 (encodes keratin 5 - important for regulating cell deformability), Kif26B (important for cell polarity and adhesion) and Adam26 (encodes an ECM-degrading protease). Note that some of the genes required both SRF- and SAP-domain-related functions of MKL. Functional studies demonstrated that migration and proliferation of HCC1 cells are significantly impaired upon abrogation of the SAP-domain activity of MKL1 further underscoring an important role of SAP-domain function of MKL1 in cell migration. Interestingly, the SAP-domain gene expression signature (elevated most prominently in triple-negative breast cancer) also correlated with poor-prognosis of breast cancer irrespective of the subtype of breast cancer. A follow-up study conducted by the same group in 4T1 breast cancer cells showed that while SRF-function of MKL1 plays a more prominent role in promoting tumor growth and lung metastasis, irradiated tumors (which causes matrix stiffening) rely on the SAP-domain function of MKL1 for tumor progression (growth and metastasis). This observation was consistent with SAP-domain function dependency for transcription of mechanosensitive genes and mechanical strain-stimulated 4T1 cell migration (107,111). Our group has recently reported

a novel role of MKL1 in co-regulating the expressions of isoforms of profilin family (profilin-1 and 2) of ABP (a key regulator of actin dynamics and cell migration), and this action of MKL1 also relies on its SAP-domain function rather than its SRF-related activity (61). However, MKL-dependent regulation of profilin was found to be indirect (through an intermediate regulation of STAT family transcription factor) and involved cellular externalization control of profilin rather than its transcription. Consistent with these findings, we also showed that either pharmacological inhibition of MKL by CCG-1423 or treatment of latrunculin (indirectly inhibits MKL function through promoting F-actin depolymerization) causes a dramatic loss of cellular level of profilin1 (as a result of increased release in the extracellular environment). In addition to stimulating profilin1 release, pharmacological inhibition of MKL also promoted cellular depletion of at least two other actin-binding proteins including VASP, Arp2 although the effect on profilin1 was most prominent (whether MKL's effect on VASP and Arp2 is also dependent on its SAP-domain function is yet to be confirmed) (88). Although the detailed mechanisms of how the SAP-domain function of MKL ultimately links to cellular retention control of profilin and possibly, other actin-binding protein are yet to be worked out, this pathway clearly represents a potential novel way of MKL-mediated regulation of cell migration that need to be explored further. Figure 4 depicts a schematic of various SRF-dependent and independent mechanistic links to cell migration as summarized from published literature to date.

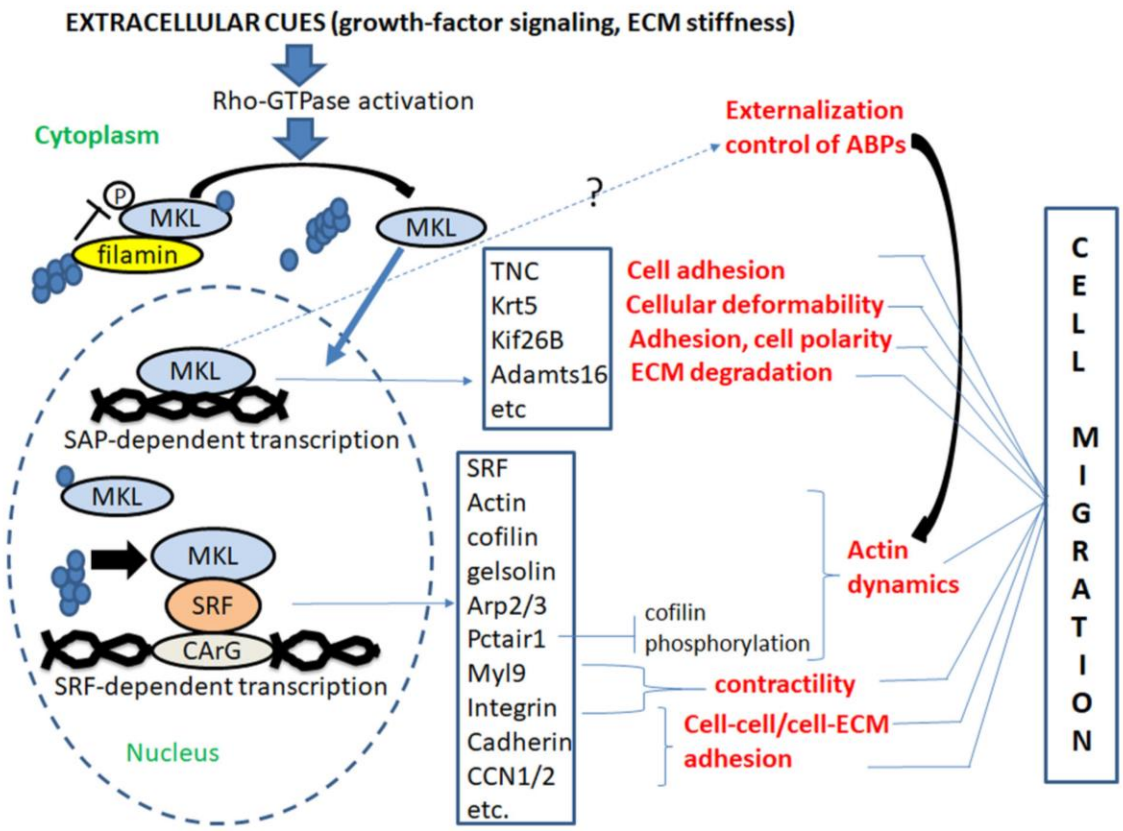

Figure 4. Schematic of MKL SAP-dependent or SRF-dependent regulation of cell migration. Extracellular cues activate Rho-GTPase signaling pathway, initiating actin polymerization, which encourages separation of MKL and G-actin binding. Free from G-actin, MKL translocates into the nucleus where it can interact with SRF and initiate MKL/SRF gene transcription. MKL/SRF transcription targets include regulators of actin dynamics (e.g. SRF, actin, cofilin, gelsolin, Arp2/3), contractility (e.g. Myl9, integrin), and cell-cell/cell-ECM adhesion (e.g. integrin, cadherin, CCN1/2). MKL can also interact with DNA through its SAP domain and initiate MKL SAP-dependent gene transcription with targets related to cell adhesion (e.g. TNC), cellular deformability (e.g. Krt5), adhesion/cell polarity (e.g. Kif26B), and ECM degradation (e.g. Adamts16). In addition, MKL is able to regulate the externalization of some ABPs by an unknown mechanism which contributes to MKL's regulation of actin dynamics and cell migration.

1.7 PROFILIN

Profilins are key players in the regulation of actin polymerization. There are four Pfns in the family. Pfns are well conserved through evolution and at least one Pfn gene is found in almost every eukaryotic cell type from yeast to plants and animals. Of the four, Profilin-1 (Pfn1) is ubiquitously expressed in all cells except skeletal muscle and was one of the first G-actin binding protein isolated (112). Homozygous knockout of Pfn1 gene results in embryonic lethality at the two-cell stage, highlighting Pfn1's importance (113). Initial studies on Pfn1 identified Pfn1 as a monomeric actin-sequestration molecule that facilitated ADP to ATP exchange on actin and prevented actin nucleation (114-116). In the presence of other actin-binding proteins (ABPs), Pfn1 acts as a promoter of actin polymerization (117-119). Pfn1 is found to localize at the lamellipodia of mammalian cells (120) and the surface of motile *listeria monocytogenes* (119) and loss of Pfn1 expression leads to a decrease of F-actin content in ECs (121). These studies suggest that Pfn1 has an important role as a promotor of actin polymerization. Related to angiogenic regulation, Pfn1 reduction led to decreased EC migration, invasiveness, proliferation, and cord morphogenesis *in vitro* (121) and also *ex vivo* (88). Furthermore, Pfn1's ability to interact with its ligands such as G-actin and polyproline are important to promote such behavior (122).

Pfn1 has various binding partners including actin, polyproline proteins (PLPs), and phosphoinositides (PPIs). Pfn1's PPI binding regions overlaps with the G-actin binding domain and also the PLP binding domain. There is some evidence that Pfn-actin interaction can be controlled by phosphorylation (123), which suggests that at least Pfn1 may also be differentially regulated in cells. Opening the possibility for another way to regulate Pfns, our lab has shown that Pfn1 can regulate cell motility through PPI signaling in an actin-independent manner (124).

However, we still do not know how Pfns are regulated and what effect this regulation has on Pfns ability to interact with its binding partners.

Regulation of Pfn1 has been previously shown through phosphorylation. Pfn1 can be phosphorylated at S137 *in vitro* by Protein Kinase C-ζ (PKCζ) when $PI(4,5)P_2$ or other PPIs are present (125,126). Phosphorylation of Pfn1 on S137 led to an increase of G-actin and PLP binding with no apparent effect to $PI(4,5)P_2$ binding (127) and this furthermore increases 2D migration of MCF7 breast cancer cells (128). Another group, however, showed that S137 on Pfn1 can be phosphorylated by Rho-associated coiled-Coil Kinase-1 (ROCK1) both *in vitro* and *in vivo* (129) which decreased Pfn1's ability to bind to both G-actin and PLPs, contradictory to previous findings. These two findings were never confirmed with mass spectrometry or phospho-enrichment to confirm the specificity of S137 phosphorylation. Another group found that phosphorylation of Pfn1 at Y128 led to an increase to G-actin binding which was shown to be crucial in sprouting angiogenesis (123). These data suggest that post-translational regulation of Pfn1 may also serve as a strategy to target Pfn1 activity.

1.8 HYPOTHESIS AND SPECIFIC AIMS

Regulation of the actin cytoskeleton is a crucial aspect of cell migration and in part angiogenesis. MKL/SRF signaling is a major contributor in the regulation of the actin cytoskeleton by initiating the *de novo* synthesis of many actin cytoskeletal proteins. Recent studies have established that MKL/SRF signaling pathway plays a crucial role in various cell type migrations, suggesting that the MKL/SRF pathway may be a potential target for regulation of cell migration. Other studies have shown that the compound CCG-1423 and analogs of CCG can inhibit MKL

activity. Furthermore, work from our lab has shown that MKL can affect expression of actin binding protein, profilin, in a SRF independent manner and that MKL's effect on migration is at least in part due to changes to Pfn1 expression. Therefore, I hypothesize that ***endothelial cell migration and angiogenesis are susceptible to small molecule-mediated intervention of either MKL directly or selective MKL-regulated molecules with pro-angiogenic function such as profilin1***. The following specific aims were formulated to address the hypothesis.

Specific Aim 1: Determine the effect of CCG-1423, a small molecule inhibitor of MKL, on EC migration and angiogenesis.

Specific Aim 2: Identify novel small molecule inhibitors targeting Profilin-1 (a downstream target of MKL) and further assess the potential inhibitors in modulating EC migration and angiogenesis.

Specific Aim 3: Identify and examine the consequence of novel phosphorylation event on actin-related function of Pfn1.

By developing MKL/SRF signaling or Pfn activity inhibitors, we will explore the potential for therapies for pathologies such as excessive angiogenesis, or even tumor metastasis. These studies will also further implicate the possibility for targeting fundamental processes as a pharmacological target. A major gap in MKL-related signaling and Pfn is a limited understanding of the implications of pharmacological inhibition of either. In addition, examining the effect of post-translational modification on Pfn may open new avenues for targeting this important actin binding protein. The work presenting in this dissertation for the most part have already been published in peer-reviewed journals. Work that has not been published will be noted throughout the text.

2.0 MATERIALS AND METHODS

2.1 CELL CULTURE AND TREATMENTS

HmVEC-1, a widely used human dermal microvascular EC line (source: ATCC; Manassas, VA; CRL-3243 – referred to as HmVEC hereafter), were cultured in MCDB-131 (Life Technologies; Carlsbad, CA) growth medium [10% (v/v) fetal bovine serum, 100U/mL Penicillin, 100µg/mL Streptomycin, 10ng/mL EGF, 1µg/mL Hydrocortisone, 10mM L-Glutamine]. HEK-293 cells (ATCC, CRL-1573) were cultured in DMEM/F12 (1:1) (Life Technologies, Carlsbad, PA, USA) growth medium [10% (v/v) FBS, 100 U-mL-1 Penicillin, 100 µg-mL-1 Streptomycin]. HEK-293 cells were maintained on culture dishes (Corning, Corning, NY, USA) coated with type I collagen (BD Biosciences, Frankin Lakes, NJ, USA) for all experiments. MDA-MB-231 cells (ATCC, HTB-26) were cultured in EMEM (Lonza, Basel, Switzerland) growth medium [10% (v/v) FBS, 100 U-mL-1 Penicillin, 100 µg-mL-1 Streptomycin]. Human VSMC (ATCC; PCS-100-012) were cultured in Human Smooth Muscle Cell Media (Cell Applications) with supplement provided by the company, 100 U/ml Penicillin, and 100 µg/ml Streptomycin. For silencing of genes, MKL1 siRNA (Santa Cruz, Dallas, TX, USA, sc-43944; Thermofisher Scientific, Waltham, MA, 133259 (#2)), MKL1 3'UTR siRNA (sense-strand sequence of a single-target siRNA 5' GUGUCUUGGUGUAGUGUAAUU-3'), MKL2 siRNA (Santa Cruz, sc-61074), SRF siRNA (Santa Cruz, sc-36563), Pfn1 siRNA (GE Dharmacon, M-012003-01-

0005), Pfn1-specific siRNA (sense-strand sequence of a single-target siRNA 5′-UAGCGACUAAACACAUCAAUU-3′) or smart-pool control-siRNA (Dharmacon, Lafayette, CO, USA) all at 100 nM, were transfected using Transfection Reagent 1 for HmVEC or Transfection Reagent 2 for MDA and 293 (Dharmacon) following the manufacturer's instructions. Phosphomimetic point mutation of Pfn1 were created on a GST-tagged *Mus musculus* Pfn1-encoding bacterial expression vector using the following primers: S57D (sense: 5'- GGCAAAGACCGGTCAGATTTTTTCGTC-3'), T89D (sense: 5'-GGATCTTCGTGACAAGAGCACCGG-3'), S91D (sense: 5'-CGTACCAAGGACACCGGAGGAG-3'), T92D (sense: 5'-CCAAGAGCGACGGAGGAGCC-3'). For expression in eukaryotic cells, myc-tagged *Mus musculus* Pfn1 cDNA was sub-cloned into pIRES2-AcGFP1 (Clontech, Mountain View, CA, USA) bicistronic expression vector. Phospho-dead point mutation was made using the following primer: T89A (sense: 5'-GGACTTCGTGCCAAGAGCACCGG-3'). Plasmid DNA transfections for HEK-293 and MDA-231 cells were performed using XtremeGENE HP transfection reagent (Roche, Basel, Switzerland) and Lipofectamine LTX Plus (Life Technologies, Carlsbad, PA, USA) according to the manufacturer's instructions. For CCG-1423 experiments, HmVEC were treated with CCG-1423 (Santa Cruz) for 24 hours under serum-starved conditions prior to extraction. For compound experiments, HmVEC were treated with compounds overnight prior to being assayed. Cell viability was assessed by a live-dead staining kit (Molecular Probes) according to the manufacturer's instruction.

2.2 ANGIOGENESIS ASSAYS

For *in vitro* angiogenesis assessment, cord formation assay in matrigel (mimics the natural basement membrane matrix of EC), was performed as previous described (121). Briefly, HmVEC were plated on top of polymerized matrigel and allowed to adhere prior to treatment with DMSO or CCG. Cord formation was assessed after 16 hours by phase-contrast microscopy. Cord-formation data was quantified by measuring the total length of all cords using the angiogenesis plugin for ImageJ. For CCG and compound experiments, cells were allowed to adhere for 4 hours before switching to serum-free media with 30 ng/ml VEGF-A (Cell Signaling) and CCG-1423 or compounds. For EC-spheroid angiogenesis assay, collagen solution [1 mg/ml collagen with 0.25% (w/v) methylcellulose diluted in MCDB-131] was pH-adjusted using 5N NaOH. EC spheroids (formed by culturing cells in ultra-low attachment plate) were mixed with chilled collagen solution and seeded into the wells of a pre-warmed 24-well plate (the seeding volume was equal to 600 µL which typically contained 15-20 spheroids). To permit complete polymerization, the gels were incubated at 37˚C for 1 hour, and then overlaid with 500 µL of MCDB-131 growth medium. End-point analysis of sprouts was performed after 24 hrs of culture.

For *ex vivo* angiogenesis assessment, aortic ring angiogenesis assay was performed. Briefly, thoracic aortas of 9-11 week-old mice were isolated, cleaned of fatty tissues and branching vessels, and excised into ~1 mm segments. When applicable, aortic segments were transfected for 24 hrs with appropriate siRNAs in Opti-MEM (Life Technologies) media, and embedded in either type I collagen (1 mg/ml - diluted in DMEM) or growth-factor reduced matrigel. After polymerizing the matrix for 45 minutes, *ex vivo* culture was maintained in Opti-MEM containing 2.5% (v/v) FBS and 30 ng/ml VEGF-A for an additional 3-4 days to allow vascular sprouting to take place. For CCG and compound experiments, DMSO or CCG-1423 or

compound was added to the media following embedding of aortic rings. For Pfn1 siRNA experiments, control of Pfn1 siRNA was added to the media following embedding of aortic rings. At the end of incubation, aortic rings were fixed with 3% (v/v) formalin for 30 minutes, stained with 0.05 mg/ml rhodamine-conjugated lectin (labels EC) for 2 hours at room temperature and further washed before acquiring images at a 4x magnification. For Pfn1 immunostaining, following fixation, aortic rings were permeabilized with two consecutive treatments of 0.25% (v/v) Triton-X-100 (Fisher Scientific) for 15 minutes. After blocking with 10% (v/v) goat serum for 1 hour, rings were stained with Pfn1 polyclonal antibody (1:200; Abcam, Cambridge, MA) overnight at 4˚C, washed extensively, labeled with FITC-conjugated Goat Anti-Rabbit (1:100; Jackson Immunoresearch) and 0.05 mg/ml rhodamine-conjugated lectin for 2 hours at room temperature and further washed several times before image acquisition.

For *in vivo* angiogenesis experiments, embryos were collected from Tg(kdrl:gfp)la116 zebrafish (Danio rerio), grown at 24˚C until the 20 somite stage [equivalent to 19 hours post-fertilization (hpf) at 28.5oC], dechlorinated, and allocated 20 per well in a six-well plate. Embryos were exposed to 1% DMSO or graded doses of CCG-1423 (0.5-50 μM) in 30% Danieau/0.003% phenylthiourea (Sigma, St. Louis, MO) for 22 hr at 28.5˚C. CCG-1423 was added directly in the water. For vessel analysis, each dose was repeated at least two times. At the end of the incubation period (41 hpf), embryos were fixed in 4% paraformaldehyde and imaged via brightfield and fluorescence on an Olympus MVX10 microscope. Selected high-resolution images were obtained using a multiphoton microscope.

2.3 GENERATION OF EC-SPECIFIC CONDITIONAL PFN1 KNOCKOUT MICE

$Pfn1^{flox/flox}$ mice (described in (130)) were bred into a Tie2-Cre background (Source: Jackson Laboratory in this transgenic C57BL/6 mouse strain, Cre expression is driven under EC-specific Tie2 promoter) to generate EC-specific heterozygous Pfn1 knockout mouse ($Pfn1^{+/-}$ [EC]). Genomic DNA was extracted from either the tails of pups or aortic segments of adult mice (following sacrifice) using a commercial kit (Promega). For genotyping, the following primers were used: LoxP (Primer 1 [forward]: TGGAGCGGATCCAGCGAAGG; Primer 2 [reverse]:GTCCCCAGCAGTCGGGACG, Tie2-Cre (forward: GCGGTCTGGCAGTAAAAACTATC, reverse: GTGAAACAGCATTGCTGTCACTT); PCR positive control (forward: CTAGGCCACAGAATTGAAAGATCT; reverse: GTAGGTGGAAATTCTAGCATCATCC). The recombinase activity of Cre was confirmed by the generation of a 700 bp knockout band using Primer 1 (as mentioned above) and Primer 3 [reverse]: GGACACCAACCTCAGCTGGC. All animal experiments were performed in compliance with an approved protocol by the Institutional Animal Care Committee of the University of Pittsburgh.

2.4 CELL MIGRATION AND KYMOGRAPHY ASSAY

HmVEC were sparsely plated in a 24-well plate coated with type I collagen (Millipore) and allowed to attach prior to switching to serum-free media overnight with DMSO or CCG. Prior to taking images, cells were stimulated with 50 ng/ml of VEGF. For compound experiments, HmVEC were sparsely plated in a 24-well plate coated with type I collagen (Millipore) and

treated with DMSO, C1, or C2 overnight in cell culture plating media described earlier. For MDA experiments, MDA were sparsely plated in a 24-well plate coated with type I collagen (Millipore) overnight in cell culture plating media described earlier. Time-lapse images of randomly migrating EC or MDA were collected using a 10x objective for 120 minutes at a 1 minute time interval using MetaMorph (Universal Imaging). The centroid of the cell nucleus was tracked using ImageJ. For kymography analyses, HmVEC-1 were plated and treated as before but imaged using a 20x objective at 20 second intervals for 20 minutes, as per procedure described before (131).

2.5 PROTEIN EXTRACTION AND IMMUNOBLOTTING

Cell lysates were prepared by a modified RIPA buffer (25 mM Tris–HCl—pH 7.5, 150 mM NaCl, 1% (v/v) NP-40, 5% (v/v) glycerol), 1 mM EDTA, 50 mM NaF, 1 mM sodium pervanadate, and protease inhibitors supplemented with 6x sample buffer diluted to 1x with the final SDS concentration in the lysis buffer was equivalent to 2%. Conditions for the various antibodies were: monoclonal Pfn1 (Abcam; 1:3000), monoclonal GAPDH (Biorad, Hercules, CA, 1:3000), monoclonal VASP (BD Biosciences, Frankin Lakes, NJ; 1:2000), polyclonal MKL1 (Santa Cruz, 1:500), polyclonal SRF (Santa Cruz, 1:500), polyclonal p34- ArpC2 (Arp2/3) (Upstate Biotechnology, Lake Placid, NY; 1:1000), monoclonal GFP (Clontech, Mountain View, CA, USA, 1:3000). monoclonal actin (BD Biosciences, Frankin Lakes, NJ, USA. 1:1000), monoclonal myc (Sigma, St. Louis, MO, USA, 1:3000), monoclonal α-tubulin (Sigma, St. Louis, MO, USA, 1:3000), monoclonal Flag (Sigma, St. Louis, MO, USA, 1:3000),

monoclonal VASP (BD Biosciences, Frankin Lakes, NJ, USA, 1:1000) and monoclonal $p27^{kip1}$ (BD Biosciences, Frankin Lakes, NJ, USA, 1:2000).

2.6 CONDITIONED MEDIA PREPARATION

Conditioned media was collected from the culture dish of HmVEC or MDA following overnight incubation of cells in serum-free media. The collected media was filtered (0.45 µm size) and concentrated using a 10 kDa cut-off filter. The concentrate was reconstituted with 2X laemmli sample buffer and boiled before being analyzed by gel electrophoresis.

2.7 IMMUNOSTAINING

Cells expressing various Flag-MKL constructs were washed with PBS, fixed with 3.7% formaldehyde for 15 min, and permeabilized with 0.5% Triton-X 100 for 5 min. Following blocking with 10% goat serum in PBS at room temperature for 30 min, cells were incubated with a monoclonal Flag antibody (Sigma Aldrich; 1:100) diluted in 5% goat serum for 1 hr at room temperature. After washing cells two times with 0.02% tween-20 and twice with PBS, cells were incubated with TRITC-conjugated secondary antibody (Jackson Immunoresearch, West Grove, PA, 1:100) for 1 hr. Cells were again washed with 0.02% tween-20 and PBS, two times each, before mounting with the mounting medium with DAPI (Sigma Aldrich). Slides were imaged using a 20X/0.4 NA objective on an Olympus IX71 inverted microscope.

2.8 PROXIMITY LIGATION ASSAY (PLA)

PLA was performed using the Duolink kit with anti-mouse plus and anti-rabbit minus probes (Sigma, DUO9210). Cells cultured on cover slips were washed with DPBS, fixed with 3.7% formaldehyde for 15 mins, permeabilized with 0.5% Triton X-100 for 5 minutes and then blocked with 10% goat serum for 1 hr at room temperature. In situ proximity ligation was performed using two primary antibodies of different species targeting either Pfn1 (Abcam, 1:200, ab124904, rabbit) or actin (BD Biosciences, 1:100, 612656, mouse), both for 1 hr at room temperature in 10% goat serum, and a pair of oligonucleotide-labeled secondary antibodies targeting each primary antibody from the Duolink kit as per the manufacturer's protocol. PLA probe hybridization, ligation, amplification, and detection were performed according to the manufacturer's protocol. To quantify PLA spots, images (acquired at an emission wavelength of 624 nm with a 60X oil-immersion objective [N.A. = 1.4] on an Olympus IX-71 inverted microscope) were first background subtracted using the mean fluorescent intensity of cells from the negative control group. A mask was then created from the images of interest and the "Analyze Particles" option was used to count the number of spots in each cell from a field of view.

2.9 ACTIN POLYMERIZATION ASSAY

Bacteria transformed with GST-Pfn1 were grown to OD 0.6-0.9 and induced with 0.1 mM isopropyl- β-D- thiogalactopyranoside (IPTG) (Sigma) for 3 hours and extracted with lysis buffer (25 mM Tris pH 7.4, 150 mM NaCl, 1% NP-40, 1 mM EDTA, 5% glycerol). Following

clarification by centrifugation at 18000g for 30 minutes, cell lysates were mixed with reconstituted glutathione-agarose beads (Thermo Fisher) for overnight. After washing the resin with a wash buffer (50 mM Tris, 150 mM NaCl, pH 8.0), GST-Pfn1 was eluted using an elution buffer (50 mM Tris, 150 mM NaCl, pH 8.0, 10 mM reduced glutathione). The eluted GST-Pfn1 was then dialyzed in the following buffer: 100 mM Tris pH 7.4, 100 mM NaCl, 0.2 mM ATP, 5% sucrose, and 1% dextran prior to use in the polymerization assay. Actin polymerization with or without GST-Pfn1 in the presence of DMSO or compound was performed using a fluorescent actin polymerization kit (Cytoskeleton, BK003) according to manufacturer's protocol downscaled to a 96-well format with a 10:1 ratio (9 µM unlabeled and 1 µM pyrene actin) between unlabeled and pyrene actin. Pyrene fluorescence signal was read using a fluorimeter with excitation wavelength of 360 nm and emission wavelength of 420 nm.

2.10 CELL PROLIFERATION ASSAY

Five-thousand cells (HmVEC or VSMC) were plated in the wells of a 24-well plate in duplicate on day 0 (D0) and cultured overnight before being subjected to either compound or vehicle treatment on Day 1(D1). Cells were trypsinized and counted on Days 2 and 4 (D2 and D4). The media was replenished on day 3 (D3) with appropriate treatment.

2.11 PHARMACOPHORE QUERY CONSTRUCTION

Pharmacophore interaction features were generated for the Pfn1:actin binding pocket by docking fragments (benzene and water) and manually selecting deeply buried interactions. Altogether, we identified two hydrophobic, one aromatic, and five hydrogen bond interaction features in the vicinity of Y169 residue of actin. As including all these features resulted in an overly-specific query without any matches, we generated all 10 possible pharmacophore queries containing any three of the five possible hydrogen bond features. Each query feature was assigned a 1Å radius and directionality was not considered.

2.12 MOLECULAR DYNAMICS FOR PFN1/ACTIN INTERACTION INHIBITORS

In order to account for receptor flexibility, the Pfn1 component of the Pfn1/Actin 2BTF complex was simulated by itself using Amber14 and the ff14SB force field (132) with TIP3P explicit water in a truncated octahedral box with a 12Å buffer, periodic boundary conditions, and particle mesh Ewald electrostatics with a 10Å cutoff. After two rounds of minimization and a 100ps equilibration run, the protein was simulated for 139ns. A greedy algorithm was then used to extract 10 diverse snapshots as measured by backbone RMSD. These snapshots were then aligned to the 2BTF structure used to define the pharmacophore queries.

2.13 CONSENSUS SCORING AND RANKING

As the hits identified through pharmacophore search are already aligned with respect to the receptor according to the desired interaction features, there is no need to perform full molecular docking. However, in order to refine the compound structures and generate a ranking, we performed local energy minimization using smina (133) with the AutoDock Vina scoring function (134). We minimized the pharmacophore aligned poses from searching the ZINC database (210,802 poses total) with respect to each of the 10 receptor structures generated through molecular dynamics simulation. Poses that moved by more than 2Å RMSD during minimization were filtered out to retain the desired pharmacophore interactions and only the top scoring pose for each compound was retained. The top 100 scoring poses for each of the 10 receptor structures were then merged and the top 300 unique compounds of this combined set (which included all 39 compounds that were top-100 ranked for at least 5 of the 10 receptors) were evaluated for acquisition. These compounds were clustered using OpenBabel FP2 fingerprints (135) and at most two compounds per a cluster were selected for screening, subject to commercial availability, up to a total of 20 compounds.

2.14 *IN VITRO* KINASE ASSAY

His-tagged Pfn1 (1.5 µg) was added to kinase Buffer [20 mM BES (Sigma, St. Louis, MO, USA) pH 7, 20 mM EGTA (Fisher Scientific, Waltham, MA, USA), 6 mM MgCl2 (Fisher Scientific, Waltham, MA, USA), 5 mM ATP (Sigma, St. Louis, MO, USA), 10 mM Phosphocreatine (Sigma, St. Louis, MO, USA), 1 mM DTT] and incubated with or without 0.5 U µL-1 catalytic

subunit of bovine PKA (Sigma, St. Louis, MO, USA) at 30˚C for 1 hour with gentle mixing every 15 minutes. The reaction was stopped by boiling the products for 5 minutes in the presence of 2-mercaptoethanol. Reaction products were run on SDS-PAGE and visualized by silver staining.

2.15 IN GEL TRYPSIN DIGESTION

In gel trypsin digestion was carried out as previously described (136). PKA treated his-tagged Pfn1 was first subjected to SDS-PAGE. The gels were washed twice with MilliQ water for 5 minutes each and then stained with Coomassie Stain [0.1% (w/v) R250 (Fisher Scientific, Waltham, MA, USA), 40% (v/v) Ethanol (Decon, King of Prussia, PA, USA), 10% (v/v) Acetic Acid (Fisher Scientific, Waltham, MA, USA)]. After destaining gels with a destaining solution [10% (v/v) Ethanol, 7.5% (v/v) Acetic Acid], regions containing his-tagged Pfn1 were excised, washed with HPLC water and destained with 50% acetonitrile (ACN)/25mM ammonium bicarbonate until no visible staining. Gel pieces were dehydrated with 100% ACN, reduced with 10mM dithiothreitol (DTT) at 56°C for 1 hour, followed by alkylation with 55mM iodoacetamide (IAA) at room temperature for 45 min in the dark. Gel pieces were then again dehydrated with 100% ACN to remove excess DTT and IAA, and rehydrated with 20 ng/µl trypsin/25mM ammonium bicarbonate and digested overnight at 37°C. The resultant tryptic peptides were extracted with 70% ACN/5% formic acid, vacuum dried and re-constituted in 18 µl 0.1% formic acid.

2.16 TANDEM MASS SPECTROMETRY ANALYSIS

Proteolytic peptides from in gel trypsin digestion were analyzed by a nanoflow reverse-phased liquid chromatography tandem mass spectrometry (LC-MS/MS). Tryptic peptides were loaded onto a C18 column (PicoChip™ column packed with 10.5cm Reprosil C18 3 µm 120Å chromatography media with a 75µm ID column and a 15µm tip, New Objective, Inc., Woburn, MA, USA) using a Dionex HPLC system (Dionex Ultimate 3000, ThermoFisher Scientific, Waltham, MA, USA) operated with a double-split system (Personal communication with Dr. Steve Gygi from Department of Cell Biology, Harvard Medical School) to provide an in-column nano-flow rate (~300nl/min). Mobile phases used were 0.1% formic acid for A and 0.1% formic acid in acetonitrile for B. Peptides were eluted off the column using a 52 minute gradient (2-40% B in 42 min, 40-95% B in 1 min, 95% B for 1 min, 2% B for 8 min) and injected into a linear ion trap MS (LTQ-XL, ThermoFisher Scientific, Waltham, MA, USA) through electrospray. The LTQ XL was operated in a date-dependent MS/MS mode in which each full MS spectrum [acquired at 30000 automatic gain control (AGC) target, 50ms maximum ion accumulation time, precursor ion selection range of m/z 300 to 1800] was followed by MS/MS scans of the 5 most abundant molecular ions determined from full MS scan (acquired based on the setting of 1000 signal threshold, 10000 AGC target, 100ms maximum accumulation time, 2.0 Da isolation width, 30ms activation time and 35% normalized collision energy). Dynamic exclusion was enabled to minimize redundant selection of peptides previously selected for CID.

The MS raw files have been deposited to Chorus (https://chorusproject.org/pages/index.html) under the project “Phosphorylation of Pfn1”.

2.17 PEPTIDE IDENTIFICATION BY DATABASE SEARCH

MS/MS spectra were searched using the SEQUEST search engine implemented in Proteome Discoverer™ software (v. 1.4.0, ThermoFisher Scientific, Waltham, MA, USA) against a UniProt human proteome database (January 2013 release) from the European Bioinformatics Institute (http://www.ebi.ac.uk/integr8). The following modifications were used: static modification of cysteine (carboxyamidomethylation, +57.05 Da), variable modification of methionine (oxidation, +15.99Da) and variable modification of serine/threonine/tyrosine (phosphorylation, +79.97Da). The mass tolerance was set at 1.4Da for the precursor ions and 0.5 Da for the fragment ions. Peptide identifications were filtered using PeptideProphet™ and ProteinProphet® algorithms with a protein threshold cutoff of 99% and peptide threshold cutoff of 95% implemented in Scaffold™ (Proteome Software, Portland, Oregon, USA).

2.18 TWO-DIMENSIONAL GEL ELECTROPHORESES (2D-GE)

Cells were scraped in the presence of 2D lysis Buffer [2 M Urea (Fisher Scientific, Waltham, MA, USA), 7 M Thiourea (Life Technologies, Carlsbad, PA, USA), 4% (w/v) CHAPS (Sigma, St. Louis, MO, USA), 50 mM DTT (Roche, Basel, Switzerland)] and collected into a Bead-beater tube (Biospec, Bartlesville, OK, USA) containing 50 mg Glass Beads (Sigma, St. Louis, MO, USA). Isoelectric focusing was performed using the Zoom IPGRunner System (Life Technologies, Carlsbad, PA, USA) according to manufacturer's instructions with modification. Briefly, lysates were reconstituted in rehydration buffer [final concentrations: 2 M Urea, 7 M Thiourea, 4% (w/v) CHAPS, 50 mM DTT, 0.5% (v/v) Carrier Ampholytes (Life Technologies,

Carlsbad, PA, USA), 0.005% (w/v) Bromophenol Blue (Fisher Scientific, Waltham, MA, USA), 50-150 µg Proteins]. IPG strips underwent isoelectric focusing using the following program: 175 V for 30 minutes; linear ramp 175-2000 V over 45 minutes; 2000 V for 45-105 minutes depending on the pH range. IPG strips were briefly washed with running buffer [25 mM Tris pH 8.3, 192 mM Glycine, 0.1% (w/v) SDS] and sealed on Tris-HCl polyacrylamide gels with running buffer containing 0.5% Agarose (Life Technologies, Carlsbad, PA, USA) and 0.005% (w/v) Bromophenol Blue before performing electrophoresis in the second dimension followed by immunoblotting.

2.19 PHALLOIDIN STAINING

Cells were washed with DPBS, fixed with 3.7% formaldehyde for 15 min, permeabilized with 0.5% Triton X-100 for 5 min and then blocked with 10% goat-serum for 1 hr at room temperature. Cells were incubated with rhodamine-phalloidin (Life Technologies, Carlsbad, PA, USA) for an hour at room temperature. Stained cells were washed two times with PBS containing 0.02% tween, two times with PBS, and then once with distilled water before mounting on slides for imaging using a 60× oil-immersion objective on an Olympus IX71 inverted microscope.

2.20 MOLECULAR DYNAMICS SIMULATION FOR PFN1 PHOSPHORYLATION

A homology model of Mus musculus Pfn1 was created from a crystal structure of bovine Pfn1 bound to actin (PDB 2BTF). The model was created by manually performing the following mutations using Pymol: N9S, N41S, I49V, I100V, and M122L. All mutations could be performed without introducing significant steric clashes. Additional Pfn1 models were created by mutating T89 to either alanine or aspartic acid to mimic phospho-dead and phosphorylated states as well as to phosphothreonine. All simulations were performed with GPU accelerated Amber version 14 with the ff14sb force field (137). Parameters for phosphothreonine were taken from a previously published study (138). The homology modules were solvated to form an octahedral TIP3P water box that extends 12 Å beyond the protein. The system was neutralized with Na+ or Cl- ions as needed. The system then underwent two rounds of minimization. A 100 ps constant volume run was performed with weak positional restraints on the protein during which the temperature was warmed from 0 K to 300 K followed by an unrestrained constant temperature and pressure equilibration run of 100 pS. Simulations were performed using the particle mesh Ewald (PME) method with a non-bonded cutoff of 10 Å. Constant pressure periodic boundaries and isotropic position scaling were used to maintain a pressure of 1 atm. Langevin dynamics were used for temperature control. Three separate simulations of each model were run with different random seeds and every simulation was run for 300ns, resulting in 900ns of simulation per a model. Analysis of the simulations was performed using MDAnalysis (139).

2.21 STATISTICS

Statistical tests were performed with either one-way ANOVA followed by Tukey's post-hoc test or student's T-test when appropriate, and $p < 0.05$ was considered to be statistically significant.

3.0 PHARMACOLOGICAL INTERVENTION OF MKL/SRF SIGNALING BY CCG-1423 IMPEDES ENDOTHELIAL CELL MIGRATION AND ANGIOGENESIS

3.1 INTRODUCTION

The contents of this section are mostly published (section unpublished will be noted in text).
Reference: **Gau D**, Veon W, Capasso T, Bottcher R, Shroff S, Roman B, Roy P. Pharmacological Intervention of MKL/SRF signaling by CCG-1423 impedes endothelial cell migration and angiogenesis. Angiogenesis. 2017; 20(4):663-672. Joy M, **Gau D**, Castellucci N, Prywes R, Roy P. The myocardin-related transcription factor MKL co-regulates the cellular levels of two profilin isoforms. Journal of Biological Chemistry. 2017; 292(28):11777-11791.

Specific Aim 1: Determine the effect of CCG-1423, a small molecule inhibitor of MKL, on EC migration and angiogenesis.

Angiogenesis is an important physiological process that occurs during expansion of the vascular network during development. However, excessive angiogenesis promotes a wide range of human pathologies such as diabetic retinopathy, cancer, atherosclerosis, and arthritis, thus providing justification of anti-angiogenic therapies in various disease contexts. Endothelial cell (EC) migration is a fundamental aspect of angiogenesis. EC activation by pro-angiogenic cues allows a selective population of EC (known as tip cells) to extend F-actin-rich filopodial protrusions, migrate toward guidance cues, and initiate the vessel sprouting, while EC trailing behind the tip cells (known as stalk cells) proliferate to elongate the sprouts. A proper coordination of continued migration of tip cells and proliferation of stalk cells is crucial for angiogenesis (81). Dynamic remodeling of the actin cytoskeleton in response to angiogenic stimuli lies at the heart

of tip cell migration, which, in part, is thought to rely on *de novo* synthesis of important structural and regulatory components of the actin cytoskeletal system by the action of transcription factor SRF [serum response factor]. SRF target genes include SRF itself and those involved in regulating actin cytoskeletal, adhesion, and contractility functions (e.g., actin, myosin, vinculin, filamin, integrin, calponin) (30,35,43,45,140). Myocardin family transcriptional co-activators (include myocardin and myocardin-related transcription factors (MRTF; also known as MKL (megakaryoblastic leukemia))) play an important role in stimulating transcriptional activity of SRF. EC-selective disruption of either SRF or MKL genes (MKL1 and MKL2) when conditionally induced in neonatal and adult mice causes prominent reduction in developmental (physiological) and tumor (pathological) angiogenesis. In line with these *in vivo* findings, knockdown of either SRF or MKL inhibits migration and angiogenic ability of both human and rodent ECs *in vitro* (18,82-85). While these findings provide compelling genetic evidence of an essential role of MKL/SRF signaling in EC migration and angiogenesis, pharmacological targeting of MKL/SRF pathway as a potential anti-angiogenic strategy has not been explored to date.

A small molecule screen of inhibitors of Rho-induced SRF-mediated transcription initially identified CCG-1423 as an inhibitor of MKL/SRF signaling (86). The molecular targets of CCG-1423 have been more recently uncovered. It has been shown that CCG-1423 binds to the nuclear localization signal (NLS) region of RPEL-domain containing proteins, such as those belonging to the MKL family of proteins (87). By virtue of this interaction, CCG-1423 prevents MKL's interaction with importin-α/β, causing inhibition of nuclear import of MKL and MKL/SRF-mediated gene transcription. CCG-1423 can also indirectly reduce nuclear accumulation of MKL and suppress SRF activation by targeting MICAL2 (an atypical actin-

binding protein) and regulating MICAL2-catalyzed redox-modification and depolymerization of nuclear actin (an inhibitor of MKL: SRF interaction) (58). Although these studies suggest that CCG-1423 has more than one cellular target, attenuation of MKL/SRF signaling is clearly one of the main downstream effects of CCG-1423.

We herein demonstrate that pharmacological intervention of MKL/SRF axis by CCG-1423 dramatically inhibits EC migration and angiogenesis *in vitro, ex vivo,* and *in vivo*. Our data suggest cellular depletion of actin-binding protein profilin1 (Pfn1), an important regulator of actin cytoskeletal dynamics, may be one of the mechanisms of the anti-angiogenic action of CCG-1423. These findings set the stage for further preclinical evaluation of CCG-1423 as a potentially novel anti-angiogenic agent.

3.2 RESULTS

3.2.1 Pharmacological intervention of MKL/SRF signaling by CCG-1423 inhibits angiogenesis

First, to determine whether CCG-1423 affects the angiogenic potential of EC in vitro, we performed matrigel-induced cord formation assay with HmVEC at different concentrations (0.5, 1, 2.5, and 5 μM) of CCG-1423 or DMSO (vehicle control). In these experiments, CCG-1423 significantly reduced the cord-forming ability of HmVEC starting at a 1 μM concentration. We found a dose-dependent inhibition in cord-forming ability of HmVEC (as judged by the measurements of total cord length) with mean inhibition equaling to 45 and 80%, at 1 and 2.5 μM concentrations, respectively. At the 5 μM concentration of CCG-1423, the cord-forming

ability of HmVEC was almost completely abolished (Figure 5a–b). By live–dead staining, we confirmed no significant cytotoxicity effect of CCG-1423 on HmVEC (Figure S 1). Immunoblot analyses of parallel culture showed that CCG-1423 not only caused a prominent reduction in the expression level of SRF (this is expected since inhibition of nuclear import of MKL by CCG-1423 should reduce SRF activation, thus diminishing transcription of SRF itself), but interestingly, it also downregulated the expression level of MKL1 (Figure 5c). CCG-1423-induced inhibition of cord formation of HmVEC was also consistent with similar effects elicited by treatment of these cells with siRNAs targeting either MKL1 or SRF (Figure 5d–e).

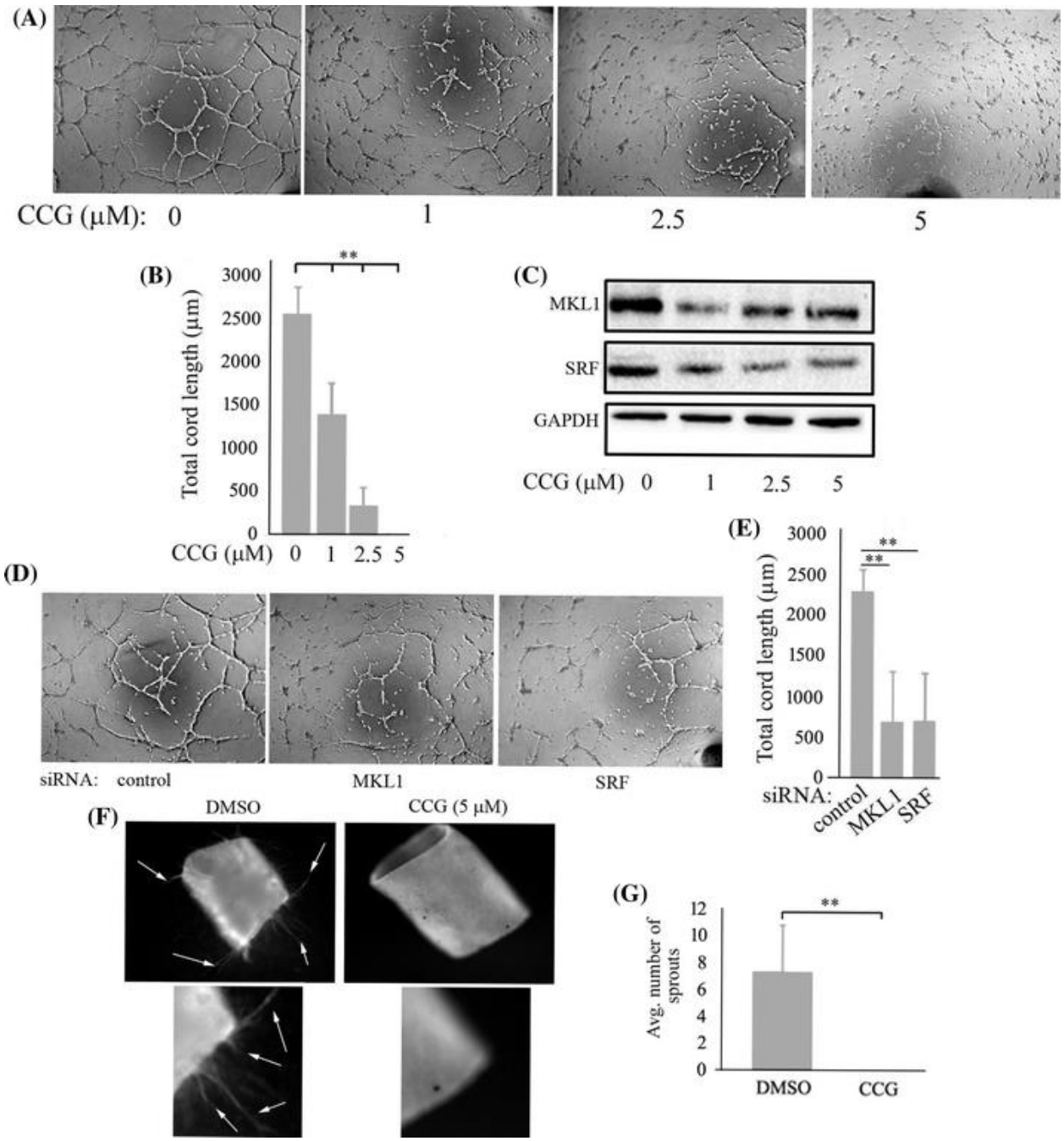

Figure 5. CCG-1423 inhibits angiogenesis both in vitro and ex vivo. a Representative images of HmVEC cord formation after treatment with either DMSO or CCG-1423 at increasing concentrations. b Quantification of angiogenesis readouts (measured by total cord length) of HmVEC in CCG-1423 versus DMSO treatment groups summarized from 3 independent experiments with 3 replicates/experiment (**$p < 0.01$). c Immunoblots of HmVEC extracts prepared at the same time-point as the end-point of cord formation assays showing the effect of increasing doses of CCG-1423 on the expression level of MKL1 and SRF (GAPDH—loading control). d–e Representative

images (panel D) and quantification (panel E) showing the effect of either MKL1 or SRF knockdown on the cord-forming ability of HmVEC (data summarized from 3 independent experiments with 3 replicates/experiment; $p < 0.01$). f–g Representative images [panel F; magnified regions of the lower right corner of the rings below show sprouts (arrows)] and quantification (panel G) of endothelial sprouts from aortic segments in collagen-I matrix under either DMSO or CCG-1423 treatment (sprouts were identified by FITC lectin staining; data summarized from aortic segments pooled from 4 mice; $^{**}p < 0.01$).

Although cord formation assay is widely used to study the morphogenetic ability (and angiogenic potential) of EC, it fails to recapitulate the sprouting behavior of EC from the preexisting blood vessels and represent the complexities of multicellular interactions that occur doing angiogenesis *in vivo*. Therefore, we next assessed EC sprouting from mouse aortic rings explanted in ECM in response to either 5 μM CCG-1423 or DMSO (vehicle control). Consistent with its effect on human EC line in vitro, CCG-1423 at 5 μM concentration nearly completely abrogated EC sprouting from the mouse aortic segments ex vivo (Figure 5f–g), further confirming the anti-angiogenic effect of CCG-1423 *ex vivo*.

We next examined the effect of CCG-1423 on sprouting angiogenesis in developing zebrafish Tg(kdrl:gfp)^{la116} embryos. These zebrafish express GFP driven by the EC-specific kdrl/flk1/vegfr2 promoter, enabling visualization of blood vessels by fluorescence microscopy (141). Embryos were exposed to CCG-1423 at 19 hpf (20 somites), just prior to the onset of intersegmental vessel (ISV) sprouting from the dorsal aorta, which initiates at 20 hpf (142). We initially performed a qualitative assessment of the effect of various doses of CCG-1423 ranging from 0.5 to 50 μM on overall development and vascular sprouting, the results of which are displayed in a tabular form in Figure 6a. At concentrations 10 μM and higher, the embryos exhibited a complete developmental arrest. Although vascular sprouting was dramatically

inhibited in the concentration range of 2.5–5 μM CCG-1423 (data not shown), there was also a prominent developmental delay of the embryos, and therefore we excluded these concentrations for the ISV analyses. Since no gross developmental anomaly was apparent within 0.5 to 1.0 μM CCG-1423 (Figure 6b), we evaluated ISV development specifically at these two doses of the compound. With DMSO treatment, ISVs sprouted normally from the dorsal aorta, and rostral and caudal branches from these primary ISVs interconnected to form the dorsal longitudinal anastomotic vessel (DLAV) (Figure 6c–e). These features were not adversely affected at 0.5 μM CCG-1423. However, at 1 μM CCG-1423, ~70% embryos exhibited defects in ISV sprouting which was marked by lower number of initiated sprouts and/or incomplete extension of ISVs. In many of those cases, DLAV formation was not apparent likely resulting from the initiation and/or extension defects. On average, there was a 25% reduction in the number of ISV and 41% decrease in the total length of ISV in response to 1.0 μM CCG-1423 relative to the vehicle control, and this difference was statistically significant ($p < 0.01$; Figure 6f–g). Taken together with foregoing *in vitro* and *ex vivo* angiogenesis data, these *in vivo* data demonstrate anti-angiogenic effect of CCG-1423.

A)

	Reagent	Replicates	N	Results at 41 hpf
	DMSO	3	60	Normal development, normal ISV sprouting
CCG-1423	0.5 µM	2	40	Normal development, normal ISV sprouting
	1 µM	2	40	normal development, ISV sprouting defect
	2.5 µM	1	20	Developmental delay; ISV sprouting defects
	5 µM	3	40	Developmental delay; ISV sprouting defect
	10 µM	1	20	Developmental arrest
	25 µM	1	20	Developmental arrest
	50 µM	1	20	Developmental arrest

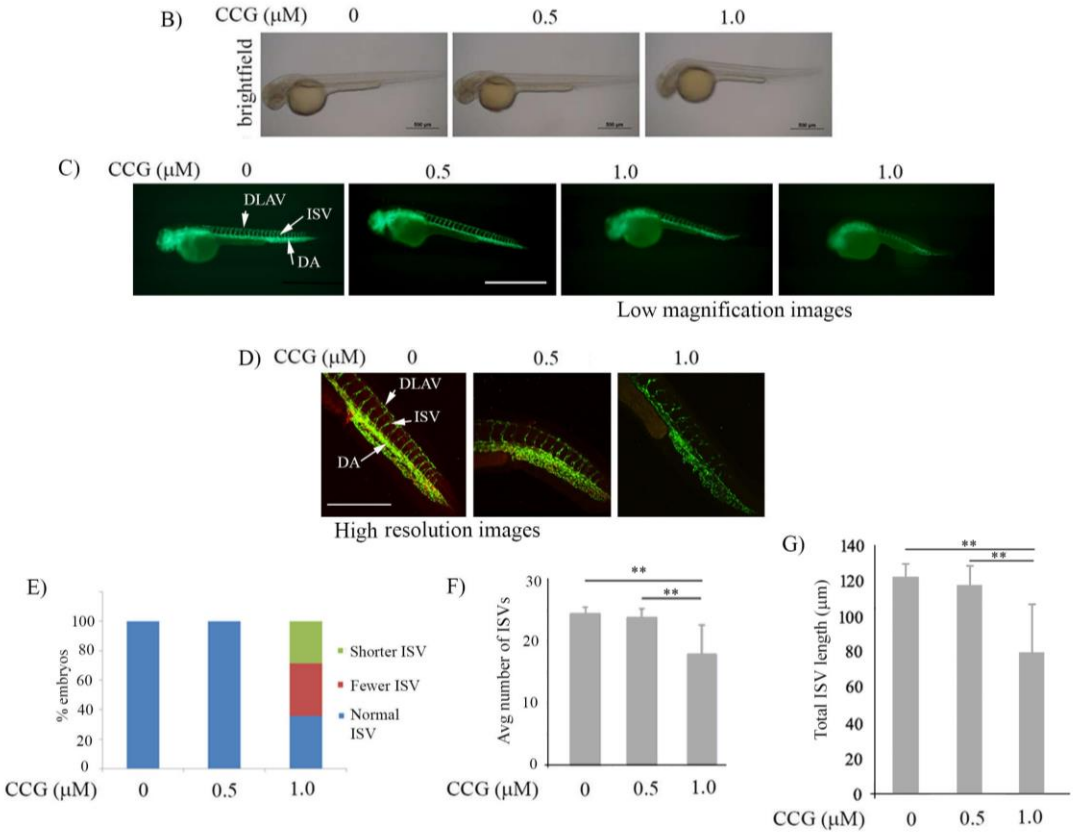

Figure 6. CCG-1423 inhibits developmental angiogenesis in zebrafish embryos. a Summary of phenotypes of Tg(flk1:gfp)lal16 zebrafish embryos at 22 h after treatment with the indicated doses of either CCG-1423 or DMSO (control); N indicates the number of embryos in each treatment group. b–d Brightfield (panel B; scale bar—500 µm) and fluorescence images [panels C (scale bar 500 µm) and D]; panel D shows multiphoton images (scale bar 50 µm) of zebrafish embryos at the indicated doses of CCG-1423 relative to DMSO (ISV: intersegmental vessel; DA dorsal

aorta, DLAV dorsal longitudinal anastomotic vessel). e–g Bar graph summarizing the ISV phenotypes (panel E), average number of ISV (panel F) and the total length of ISV (panel G) per embryo at 41 hpf under DMSO vs low concentration CCG-1423 treatment (**$p < 0.01$).

3.2.2 CCG-1423 inhibits membrane protrusion and impedes EC migration

Since cell migration is an important event in sprouting angiogenesis, we next assessed the effect of CCG-1423 on EC migration. Specifically, we analyzed random migration of HmVEC in serum-starved vs VEGF-stimulated conditions without or with 5 μM CCG-1423 treatment (Figure 7a). In the absence of CCG-1423, VEGF stimulation increased the average speed of migration of HmVEC by approximately twofold. CCG-1423 treatment not only reduced both basal (i.e., in serum-starved state) and VEGF-induced migration dramatically, but also abrogated VEGF-induced motility response, demonstrating that CCG-1423 has a prominent anti-migratory effect in EC.

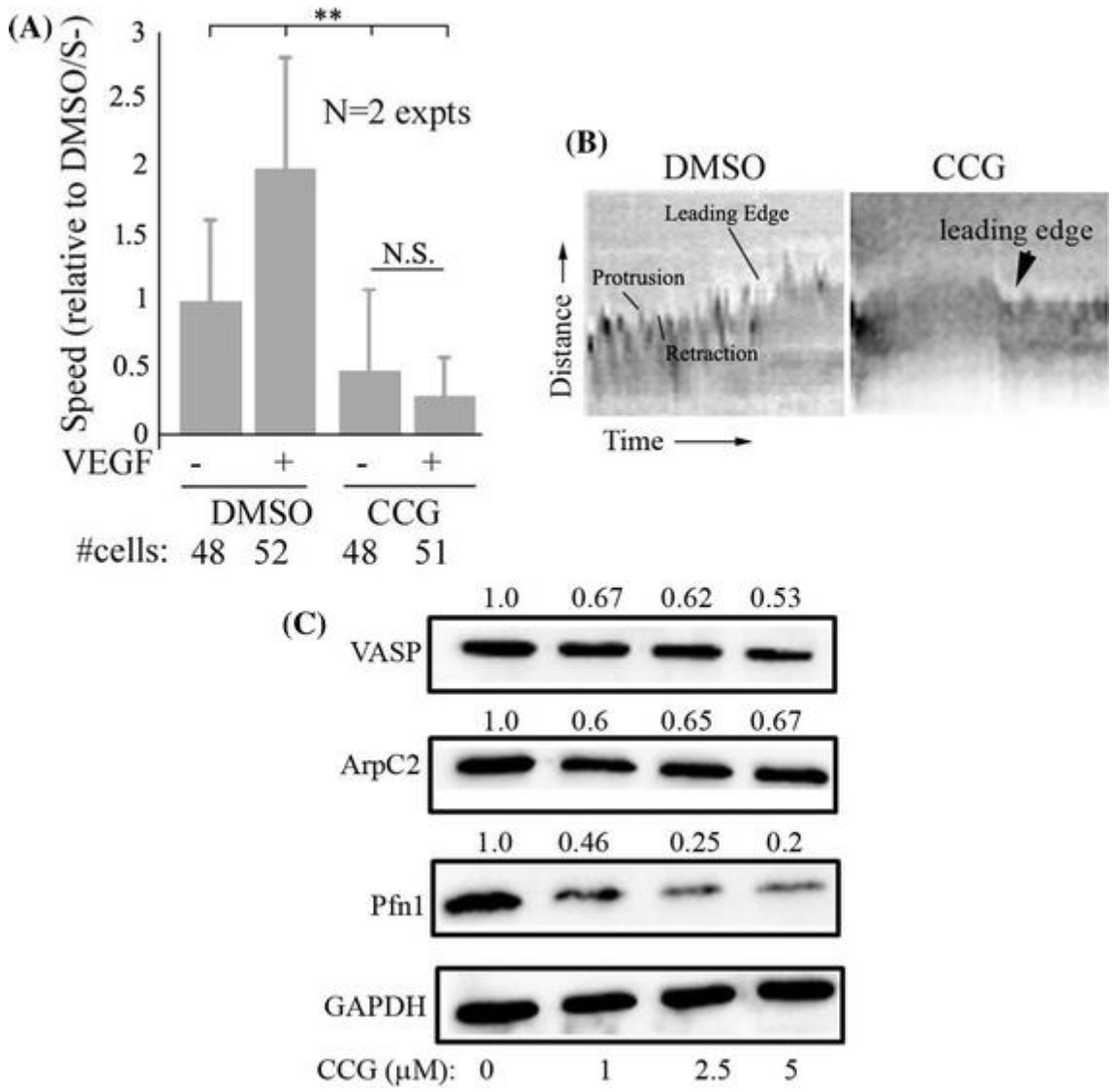

Figure 7. CCG-1423 attenuates expression of several actin-binding proteins and suppresses membrane protrusion and motility of HmVEC. a Quantitative analyses of the effect of 5 μM CCG-1423 treatment on VEGF-induced motility of HmVEC (these data are based on time-lapse analyses of randomly migrating HmVEC cells for 2 h) (**p < 0.01; data summarized from 2 independent experiments; N.S: not significant; S-: serum-starved state). b Representative images of kymograph traces of VEGF-stimulated cells under DMSO vs CCG-1423 (5 μM) treatment. c Representative immunoblots of HmVEC extracts for VASP, ArpC2, Pfn1, and GAPDH (loading control) at various concentrations of CCG-1423 treatment (the numbers indicate the expression level relative to DMSO control averaged from 2 independent experiments). HmVEC lysates were prepared at the same time-point as the end-point cord formation or cell motility assay.

Lamellipodial protrusion is the defining step of cell migration. To determine whether CCG-1423 has any effect on protrusion dynamics of EC, we performed kymography analyses of the dynamic behavior of the leading edge in migrating HmVEC. Representative kymography traces show that within the 20-min time frame, control cells (i.e., subjected to DMSO) exhibited many cycles of membrane protrusions and retractions (marked by the saw-tooth waveform—protrusions and retractions are denoted by the ascending and descending portions of saw-tooth waveform, respectively), with an overall positive slope indicating a net protrusive behavior (Figure 7b). By contrast, the generally flatter kymograph traces of CCG-1423-treated cells suggested that membrane protrusion is dramatically suppressed by the action of CCG-1423.

3.2.3 CCG-1423 reduces the expression of several key regulators of actin assembly with most dramatic effect on Pfn1

Actin polymerization at the leading edge drives membrane protrusion. The above results promoted us to probe for expression of a few key regulators of actin assembly the actions of which are critical for membrane protrusion including ArpC2 (a key component of the Arp 2/3 complex), VASP and Pfn1, in response to different doses (1–5 μM) of CCG-1423. This dose range was selected because of anti-angiogenic effect of CCG-1423 in this range of concentrations. We chose these three proteins because they belong to different classes of actin-binding proteins and stimulate actin polymerization through different mechanisms of action, albeit in a coordinated fashion (143). Specifically, the action of Arp 2/3 facilitates the nucleation step of actin assembly. VASP, a key member of the Ena/VASP family of actin-binding proteins, promotes the elongation of actin filaments. Finally, Pfn1 promotes actin assembly by (a) facilitating an ADP-to-ATP nucleotide exchange on actin and (b) delivering ATP-G-actin to

various F-actin elongating factors (including Ena/VASP proteins) through its direct interaction. We have also found that Pfn1 expression can be influenced post-transcriptionally by either perturbations (knockdown and overexpression) of MKL or high concentration of CCG-1423 (61). Whether CCG-1423 has any dose effect on Pfn1 expression in cells and is capable of affecting Pfn1 expression in a low concentration range is not known. Immunoblot analyses of HmVEC extracts showed attenuation in the expression of all three actin-binding proteins in response to CCG-1423 with the effect being most pronounced for Pfn1 (Figure 7c). The cellular level of Pfn1 was depleted by almost 80% at 5 μM concentration of CCG-1423; in comparison, VASP and ArpC2 levels were reduced by 30–40%. Even at 1 μM concentration of CCG-1423, reduction of Pfn1 expression was fairly dramatic (~54%). Among these three proteins, a dose-dependent trend of CCG-1423 was observed mainly for Pfn1. Attenuation of these actin assembly factors was clearly consistent with the defective protrusion phenotype of CCG-1423-treated cells. CCG-1423-induced downregulation of Pfn1 expression and concomitant defects in migration and cord morphogenesis of EC are consistent with our previously reported findings of similar phenotypes associated with loss of expression of Pfn1 in EC including HmVEC (121,122).

3.2.4 Pfn1 depletion causes defects in sprouting angiogenesis

All data from this section was performed by Dr. William Veon (thesis title: PKA-mediated regulation of Profilin-1 implication in sprouting angiogenesis). Given the drastic effect of CCG-1423 on the expression of Pfn1 and previous evidence of impaired cord morphogenesis of EC upon knockdown of Pfn1 expression, we further asked whether loss of function of Pfn1 alone is sufficient to impair sprouting angiogenesis, phenocopying the action of CCG-1423. To test this,

we first performed spheroid-based EC sprouting assay with HmVEC following treatment with either non-targeting control or Pfn1-specific siRNA. Our experiments revealed that knockdown of Pfn1 expression dramatically inhibited EC sprouting as judged by a 55% reduction in the average number of sprouts from the EC spheroids. To further extend the relevance of these findings *ex vivo*, we treated mouse aortic segments with either control or Pfn1 siRNA and performed aortic ring angiogenesis assay. These experiments also showed a significantly lower number of endothelial sprouts from the aortic segments in Pfn1 siRNA-treated culture compared to the control culture. Pfn1 immunostaining performed at the end of the experiment revealed a reduction but not complete loss of Pfn1 expression throughout the aortic ring and in sprouts. Note that the apparent large variation in aortic sprouting can be due to several biological and experimental factors including sensitivity of EC sprouting to the age of mice the aortic segments are prepared from, zonal variation in EC sprouting even within an aortic segment and possibly unequal exposure of EC in aortic ring to siRNA in an embedded condition. Since siRNA is not likely to be targeted selectively in EC in this experimental setup, we also examined the effects of EC-specific gene deletion of Pfn1 on vascular sprouting from mouse aortic segments ex vivo. Note that $Pfn1^{+/-[EC]}$ mice were born at the expected frequency (~50%); however, in three rounds of breeding yielding in a total of 21 pups, no $Pfn1^{-/-[EC]}$ mice were born (expected frequency: 25%) which may suggest that complete deficiency of Pfn1 in EC might be embryonically lethal. Therefore, we compared angiogenic sprouting between aortic segments derived from wild-type (WT) and $Pfn1^{+/-[EC]}$ mice. Although heterozygosity of Pfn1 did not result in any obvious defect in vascular sprouting in collagen-I matrix (data not shown), in matrigel $Pfn1^{+/-[EC]}$ aortic rings exhibited significantly lower number of sprouts than WT aortic rings at 72 hr. Overall, these *in vitro* and *ex vivo* studies demonstrate that Pfn1 is an important molecular player for sprouting

angiogenesis. Conditional knockout experiments further suggest that angiogenesis in certain ECM environment is sensitive to even a partial loss of Pfn1 in EC. Note that although $Pfn1^{+/-[EC]}$ mice do not exhibit any obvious phenotype, possibility of certain subtle vascularization-related developmental delay upon heterozygosity of Pfn1 cannot be absolutely ruled out which should be investigated in the future. Given that cellular depletion of Pfn1 alone is sufficient to cause a prominent defect in sprouting angiogenesis and at least qualitatively phenocopies the anti-angiogenic effect of CCG-1423, cellular attenuation of Pfn1 may be one the possible mechanisms of the anti-angiogenic action of CCG-1423. Note that the degree of inhibition of sprouting angiogenesis upon Pfn1 depletion is lower than that elicited by CCG-1423 (this is discussed later).

3.2.5 MKL regulates Pfn expression via increase of Pfn externalization

Some data from this section was performed by Dr. Marion Joy (thesis title: Molecular insights into profilin regulation and its role in breast cancer). To gain insight into the mode of regulation of Pfn by MKL, we analyzed the mRNA levels of Pfn in control versus MKL1 siRNA-transfected HEK-293 cells by quantitative RT-PCR. Although silencing of MKL1 elicited a 60% decrease in the expression of Pfn1 at the protein level, surprisingly, we found no significant difference in the mRNA level of Pfn1 between control and MKL1 knockdown HEK-293 cells. We detected a small ~20% difference in the average Pfn2 mRNA level between the control and MKL1 knockdown groups, which also clearly did not correlate with the robust 70% change in the corresponding protein expression. With knockdown using MKL1 siRNA#2, we did not detect any significant change in the mRNA level of either Pfn1 or Pfn2 in HEK-293 cells. Similarly, the mRNA levels of Pfn isoforms were also not significantly affected when STAT1 expression was

knocked down. These data suggest that Pfn expression is altered upon MKL1 knockdown in a post-transcriptional manner. We further asked whether altered protein stability might be responsible for MKL1-dependent changes in Pfn expression. However, blocking either the proteasomal (by MG-132 treatment)- or lysosomal (by ammonium chloride treatment)-mediated protein degradation pathway failed to reverse MKL1 knockdown-induced down-regulation of Pfn expression. These experimental observations tend to further rule out the possibility of accelerated protein degradation accounting for Pfn down-regulation upon loss of MKL1 function.

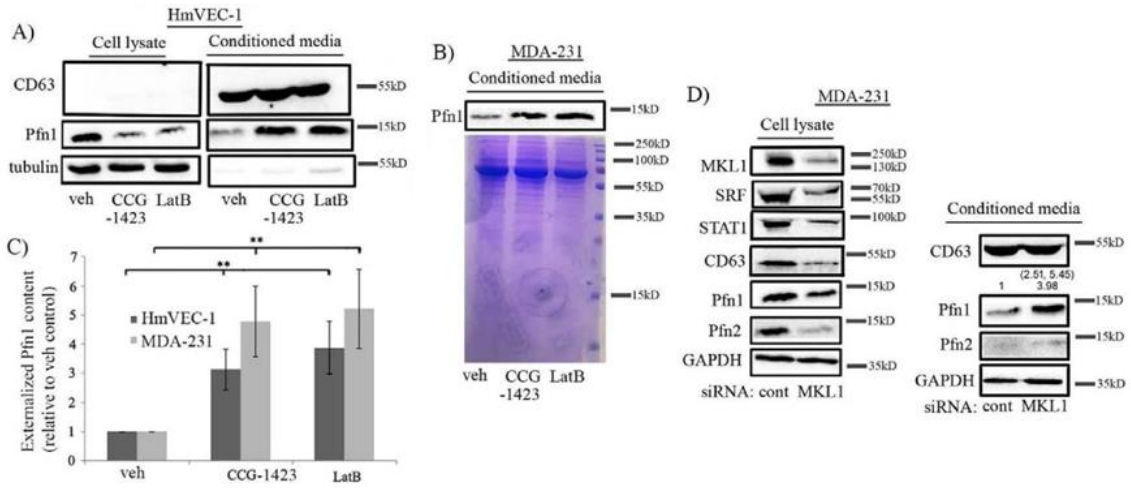

Figure 8. Loss-of-function of MKL1 down-regulates Pfn expression by promoting its extracellular release rather than its transcription. *A–C*, representative immunoblot analysis of Pfn1 level in the conditioned media prepared from HmVEC (*A*) and MDA-231 (*B*) cells following overnight treatment with either vehicle (*veh*) or LatB or CCG-1423. CD63, a well-known marker of extracellular vesicles, including exosomes, was used as a loading control for conditioned media samples in HmVEC-1 experiments. Coomassie staining of the SDS-PAGE of conditioned media derived from MDA-231 cells confirmed equal loading. *C* summarizes the quantification of fold-changes of Pfn1 (*n* = 3 experiments; **, $p < 0.01$). *D*, representative immunoblot analyses of Pfn1 along with the other indicated proteins in cellular extracts *versus* the conditioned media prepared from MDA-231 cells following transfection with either control or MKL1 siRNA (note that MKL1, STAT1, and SRF were not detected in the conditioned media). The

numbers in *parentheses* represent the individual fold-changes in the released Pfn1 content in each of the two experiments with the mean fold-change equaling ~4-fold.

Although Pfn is mainly an intracellular protein, a previous study reported the presence of Pfn1 along with several other cytoskeletal proteins in exosomes (144). Pfn1 has been also detected in the secretome of pancreatic cancer cells (145) and serum (146). These observations suggest that a certain fraction of cellular Pfn1 may be externalized into the extracellular milieu. Therefore, to explore whether loss-of-function of MKL could affect the intracellular level of Pfn by somehow impacting its externalization, we next analyzed the Pfn1 and Pfn2 levels in the conditioned media of HmVEC-1 and MDA-231 cells following overnight treatment of either LatB or CCG-1423. For both cell types, we observed a significantly elevated level (depending on the cell type and the treatment, the mean fold-increase ranged from 3- to ~5-fold) of Pfn1 in the conditioned media concomitant with the expected decrease in the corresponding cellular fractions in response to either LatB or CCG-1423 treatment (Figure 8A-C). In alignment with these results, knockdown of MKL1 expression also led to a prominent increase in the level of externalized Pfn1 in the conditioned media of MDA-231 cells (Figure 8D). Interestingly, we also detected GAPDH and tubulin in the conditioned media in our experiments; this is consistent with the previously reported findings of the presence of these two proteins in the exosomes (147,148). Unfortunately, because of general low abundance of Pfn2 in non-neuronal cells, we were not able to detect Pfn2 in the conditioned media by immunoblot analyses. We also performed live-dead staining of HmVEC-1 and MDA-231 cells for either CCG-1423 treatment or MKL knockdown settings, which showed 97–99% cell viability under these experimental conditions (data not shown). Note that CCG-1423 reduced cell proliferation (accounting for ~15–20% lower overall cell number compared with the DMSO-treated group) and spreading. A more

obvious phenotypic change elicited by CCG-1423 compared with MKL knockdown was not entirely surprising for at least two reasons. First, MKL knockdown was not complete by siRNA treatment. Second, there is evidence of at least one other cellular target (MICAL) of CCG-1423 besides MKL (58), and therefore the biological effect of CCG-1423 likely extends beyond its action on MKL. Nonetheless, no biologically significant difference in cell viability between the different experimental settings strongly suggests that our observation of a substantial increase in the released amount of Pfn1 upon loss-of-function of MKL is not a result of compromised cell viability.

3.2.6 MKL regulates cell migration in a SAP- and SRF-independent manner

Some data from this section was performed by Dr. Marion Joy (thesis title: Molecular insights into profilin regulation and its role in breast cancer). Given that we demonstrated that MKL can regulate the expression of Pfn1, we next asked which domain function on MKL was important for this regulation. We initially analyzed the effect of silencing of SRF on Pfn expression in various cell lines. Surprisingly, transient knockdown of SRF in HEK-293, MDA-231 and HmVEC-1 cells did not elicit any significant change in the basal level of expression Pfn1 isoforms (the average knockdown efficiencies of SRF in HEK-293, MDA-231 and HmVEC-1 cells were 70%, 70% and 90%, respectively). However, since SRF knockdown was not complete, we could not completely rule out a possibility that some low levels of residual SRF activity in SRF-silenced cells may be sufficient to maintain Pfn1 expression. We next investigated the effect of disrupting SRF-activating function on MKL's ability to stimulate Pfn1 level in HEK-293 cells. Mutagenesis studies revealed that K237, Y238, H239 and Y241 residues located in the B1 domain of MKL1 are critical for its SRF interaction, and that alanine

substitution on these residues abrogates MKL1:SRF interaction and MKL1-mediated SRF activation (40). Therefore, we overexpressed either WT MKL1 or a triple-point-mutant version of MKL1 (K237A/Y238A/H239A – denoted as $MKL1^{3p(mut\text{-}B1)}$) in HEK-293 cells, and analyzed the changes in Pfn expression. Overexpression of WT-MKL1 but not $MKL1^{3p(mut\text{-}B1)}$ led to increased SRF expression which confirmed the inability of this MKL1 mutant to activate SRF. However, $MKL1^{3p(mut\text{-}B1)}$ was able to elevate Pfn expression and to an extent comparable to that seen in WT-MKL1 overexpressers. These results argue against SRF being a direct downstream mediator of MKL1-dependent regulation of Pfn.

A previous study demonstrating differential gene expression and phenotypic distinctions between MKL- and SRF-knockout megakaryocytes suggested that MKL can have SRF-independent transcriptional activity in cells (110). It has been shown that MKL can transcriptionally regulate gene expression in breast cancer cells in an SRF-independent manner that is dependent on its SAP-domain (a homology domain that is found in SAF-A/B, Acinus and PIAS proteins, and thought to facilitate DNA-binding of MKL) function (note that some of the MKL-regulated genes require both SAP- and SRF-related function) (111). Since our findings suggested that MKL likely regulates Pfn expression without a direct involvement of SRF, we wondered whether SAP-domain-directed transcriptional function of MKL1 might be important in the context of Pfn regulation. To address this question, we next investigated the effect of deletion of either the SAP or the transcriptional activation (TA) domain on MKL1's ability to promote Pfn expression in HEK-293 cells. We found that upon deletion of either the SAP (ΔSAP-MKL1) or the transcriptional activation (ΔTA-MKL1 – this construct is completely impaired in transcriptional activity) domain, MKL1 was unable to induce Pfn1 elevation when overexpressed

in HEK-293 cells. These data are consistent with a scenario in which MKL regulates Pfn expression through its SAP-domain directed transcriptional activity.

Finally, to explore a possible functional connection between MKL1 and Pfn1, we next asked whether Pfn1 plays any role in MKL-mediated regulation of actin-dependent cellular events such as cell migration. Specifically, we investigated the effect of MKL1 knockdown on random motility of MDA-231 cells without or with transient overexpression of Pfn1. We found that knockdown of MKL1 reduced the basal level of Pfn1 as expected and increased the average speed of MDA-231 cells by ~1.9 fold (this result was further confirmed by the use of a second MKL1 siRNA [MKL siRNA #2]). This is consistent with our previously published finding of enhanced motility of MDA-231 cells upon Pfn1 knockdown, a phenotype that was related to altered phosphoinositide signaling (124). Hypermigratory phenotype of MDA-231 cells upon MKL1 depletion was completely reversed when Pfn1 expression was forcibly elevated thus suggesting that downregulation of Pfn1 expression contributed to enhanced motility of MKL1-silenced MDA-231 cells. In the absence of MKL1 knockdown, transient overexpression of Pfn1 also reduced the average speed of MDA-231 cells which is consistent with our previously published findings related to the effect of stable overexpression of Pfn1 on MDA-231 cell motility (149). Lastly, we performed rescue experiments to investigate the importance of the SAP-domain and SRF activation of MKL on cell motility. Our preliminary data (the following data has not been published yet) show that double knockdown of MKL1 and MKL2 increased the random speed of MDA-231. Not only that, upon rescue with wild-type MKL1, ΔSAP MKL1, or $MKL1^{3p(mut\text{-}B1)}$, motility returned to that of control siRNA group (Figure 9A-B). These data provided a proof-of-principle of MKL's ability to impact cellular phenotype through modulating Pfn expression although the importance of the various domains of MKL1 is still unclear.

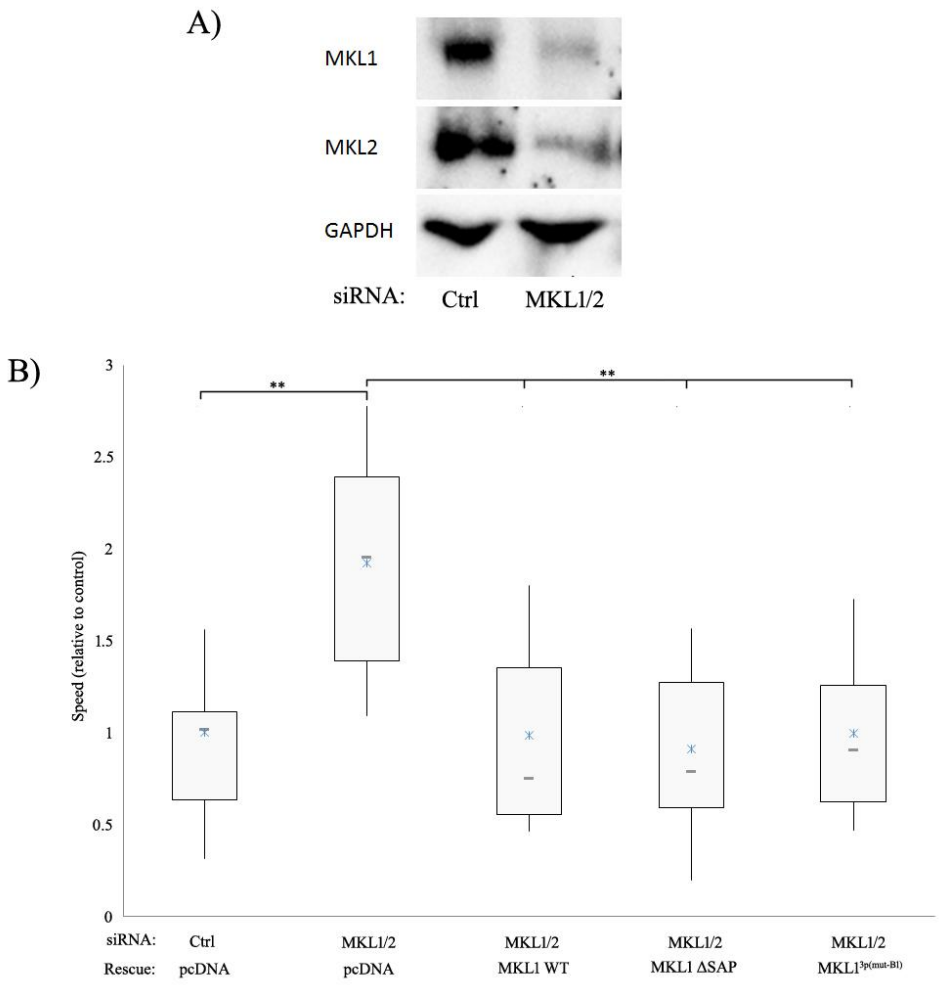

Figure 9. Loss-of-function of MKL1 and MKL2 promotes MDA-231 cell motility and can be reverted by rescue with MKL1 WT and/or various MKL1 mutants. A) Immunoblots depicting MKL1 and MKL2 knockdown upon MKL1/2 siRNA treatment. B) Box-whisker plot summarizing the average speed of migration of these five groups of cells (transfected cells were identified by FLAG immunostaining) in random motility assays. In the plot, the middle line, the upper and lower hinges of the box represent the median, 75th and 25th percentile of data, and the whiskers represent the maximum and minimum values (data summarized from two experiments with n = 60 cells per group pooled from all experiments; ** < 0.01).

3.3 DISCUSSION

Clinical efforts to develop anti-angiogenic therapies have largely focused on inhibiting the action of pro-angiogenic factor VEGF. While these therapies have shown promise in some clinical settings, in other cases therapeutic resistance (partly due to compensatory action of other pro-angiogenic factors) and/or toxicities have been encountered (150). Therefore, there is a need to discover new anti-angiogenesis targets and therapy. Since its initial discovery as an inhibitor of Rho-induced SRF-mediated transcription, CCG-1423 has demonstrated significant promise in various preclinical disease models to date, such as an anti-fibrotic agent (151) or a possible therapeutic agent in Type II diabetes (152). The findings from the present study further extend the utility of CCG-1423 as a novel anti-angiogenic agent.

Therefore, anti-angiogenic effect of CCG-1423 is consistent with the genetic proof-of-principle of importance of MKL and SRF in angiogenesis. The molecular links between MKL activity and EC migration/angiogenesis are still not completely understand. This insufficiency in the knowledge partly stems from the fact that MKL/SRF signaling controls the expression of a large number of genes. Several MKL/SRF-regulated genes that have been identified as pro-angiogenic (e.g. subunits of integrin, VE-cadherin and Myl9) are also required for homeostatic functions of EC and vascular integrity. Those studies either lacked detailed phenotypic comparisons between loss-of-function of MKL and the putative downstream genes, or in some cases, knockdown of those genes failed to recapitulate MKL-associated EC phenotypes, or the role of those genes as mediators of MKL-directed angiogenesis was not conclusively proven (18,82,89-91). A recent study has linked MKL1 and its transcriptional targets CCN1 and CCN2 to angiogenesis-promoting effect of actin-binding protein thymosin b4 (84); however, whether the defects in tip cell-driven angiogenesis caused by MKL deficiency is linked to alterations in

CCN isoforms is not known. The present study shows that CCG-1423 treatment leads to attenuation of several key promoters of actin assembly (such as ArpC2, VASP and Pfn1) and defect in protrusive activity and migration of EC, and Pfn1 depletion phenocopies the anti-angiogenic effect of CCG-1423, at least from qualitative standpoints. These data now open up additional avenues by which suppression of MKL/SRF signaling inhibits angiogenesis. Since the degree of inhibition of sprouting angiogenesis upon Pfn1 depletion is lower than that elicited by CCG-1423, we speculate that Pfn1 depletion is one of the several mechanisms underlying the anti-migratory and anti-angiogenic actions of CCG-1423. This is not surprising given the broad nature of gene expression program elicited by MKL/SRF pathway. Interestingly, a recent microarray study performed in PC3 prostate cancer cell line showed that CCG-1423 causes downregulation in transcription of VEGF-A gene (93). If this also occurs in EC, it can partly account for the anti-angiogenic action of CCG-1423, and furthermore, since VEGF signaling regulates VEGFR (VEGF receptor) expression, it may also partly explain why CCG-1423-treated EC fail to acquire motile phenotype in response to VEGF-stimulation. To what extent Pfn1 depletion contributes to the anti-migratory and anti-angiogenic action of CCG-1423 should be evaluated in the future by rescue experiments involving forced overexpression of Pfn1. Along this line, although we have only examined the effect of CCG-1423 on the protrusive activity of cells, it is possible that other aspects of cell migration such as adhesion and/or contractility are altered upon CCG-1423 treatment given that MKL/SRF signaling regulates transcription of genes (e.g. integrin, myosin) involved in these processes.

The mechanisms by which the various actin-binding proteins are coordinately downregulated by CCG-1423 are currently under investigation in our laboratory. Currently, we have found that MKL regulates Pfn1 expression via an externalization mechanism, but the exact

details have yet to be elucidated. Although CCG-1423 has been identified as an inhibitor of nuclear translocation of MKL, interestingly, we show that CCG-1423 can also substantially reduce the expression level of MKL1. Since MKL1 promoter has an SRF-binding site (153), it is possible that CCG-1423 transcriptionally downregulates MKL through suppressing SRF activation. Another possibility is that alterations in MKL's subcellular localization and/or interaction with other binding partners by CCG-1423 may somehow impact the protein stability of MKL. These questions need to be addressed in the future. Finally, a global assessment of transcriptomic and/or proteomic changes in EC will be valuable for a better understanding of pro- or anti-angiogenic pathways that are affected by CCG-1423 treatment.

Finally, it was previously shown that co-depletion of MKL isoforms (MKL1 and MKL2) leads to faster migration of strongly adherent cells (such fibroblasts) but has an opposite effect on the motility of weakly adherent transformed epithelial cells and breast cancer cells including MDA-231 cells (43). Inhibition of MDA-231 motility upon co-depletion of MKL1 and MKL2 was attributed to impairment in cell-substrate adhesion. Our studies demonstrate that MDA-231 cells actually become hypermotile if expression of only one of the isoforms of MKL (MKL1 in our case) is selectively suppressed or even both isoforms of MKL, a phenotype that is related to downregulation of Pfn1 expression. Although we do not have sufficient evidence yet to propose a generalizable hypothesis, it is possible that there may be an optimum range of MKL activity that is most productive for migration of certain types of cells (such as MDA-231 cells) which may be one reason for the discrepancy between our motility data with others showing invasive cell lines slowing down upon loss of MKL. In addition, our experiments examined random migration where previous studies investigated directed motility (i.e. by transwell assay or scratch

assay). Future structure-function studies dissecting the role of various functional domains of MKL on cell migration will likely yield mechanistic insights into this phenomenon.

4.0 STRUCTURE-BASED VIRTUAL SCREENING IDENTIFIES SMALL MOLECULE INHIBITOR OF THE PROFILIN1-ACTIN INTERACTION

4.1 INTRODUCTION

The contents of this section are published (section unpublished will be noted in text).
Reference: **Gau D**, Lewis T, McDermott L, Wipf P, Koes D, Roy P. Sturcture-based virtual screening identifies small molecule inhibitor of profilin1-actin interaction. Journal of Biological Chemistry. 2017; doi: 10.1074/jbc.M117.809137.

Specific Aim 2: Identify novel small molecule inhibitors targeting Profilin-1 (a downstream target of MKL) and further assess the potential inhibitors in modulating EC migration and angiogenesis.

Dynamic remodeling of the actin cytoskeleton is an integral aspect of many fundamental cellular activities (example: cell migration and cell proliferation) and therefore crucial to regulation of biological processes that rely on actin-based events, whether physiological or pathological. Actin cytoskeletal remodeling is regulated by orchestrated actions of a wide range of actin-binding proteins. One of the key players in the regulation of actin polymerization is profilin-1 (Pfn1), a ubiquitously expressed member of the Pfn family of actin-monomer-binding proteins. Pfn1 inhibits nucleation and elongation of actin filaments at the pointed end, but promotes barbed-end elongation of filamentous actin through collaboration with various polyproline-domain containing promoters of actin nucleation and elongating factors. Pfn1 also stimulates actin polymerization through its ability to promote ADP-to-ATP exchange on monomeric actin (reviewed in (154)). There is compelling evidence in the literature that Pfn1 plays an important

role in cell migration. With the exception of certain cancer cells, in most physiological contexts, either loss of Pfn1 expression or disruption of actin-binding ability of Pfn1 is generally associated with defects in membrane protrusion (the initiating event of cell migration that is primarily driven by actin polymerization) and slower cell migration (121,122,139,155-157). Similarly, gene silencing and knockout studies demonstrated defects in cytokinesis (an aspect of cell division that is dependent on the action of actin cytoskeleton) and reduced cell proliferation upon Pfn1 depletion (121,130). Collectively, these findings demonstrate Pfn1's important role in various actin-dependent cellular functions, further begging the question whether some of these cellular functions are susceptible to chemical inhibition of Pfn1 function. However, currently no inhibitor of Pfn1 function exists. In this study, we demonstrate for the first time that the Pfn1:actin interaction is susceptible to small-molecule inhibition. Guided by structure-based virtual screening of small molecule libraries, we identified two compounds with similar chemical structures that are capable of reversing Pfn1's effect on actin polymerization *in vitro*. As a further proof-of-concept test for cellular effects of these compounds, our experiments in endothelial cells (EC) demonstrated that treatment of these compounds led to attenuation of cellular Pfn1:actin interaction, slower migration and proliferation, and prominent suppression of angiogenic activity of EC.

4.2 RESULTS

4.2.1 Pharmacore-based virtual screening of small molecules that can mimic and competitively inhibit Pfn1:actin interaction *in vitro*

Since the Pfn1:actin complex structure has been resolved (158) (Figure 10A), we used structure-based virtual screening of small molecule libraries to identify compounds that can mimic the Pfn1:actin interaction, and therefore have the potential to act as competitive inhibitors of this interaction. Structure-based virtual screening has been successfully applied to protein-protein interactions (e.g. p53/MDM2 (159), BH3/Bcl-xL (160), TNF-alpha (161)). Pfn1:actin has a classical "large and flat" interface, but a few residues are identified as potential hot spots by PocketQuery (162) and their interactions can potentially be exploited for molecular design. The most critical actin residue of the Pfn1:actin structure, as determined by an analysis of PDB 2BTF, is Y169 of actin, which forms a hydrogen bond with the H119 residue of Pfn1. Consistent with the computational analysis, the H119E mutant of Pfn1, which eliminates this bond, loses affinity to actin (149,163) . In order to expand beyond the limited interactions of Y169, we considered the small pocket on Pfn1 adjacent to Y169 that the C-terminus of actin (F375) buries in (Figure 10B-i). As the F375 pocket in the crystal structure was too small to accommodate a ligand, we simulated the Pfn1 monomer with molecular dynamics and identified structures where the pocket was enlarged (Figure 10B-ii). Potential interactions with residues in this pocket were identified by docking small fragments (benzene and water) to structures extracted from the simulation (Figure 10B-iii).

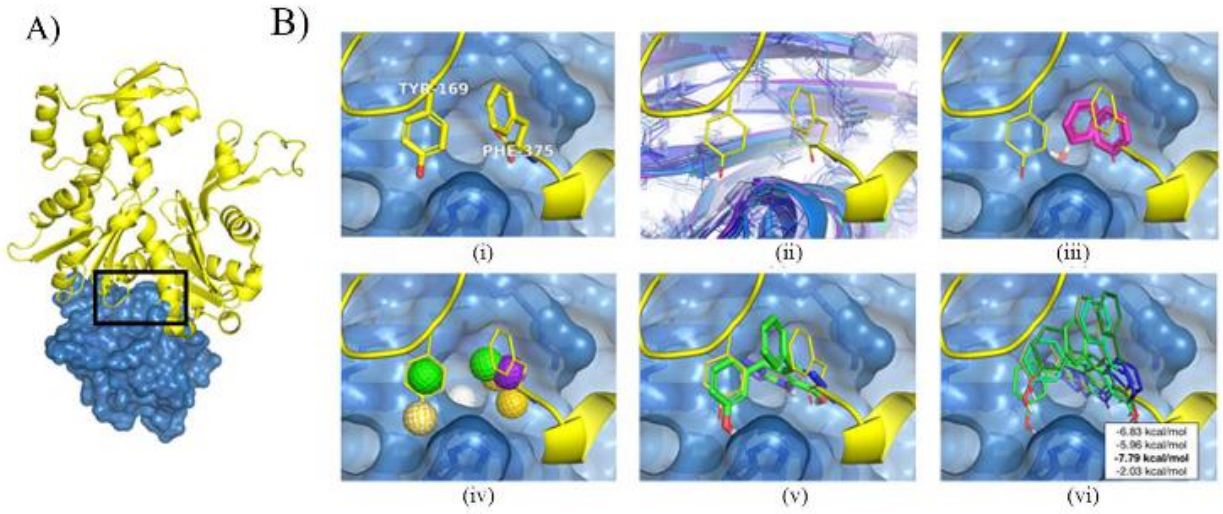

Figure 10. Structure-based workflow for identifying inhibitors of Pfn1:actin interaction. A) The Pfn1-actin interface (PDB 2BTF) with the targeted interface region highlighted. B(i-vi)): (i) Interface residues critical to binding were computationally identified. (ii) The flexibility of the Pfn1 interface was explored with molecular dynamics. (iii) Fragments were docked to molecular dynamics snapshots. (iv) Pharmacophore features were identified from interface residues and docked fragments. (v) Pharmacophore search identified compounds matching subsets of these features. (vi) Energy minimization refined and scored the ligand structures with respect to molecular dynamics snapshots. A consensus score across the receptor and ligand structures was used to select compounds for testing. This figure is courtesy by Dr. David Koes.

The native interactions of actin and the putative interactions identified through fragment docking were combined to construct pharmacophore queries. A pharmacophore represents the spatial arrangement of the essential features of an intermolecular interaction, such as hydrophobic groups and hydrogen bond donors. We generated ten pharmacophore queries, where every query contained a hydrophobic core targeting the F375 pocket and three additional hydrogen bond features selected from five possible interactions. The pharmacophore features used are shown in Figure 10B-iv and primarily target the H119, R74, D86, L87, and R88 residues of Pfn1. Pharmer (164) was used to search the ZINC database (165) for compounds that

matched each of the queries. Matching compounds are aligned to the query pharmacophore, as shown in Figure 10B-v, and need to be optimized with respect to atomistic interactions with the Pfn1 receptor in order to be effectively ranked. The steric energy of hit compounds was minimized to identify a locally optimal conformation of the ligand and a predicted binding affinity (Figure 10B-vi). Ligands were minimized and consensus scored against an ensemble of Pfn1 structures generated using molecular dynamics in order to account for receptor flexibility. The top 20 scoring hits after filtering for structural diversity were initially acquired for screening (see supplementary Table 1 for a complete list and structures of the initial batch of 20 compounds [annotated as C1 through C20]).

For biochemical screening of the compounds, we performed a pyrene-based actin polymerization assay. This type of assay was previously used to screen a library of chemical compounds to identify inhibitors against the formin family of actin-binding proteins (166). In this assay, Pfn1 reduces actin polymerization by its monomer-sequestering action. Essentially, we searched for compounds that can reverse Pfn1's inhibitory effect on actin polymerization but are unable to impact actin polymerization in the absence of Pfn1 (we bacterially expressed and purified GST-tagged Pfn1 as our source of Pfn1 [Figure 11A]). After screening the compounds, we ascertained that the two highest scoring small molecules from our virtual screen (identified as compound 1 [C1: 8-(3-hydroxyphenyl)-10-(4-methylphenyl)-2,4,5,6,7,11,12-heptaazatricyclo[7.4.0.0^{3,7}]trideca-1(13),3,5,9,11-pentaen-13-ol] and compound 2 [C2: 8-(3-hydroxyphenyl)-10-phenyl-2,4,5,6,7,11,12-heptaazatricyclo[7.4.0.0^{3,7}]trideca-1(13),3,5,9,11-pentaen-13-ol]) showed promise as demonstrated by a recovery of actin polymerization after addition of the compound in a dose-dependent and Pfn1-dependent manner (Figure 11B-C). These two compounds, used as racemic mixtures, completely abrogated Pfn1's inhibitory effect

on actin polymerization at 2.5-fold molar excess compared to Pfn1. In the absence of Pfn1, neither of these two compounds had any significant effect on actin polymerization on their own, further implying that their action on actin polymerization in Pfn1:actin setting was through inhibition of Pfn1. Mass-spectrometry and NMR analyses confirmed the purity and structure of these compounds, respectively (Figure S 3, Figure S 4). Note that compounds C1 and C2 are nearly identical, differing by a single methyl group.

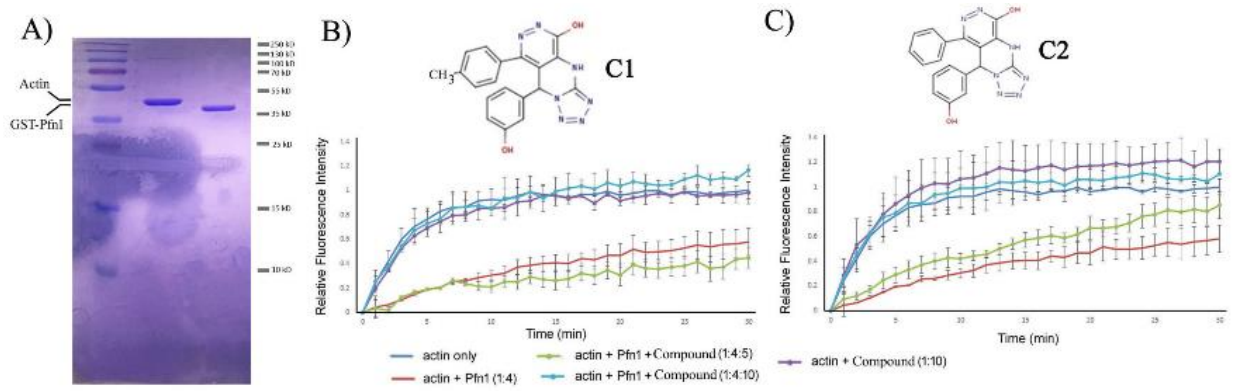

Figure 11. Effects of compounds C1 and C2 on actin polymerization with or without Pfn1 in vitro. A) Coomassie staining of an SDS-PAGE showing the purity of actin and GST-Pfn1 used in the pyrene-actin assay. B-C) Pyrene-actin polymerization assay curves for the indicated experimental conditions (panel B: compound C1; panel C: compound C2) recorded for 30 minutes after the addition of the polymerization buffer. Each time-point represents the mean±stdev values of fluorescence intensity of polymerized pyrene actin relative to the maximum fluorescence intensity for actin alone condition (data summarized from N = 3 experiments). The insets show the chemical structure of the two compounds. The numbers in the parentheses indicate relative concentrations of actin, GST-Pfn1 and the compounds. The actual concentrations of actin and Pfn1 were 10 µM and 40 µM, respectively. Compounds C1 or C2 were added either at a 50 µM (Pfn1:compound=1:1.25) or 100 µM (Pfn1:compound=1:2.5) concentration.

For a limited structure-activity relationship (SAR) analysis, we performed the pyrene-actin assay with 22 additional compounds (annotated as C21 through C42 - see Supplementary Table 2) that had an identical scaffold to C1 and C2. None of these analogous compounds exhibited comparable activity. The SAR suggests that the hydroxyl of the phenol group that mimics the Y169 of actin (Figure 10B-v) is essential: moving it to the para-position (C32) or replacing it with an ether (C24) abrogated activity as did other transformations of this phenol (C23-C42). Unfortunately, the commercially available compounds with this scaffold did not support the development of an SAR of other aspects of C1 and C2, other than revealing that the addition of a charged nitro group to the phenyl ring removes activity (C22). Considering the positional importance of the hydroxyl of the phenol group that mimics the Y169 residue of actin, it is also not clear why compounds C7 and C8 (which also contained that feature) failed to show any activity. These compounds differ from C1 and C2 through decorations of the solvent-exposed phenyl group (Figure 10B-v). This suggests there may be intra- or inter-molecular interactions missing from our model, and further refinement of the model remains an avenue of future research.

4.2.2 Compounds C1 and C2 inhibits angiogenic ability of vascular EC

We previously showed that loss-of-function of Pfn1 (either by depletion or disruption of actin-binding function by point mutation) can lead to actin cytoskeletal changes (marked by prominent reduction of actin stress-fibers and overall cellular F-actin content), slower migration and proliferation, and prominent reduction in angiogenic ability of vascular EC (121,122). Along this line, another study showed that Pfn1:actin interaction in EC is stimulated in response to pro-angiogenic growth factor signaling through a specific tyrosine (Y129) phosphorylation-

dependent mechanism *in vitro* and *in vivo*. Blockade of Y129 phosphorylation (which reduces Pfn1:actin interaction to its basal level) reduces VEGF-induced motility and angiogenesis of EC *in vitro* and angiogenesis associated with tissue repair and tumors *in vivo* (123). Pfn1 phosphorylation also promotes angiogenic growth factor secretion in the tumor microenvironment through HIF1 (hypoxia-inducible factor-1) stabilization in a VHL (von Hippel Lindau)-dependent mechanism, contributing to tumor progression (167). Therefore, as a proof-of-concept test for the cellular effects of these compounds, we performed a series of experiments in EC to determine whether some of the above phenotypes can be recapitulated in the settings of chemical inhibition of Pfn1:actin interaction by compound treatment as described in the following sections.

First, to determine the effects of compounds C1 and C2 on angiogenesis, we performed matrigel cord-formation assays (a commonly used in vitro morphogenetic assay to assess the angiogenic potential of ECs) with HmVEC-1 (a widely used immortalized human dermal microvascular cell line – referred to as HmVEC hereafter) at different concentrations (25, 50 and 100 μM) of each of the two compounds. As control, cells were treated with vehicle control DMSO. Although there was a general trend of dose-dependent decrease in the cord-forming ability of HmVEC (as measured by the total cord length) in response to either of the compounds, the difference in the cord-formation readout between the control and the compound-treated groups was statistically significant only in the 50-100 μM dose range with the most dramatic reduction (by ~90%) in angiogenesis seen in response to 100 μM compound treatment (Figure 12A-B). Depending on the compound, the average reduction in the cord formation ranged from 50-80% for 50 μM compound treatment. To ensure that compounds C1 and C2 were not cytotoxic at this high dose, we performed live-dead staining of HmVEC which showed near

100% cell viability even after overnight treatment of the compounds at a 100 μM concentration (Figure 12C), thus suggesting lack of any obvious cytotoxic effects of these compounds in ECs. Note that we also performed cord-formation assays with four additional compounds (C7, C8, C24 and C29) given that these compounds had the same general structural scaffold as C1 and C2 but did not show any activity in the actin polymerization assay. Correlated with their lack of biochemical activity in the actin polymerization assay, these compounds also did not have any anti-angiogenic effect in EC even when added to the culture at a 100 μM concentration (Figure 12D). The general correlation between biochemical and biological activities (or lack of activities) of the compounds suggest that the core structural scaffold of compounds C1 and C2 alone per se does not confer the anti-angiogenic action, further underscoring the importance of specific functional groups attached to this scaffold for the biological action of the two compounds. Although widely used, the cord formation assay fails to recapitulate the sprouting behavior of EC from preexisting blood vessels and therefore does not represent the complexities of multicellular interactions that occur doing angiogenesis *in vivo*. Therefore, we also assessed EC sprouting from mouse aortic rings explanted in ECM in response to compounds C1 and C2. Consistent with our cord morphogenesis assay results, *ex vivo* endothelial sprouting (identified by lectin-staining) of aortic rings was almost completely impaired upon treatment with either compound C1 or C2 (Figure 12E-F; representative phase-contrast images of the sprouts in control vs compound C2-treated groups are shown in supplementary Figure S 5). Collectively, these data demonstrated anti-angiogenic effects of these compounds.

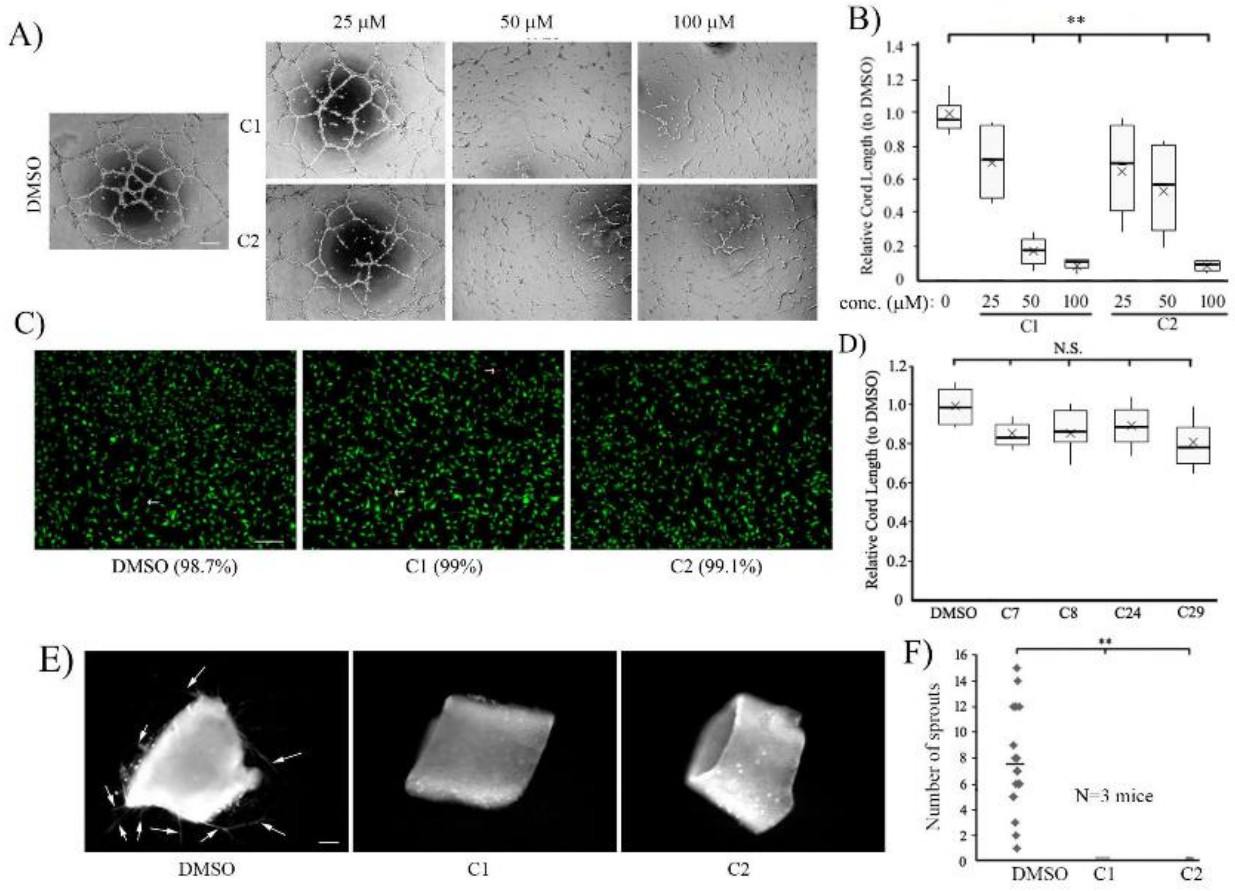

Figure 12. Effects of small molecule inhibitor of Pfn1:actin interaction on angiogenesis *in vitro* and *ex vivo*: A-B) Representative phase-contrast images of cord formation by HmVEC on matrigel after treatment with either DMSO or the indicated concentrations of C1 and C2 (images were acquired with a 4x objective; scale bar - 200 µm). The associated box and whisker plot in panel B summarizes the mean values of the cord length for the different experimental conditions relative to the mean value scored for DMSO control (N = 3 experiments with 2 technical replicates/condition in each experiment; ** $P < 0.01$). In box and whisker plots, the x's represent the mean, middle lines of box indicate median, top of the box indicates 75th percentile, bottom of the box measures 25th percentile and the two whiskers indicate the 10th and 90th percentiles, respectively. C) Live/dead staining of HmVEC following overnight treatment with either DMSO or compounds C1 or C2 at 100 µM concentration (live and dead [arrow] cells are labeled green and red, respectively; scale bar - 200 µm). The numbers in the parentheses indicate the percentage of live cells for different experimental conditions summarized from 2 experiments. D) A box and whisker plot summarizing the mean values of the cord length for the indicated compounds with similar structural scaffold as C1 and C2 (as designated in Supplementary Table S2) relative to the mean value scored for DMSO

control (N = 3 experiments. NS – not significant). E-F) Representative fluorescence images (panel E) of mouse aortic segments embedded in matrigel and stained with rhodamine-conjugated lectin for the indicated experimental conditions (arrows show the lectin-positive endothelial sprouts; scale bar - 200 μm). Panel F shows the quantification of sprouts pooled from 20 rings/condition isolated from a total of 3 mice from 3 independent experiments (the dashed line shows the mean; **: $P<0.01$).

4.2.3 Evidence of inhibition of cellular Pfn1:actin interaction by compound C2

As a proof-of-principle test to verify that our compounds can actually inhibit the Pfn1:actin interaction in EC, we performed proximity-ligation assay (PLA) to detect endogenous Pfn1:actin interaction with or without overnight treatment of ECs with compound C2. We found a dramatic 70% reduction in the average number of PLA spots (denotes Pfn1:actin interaction) per cell after treatment with compound C2 (Figure 13). These data indicate decreased proximity of Pfn1 and actin, thus suggestive of reduced interaction of these proteins in ECs resulting from compound C2 treatment. Note that we also attempted to biochemically verify these compounds' ability to inhibit actin's interaction with Pfn1 by either co-immunoprecipitation (co-IP) method in both HmVEC and HEK-293 cells or polyproline (PLP) pull-down assay (a method commonly adopted for Pfn1 purification because of Pfn1's affinity for PLP sequences) with HEK-293 cell lysate. Unfortunately, these biochemical assays did not reveal any discernible effect of the compounds on Pfn1:actin interaction (data not shown). Possible reasons for the apparent discrepancy in the results between the PLA and biochemical experiments have been elaborated later in the "Discussion" section.

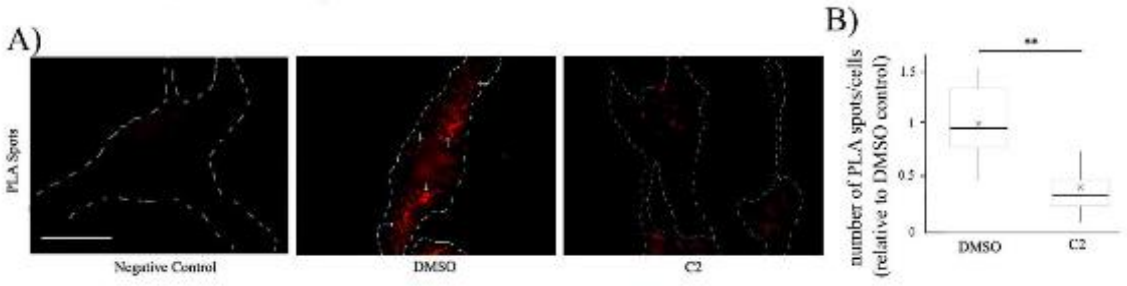

Figure 13. Effect of compound C2 on endogenous Pfn1:actin interaction in EC. A) Representative fluorescence images of Pfn1:actin PLA spots (arrows) in HmVEC following overnight treatment of either DMSO (control) and compound C2. An image of the negative control PLA stain (i.e. involving one antibody) only is shown alongside for comparison. Dashed lines indicate the boundary of the cells (scale bar - 20 µm). B) A dot plot displays the number of PLA spots in C2-treated cells relative to the mean value scored for DMSO control (the dashed lines represent the mean values (n=40 cells/group pooled from 2 independent experiments; ** $P < 0.01$).

4.2.4 Compounds C1 and C2 affect actin cytoskeleton, migration and proliferation of EC

To further test the effect of these compounds on the actin cytoskeleton of EC, we performed rhodamine-phalloidin staining of HmVEC following overnight treatment with either of the two compounds (at 50 µM concentration) or DMSO (vehicle control). We observed a noticeable decrease in the actin stress-fibers and the overall F-actin content (as measured by the average intensity of rhodamine fluorescence per cell) in HmVEC in response to the treatment with either compound C1 or C2 (Figure 14A-B), suggesting an inhibitory effect of these two compounds on actin polymerization in cells. Morphometric analyses revealed that the average spread area of EC was significantly lower in compound-treated groups than the control group (Figure 14C), an observation that is consistent with the inhibitory effect of the compounds on actin polymerization (expected to reduce the efficacy of membrane protrusion and therefore cell spreading).

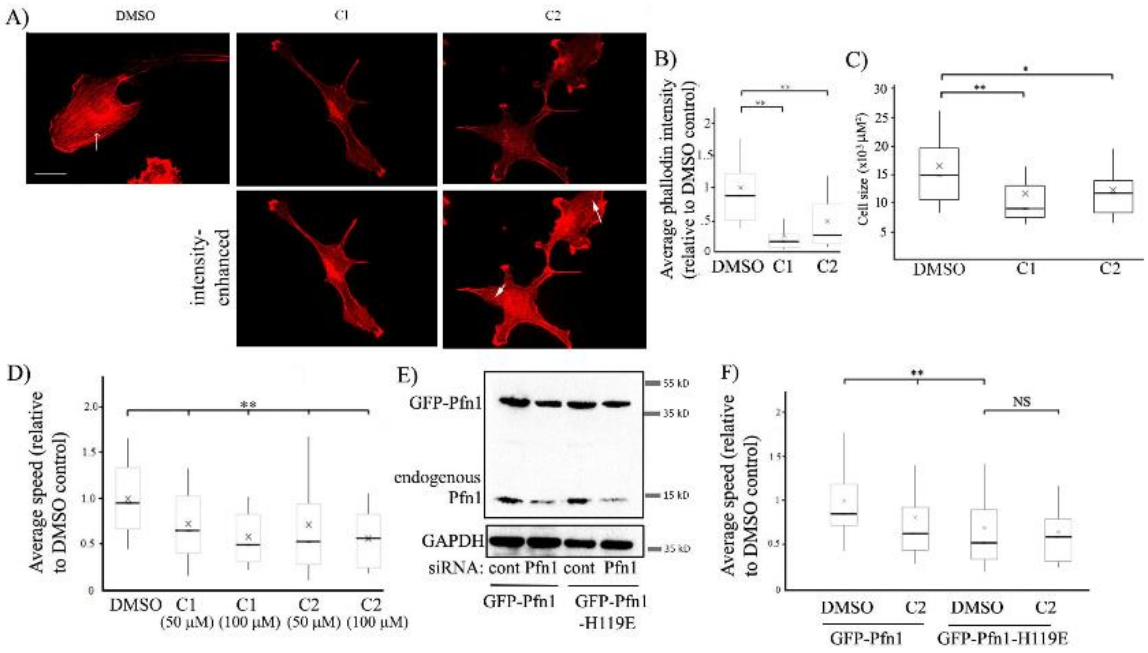

Figure 14. Effects of small molecule inhibitor of Pfn1:actin interaction on actin cytoskeleton and random 2D motility of EC. A-C) Representative fluorescence images (panel A) of rhodamine-phalloidin stained HmVEC (acquired with a 60X objective) following overnight treatment of either DMSO or C1 or C2 at 50 μM concentration (the arrow shows actin stress-fibers; scale bar – 20 μm). The upper panel shows images at identical brightness/contrast setting. Images in the bottom panel were brightness enhanced to reveal stress fibers (arrows) in compound-treated cells, albeit in much lower abundance than control cells. The box and whisker plots in panel B summarizes the mean values of the integrated fluorescence intensity of rhodamine-phalloidin relative to the average value of DMSO control group. The mean values of the cell area for the indicated treatments are summarized in a box and whisker plot in panel C (N = 50-60 cells/group pooled from 3 experiments; ** $P < 0.01$; * $P < 0.05$). In box and whisker plots, the x's represent the mean, middle lines of box indicate median, top of the box indicates 75th percentile, bottom of the box measures 25th percentile and the two whiskers indicate the 10th and 90th percentiles, respectively. D) A box and whisker plot depicting the relative speed of randomly migrating HmVEC after treatment with DMSO or the indicated concentrations of compounds C1 or C2 (N = 100-120 cells/group pooled from 3 independent experiments; ** $P < 0.01$). E) Pfn1 and GAPDH (loading control) immunoblots of total extracts of HmVEC stably expressing either GFP-Pfn1 or GFP-Pfn1-H119E and following transfection with the indicated siRNAs. F) A box and whisker plot summarizing the effect of compound C2 on the relative speed of WT-Pfn1 vs

H119E-Pfn1 expressers of HmVEC treated with control or Pfn1 siRNA (N = 60-70 cells/group pooled from 3 independent experiments; ** $P < 0.01$; NS = not significant).

Pfn1's interaction with actin is an important requirement for efficient cell migration (a crucial aspect of angiogenesis). We previously showed that interfering with the actin interaction of Pfn1 by H119E mutation, which reduces Pfn1's affinity for actin by ~25 fold (163), reduces the speed of randomly migrating HmVEC by approximately 40% (122). To determine whether the small molecule inhibitors of the Pfn1:actin interaction have a similar effect on EC migration, we analyzed 2D random migration of HmVEC without or with the compounds at two different concentrations (50 and 100 μM). At both concentrations, compounds C1 and C2 reduced the average speed of HmVEC by ~30% (Figure 14D). Next, we analyzed the effect of compound C2 on random motility of HmVEC sublines engineered to stably express either wild-type (WT) form or actin-binding deficient H119E mutant of Pfn1 as GFP-fusion proteins (the expression of endogenous Pfn1 was suppressed by siRNA treatment – see Figure 14E). The knockdown efficiency of endogenous Pfn1 in WT and H119E-Pfn1 expressers were roughly equal to 80 ± 10% (summarized from 3 experiments). The expression levels of WT-Pfn1 and H119E-Pfn1 relative to endogenous Pfn1 (based on the level in control-siRNA transfected cells) were equal to1.05±0.12 and 0.9±0.16, respectively (summarized from 3 experiments). As expected, the basal speed (in the absence of the compound) of H119E-Pfn1 expressers was ~30% lower than that of the WT-Pfn1 expressers. Compound C2 reduced the speed of WT-Pfn1 by 20% (at a slightly lower efficiency than the parental cell line which may be due to different affinities of C2 for endogenous vs GFP-tagged Pfn1) but did not reduce the average speed of H119E-Pfn1-expressers any further (Figure 14F). Although these data do not necessarily rule out the possibility of off-target effects of the compound, dependency of a functional actin-binding

capability of Pfn1 for the anti-migratory effect of the compound is consistent with a scenario in which the anti-migratory effect of any of the compounds is at least partly mediated through inhibition of the Pfn1:actin interaction.

Given that EC proliferation is also an important aspect of angiogenesis and Pfn1 plays an important role cell proliferation (121,130), we next examined the effect of compound C2 on HmVEC proliferation in a 2D culture setting. Our experiments revealed that the average cell counts in response to 3 days of incubation with the two test doses (50 and 100 μM) of the compound C2 were approximately 2- and 2.5-fold lower, respectively, than the same in the control group setting (Figure 15A-B), thus indicating an anti-proliferative effect of compound C2 on EC.

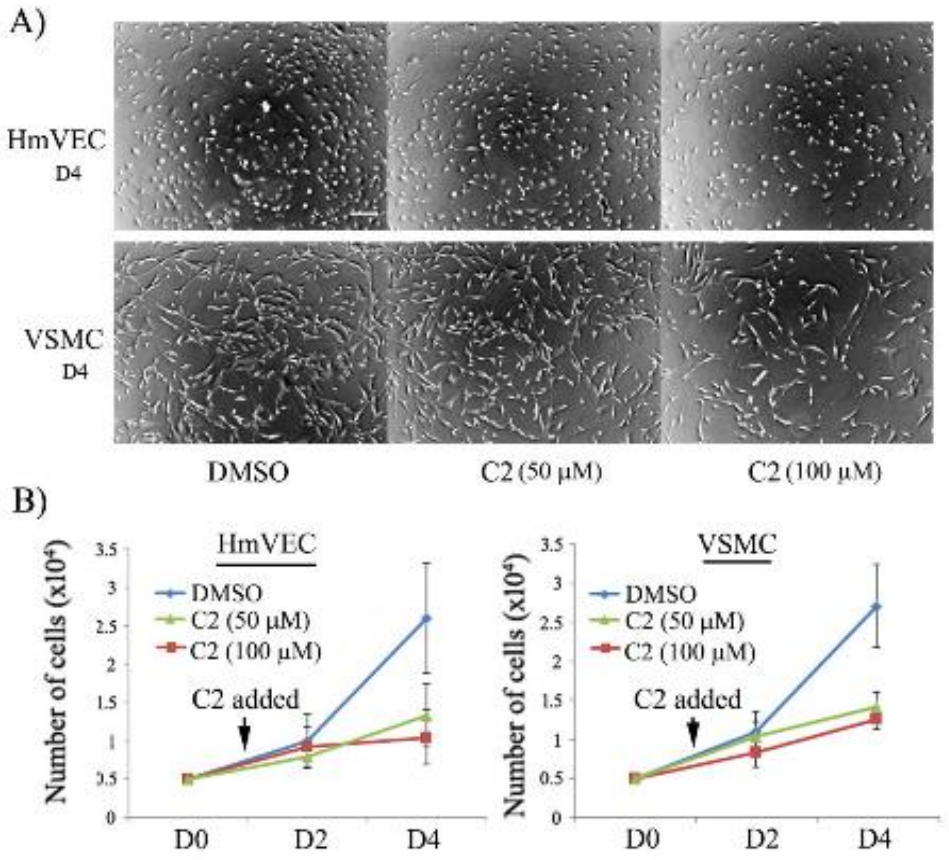

Figure 15. Effects of small molecule inhibitor of Pfn1:actin interaction on proliferation of EC and VSMC in 2D culture. A) Representative bright-field images (acquired with a 4x magnification objective) of HmVEC and VSMC in 2D culture 3 days after treatment (representing Day 4 [D4] of the experiment) with either DMSO or C2 at the indicated concentrations show dose-dependent inhibition of culture growth by compound C2 (scale bar - 200 µm). B) Line graphs summarizing the quantification (mean and stdev) of proliferation assay of HmVEC and VSMC (cells were plated on day 0 [D0]; the mean and stdev values are based on cell count data on D2 and D4 from 3 independent experiments with 2 technical replicates/condition in each experiment; **P<0.01 for D4).

4.2.5 Anti-proliferative action of compound C2 is not restricted to EC

Finally, given that Pfn1 is a ubiquitously expressed protein, we wanted to further explore whether compound C2 has similar anti-proliferative effect on other types of cells. Therefore, we performed similar proliferation experiments with human vascular smooth muscle cells (VSMC – we chose this cell type as it is relevant to the vascular system) which also showed robust suppression of VSMC proliferation in 2D culture in response to compound C2 treatment (Figure 15A-B). Although we have not extended these studies to a broad range of cell types, these preliminary findings with VSMC still suggest that our compound's action is not specific to EC only.

4.3 DISCUSSION

Pfn is a vital regulator of actin dynamics and cell motility, and, therefore, interfering with Pfn1's function could be a useful strategy to perturb physiological and pathological processes that rely on actin-based cell motility. Since no small molecule inhibitors for Pfn1:actin interaction existed to date, we sought to identify putative inhibitors of Pfn1:actin interaction. The present study demonstrates for the first time that the Pfn1:actin interaction is susceptible to small molecule-mediated inhibition. We provided evidence of anti-migratory, anti-proliferative and anti-angiogenic actions of the class of compounds identified herein. Since the biological effects of these compounds were observed only in a somewhat high concentration range (50-100 μM), these compounds should be only regarded as first-generation inhibitors of Pfn1:actin interaction at this stage. Further characterization and expansion of their chemotype will be necessary to

develop a more effective inhibitor class of Pfn1:actin interaction. The structural model used to identify C1 and C2 will serve as a useful guide in the development of such analogs. Although additional experimental characterization, such as X-ray crystallography or NMR, is needed to validate the model, the preliminary SAR (Supplementary Table 2) and our H119E-Pfn1 EC migration results are consistent with the proposed binding mode where the compound mimics the interaction of Y169 of actin with H119 of Pfn1.

Despite supportive data for the compound's inhibitory effect on Pfn1:actin interaction (as suggested by the PLA and pyrene-actin assay results), unfortunately, we were unable to biochemically validate the compound-induced changes in Pfn1:actin interaction by either co-IP or PLP pull-down method. The negative results of biochemical experiments could be due to several plausible reasons. First and foremost, these compounds are likely to be weak inhibitors of the Pfn1:actin interaction, and therefore any subtle change in the interaction would be difficult to detect in a gross biochemical assay. Moreover, use of detergent in the biochemical assays may preclude the binding of the compound to Pfn1 or dissociate weak interactions of Pfn1:compound during extraction and the pull-down phase. Second, our compound may be only effective in blocking the formation of a direct Pfn1:actin complex that is not associated with other proteins (possibly due to conformational changes induced by other interacting proteins causing steric hindrance). Similarly, indirect protein complexes containing Pfn1 and actin involving other intermediate proteins (e.g. actin nucleation and elongation-promoting factors) may not be targeted by the compounds. Biochemical assays will likely capture different types of complexes containing Pfn1 and actin, whether through direct or indirect interactions. Another potential issue in the PLP pull-down assay is that in addition to pulling down actin via Pfn1, this technique could in principle capture actin through other SH3-domain containing proteins (also have strong

affinity for PLP) as well. The theoretical maximum distance between two interacting proteins of interest is roughly 40 nm in order to be able to generate PLA signals. Given the small size of both actin (average diameter ~ 5.5 nm) and Pfn1 (even smaller than actin), although the PLA assay should not be technically limited to detection of only direct Pfn1:actin complex, we do not know whether Pfn1:actin interaction is detected with equal efficiency by PLA when this interaction is direct vs indirect (part of either small or large protein complexes). Because of the extreme sensitivity of PLA signal to the distance between the antibodies concerned, it is highly possible that PLA assay could be more efficient for detecting direct Pfn1:actin complex (either exclusive or part of a small complex involving other binding partners) or at best small indirect complexes than those involving indirect interactions as a part of large protein complexes. In essence, PLA assay may detect only a fraction of all cellular Pfn1:actin interactions (that is captured by biochemical assays), and be biased towards those interactions that are more likely to be affected by the compounds.

There could be several reasons why at least 50 µM concentration of our first-generation inhibitor was required for biological effects. First, literature has reported that the cellular concentration of Pfn1 is generally in the low tens of micromolar range (e.g. human EC [most relevant to this study]: 10.6 µM (168), mammary epithelial cells and breast cancer cells [in the range of 13-30 µM] (169), chicken hamster ovary cells: ~10 µM (170)). The compounds identified herein may be low-affinity inhibitors of Pfn1:actin interaction and at least, as per pyrene-actin assay, a 2.5-fold molar excess of the compound over Pfn1 appeared to be necessary to completely reverse Pfn1's effect on actin polymerization. Second, we do not have a clear understanding of what the relative stoichiometry of Pfn1 in its free vs bound (either exclusively with actin or PLP ligands or both) states is and whether the compound is effective in blocking

the Pfn1:actin interaction if Pfn1 is simultaneously bound to other ligands. Third, the actual intracellular concentration of the compounds may be low if they do not efficiently cross through the membrane lipid bilayer. Fourth, although the results of our motility studies in WT- vs H119E-Pfn1 expressers of EC are consistent with a cellular mechanism of action of the compounds involving Pfn1, we cannot absolutely rule out the possibility of targeting of the compound to some other cellular ligands besides Pfn1, thereby necessitating high concentrations of the compounds for biological effects. However, based on the dependency of a functional actin-binding capability of Pfn1 for the anti-migratory effect of the compound C2 and a general correlation between biochemical and cord-angiogenesis data of the compounds, it is highly unlikely that phenotypes elicited by our first-generation compounds are solely attributed to possible off-target effects.

The inhibitory effect of the compounds on angiogenesis (in both cord and aortic ring assays) was much more pronounced than it was on 2D random motility of EC on tissue culture substrate. One likely explanation could be that EC migration on a compliant ECM substrate (e.g. matrigel used in the cord angiogenesis assay) and spreading may be more sensitive to a loss-of-actin binding function of Pfn1 than 2D cell migration on a rigid tissue-culture substrate. We and others have shown that loss-of-function of Pfn1 also leads to reduced cell adhesion (155) – a defect that may be more consequential in impacting the motile phenotype of cells in 3D ECM substrate (thus affecting cord morphogenesis) than on 2D rigid tissue-culture substrate. Pfn1 also competes with Arp2/3 complex (a major actin nucleator) for actin-binding. Therefore, reduced Pfn1:actin interaction in response to the compound treatment can enhance Arp2/3-mediated membrane protrusion thereby partly mitigating the defect in migration, as previously demonstrated in the case of fibroblasts (171). We also showed that in addition to affecting

migration, our compound had a major suppressive effect on EC proliferation (a key factor for sprouting angiogenesis) and this might also explain why our compound exhibited such a dramatic impact on sprouting angiogenesis. In the future, it will be also interesting to study whether the compounds identified herein can lead to regression of already formed vessels.

Finally, the compounds identified herein could have potential utility in cell biology research as novel chemical tools for perturbing actin cytoskeletal dynamics and actin-dependent biological processes. We also need to carefully consider the potential implications of our findings related to the anti-angiogenic effects of the compounds. While angiogenesis is important for growth, development and tissue repair, it can exacerbate a wide range of human pathologies including diabetic retinopathy, cancer, atherosclerosis, and arthritis, if uncontrolled. Anti-angiogenic therapies to date have been primarily targeted against the action of VEGF (vascular endothelial growth factor – a potent pro-angiogenic growth factor) signaling. However, the therapeutic benefits of the anti-VEGF strategy have been stymied in many instances because of the involvement of alternative pro-angiogenic signaling pathways and acquired resistance to the anti-VEGF treatment (150). Therefore, it is conceivable that targeting molecules that are fundamentally important for angiogenesis-related activities of vascular EC may be an alternative strategy. As an example, attenuation of glycolysis by pharmacological blockade of certain metabolic enzymes has recently shown significant promise in diminishing pathological angiogenesis) (172-174). At least at the conceptual level, there are certain advantages of a Pfn1-centric angiogenesis-modulating strategy. First, Pfn1:actin interaction is fundamentally important for dynamic actin remodeling and EC migration, and also stimulated in ECs in response to proangiogenic growth factor (122,123). Second, Pfn1 is not absolutely essential for actin polymerization (this likely explains why differentiated cells generally tolerate even the genetic

disruption of Pfn1:actin interaction) but it is utilized by multiple actin assembly pathways to enhance the efficiency of actin polymerization, and therefore occupies a critical node of convergent pathways. This nodal positioning may reduce resistance to Pfn1:actin interaction inhibitor that could otherwise occur from alternative compensatory pathways. However, a major disadvantage of targeting Pfn1 is that it is a broadly expressed protein and presumably there is requirement for Pfn1:actin interaction in all somatic cell types. Clearly, our data showing that the anti-proliferative action of our compound is not restricted to EC only support this notion. Therefore, there is always a general concern of potential wide-spread *in vivo* effects associated with targeting Pfn1's interaction with actin. Unless these issues are experimentally addressed through *in vivo* studies in the future, it is still premature to justify an inhibitor of Pfn1:actin interaction as an anti-angiogenic agent for any therapeutic purpose.

5.0 THREONIN 89 IS AN IMPORTANT RESIDUE OF PROFILIN-1 THAT IS PHOSPHORYLATABLE BY PROTEIN KINASE A

5.1 INTRODUCTION

The contents of this section are published (section unpublished will be noted in text).
Reference: **Gau D***, Veon W*, Zeng X, Yates N, Shroff S, Koes D, Roy P. Threonin 89 is an important residue of profilin-1 that is phosphorylatable by protein kinase A. PLoS One. 2016; doi: 10.1371/journal.pone.0156313. * designates co-first authors.

Specific Aim 3: Identify and examine the consequence of novel phosphorylation event on actin-related function of Pfn1.

Actin-based cell migration is fundamental to a number of physiological processes including, but not limited to, embryonic development, wound healing and inflammatory response. Cell migration correlates with marked changes in the actin cytoskeleton where a motile cell has extremely rapid and directed actin polymerization and turnover (175). Membrane protrusion of the leading edge is the initiating event of cell migration and requires de novo actin nucleation followed by filament elongation and/or elongation of pre-existing filaments, catalyzed by various nucleation-promoting and elongating factors (e.g. N-WASP/WAVE, formins and Ena/VASP). These factors harbor poly-L-proline (PLP) domains through which they interact with profilins (Pfn), a family of actin-monomer binding proteins that strongly inhibits spontaneous nucleation and elongation at the pointed ends of actin filaments but promotes barbed-end elongation through the addition of ATP-bound monomeric actin (154). Interaction with Pfn1 (the most

abundant isoform of Pfn in mammals) enhances the actin polymerizing abilities of nucleation-promoting and elongating factors *in vitro* and *in vivo* (176-179).

How Pfn1's interactions with its ligands are regulated in cells is still not clearly understood. At least three types of regulatory mechanisms have been proposed in the literature. First, based on findings that Pfn1 exhibits affinity for membrane phosphoinositides (PPI), and $PI(4,5)P_2$ (the most abundant PPI species in cells) micelles can dissociate the Pfn1:actin complex, it has been speculated that phospholipase C-mediated $PI(4,5)P_2$ hydrolysis could trigger the release of Pfn1 from the plasma membrane enabling its interaction with actin (180). Whether this actually occurs in cells has not been examined yet. Second, it was shown that when treated with peroxynitrile, Pfn1 becomes nitrated on a single tyrosine residue at the C-terminus, and this type of modification increases and decreases Pfn1's affinities for PLP ligands and actin, respectively (181). It was further demonstrated that activation of inducible Nitric Oxide synthase results in Pfn1 nitration in platelets (182). Therefore, nitric oxide signaling could potentially modulate ligand interactions of Pfn1. Third, there is also evidence that Pfn1 can be phosphorylated on tyrosine and serine residues. For example, in endothelial cells, VEGFR2 activation leads to Src-mediated phosphorylation of Pfn1 on residue Y129 which increases its affinity for actin (123). Similarly, activation of the Rho pathway causes ROCK (Rho-associated coiled-coiled kinase)-mediated phosphorylation of Pfn1 on residue S137 (129) impacting its binding to PLP ligands (note that phosphorylation at this site can be also mediated by PKC at least *in vitro* (127)). These studies suggest that acute activation of certain signaling pathways can modulate ligand interactions of Pfn1 through phosphorylation.

The overall goal of this study was to identify other novel phosphorylation events of Pfn1 that can have important functional consequences. We here report that PKA can directly

phosphorylate Pfn1 at multiple residues including T89, a residue that is involved in its interaction with actin. Consistent with molecular dynamics simulations, expression studies of phosphomimetic variant of Pfn1 further suggest that T89 is a structurally important residue, phosphorylation of which is likely to influence actin-binding of Pfn1.

5.2 RESULTS

5.2.1 PKA phosphorylates Pfn1 on multiple residues *in vitro*

All data from this section was performed by Dr. William Veon (thesis title: PKA-mediated regulation of Profilin-1 implication in sprouting angiogenesis). To predict potential phosphorylation sites of Pfn1 and the likely kinases associated with these sites, we performed sequence analyses of both human and mouse Pfn1 using two different bioinformatics tools (NetphosK, KinasePhos). As per these analyses, the abundance of predicted phosphorylation sites is higher for serine/threonine residues than tyrosine residues, and among the various candidate serine-threonine kinases considered, PKA and PKC, the two AGC-family kinases, are associated with the most number of predicted phosphorylation sites. PKC-mediated phosphorylation of Pfn1 on S137 residue has been characterized previously (127,129). Based on alterations in post-translational modification patterns of Pfn isoforms in astrocytes upon treatment with FSK (an activator of cyclic AMP-PKA pathway), it has been recently suggested that PKA may be involved in post-translational regulation of Pfn isoforms (139). Whether Pfn1 is a phosphorylation substrate of PKA however remains unknown. Therefore, as a potential strategy to uncover novel phosphorylation sites of Pfn1, we performed in vitro phosphorylation

assays using recombinant His-tagged Pfn1 and the catalytic subunit of PKA. We observed acidic shift of a significant population of His-Pfn1 (unmodified isoelectric point ~6.5) as evident from several new charged states demonstrating that PKA is capable of directly phosphorylating Pfn1 at multiple residues at least *in vitro*. To identify these phosphorylation sites of Pfn1, PKA-treated His-Pfn1 was trypsin-digested and subjected to LC-MS/MS analysis. A number of Pfn1 peptides covering 53% of Pfn1 sequences were identified, including three singly phosphorylated peptides. Fragmentation patterns of these phosphopeptides were able to narrow down the potential phosphorylation sites to 3 serine/threonine residues: S56/S57, T89, S91/T92. Note that the MS/MS spectra are not able to locate the exact modification sites for some phosphopeptides due to the presence of multiple serine/threonine residues (e.g. S56/S57 and S91/T92) and the absence of signature fragment ions for site specificity. Multiple sequence alignment of Pfn1 in vertebrates revealed a high degree of conservation of S56, S57, T89, S91, T92 and the surrounding residues. As the protein coverage was incomplete, we could not rule out the possibility of other PKA-phosphorylation sites of Pfn1.

5.2.2 Activation of cAMP/PKA pathway induces acidic charge shift of Pfn1 in non-neuronal cells

Next, to determine whether activation of cAMP-PKA pathway has any effect on the isoelectric profile of Pfn1 in non-neuronal cells, HEK-293 cells overexpressing myc-Pfn1 were either serum-starved or acutely stimulated by FSK before performing 2D-GE analyses of cell extracts. We chose to investigate FSK's effect on isoelectric profile of myc-Pfn1 instead of endogenous Pfn1 for two main reasons. First, we reasoned that small changes in the isoelectric profile would be easier to detect in an overexpressed condition. Second, our pilot experiments demonstrated

that myc-Pfn1 (theoretical PI: 6.3) is much better resolvable than endogenous Pfn1 (theoretical PI—8.3) on IEF, likely owing to its acidic nature (it circumvents the problem of reducing agent DTT migrating away the protein). We found that even under serum-starved condition, myc-Pfn1 exists in multiple charged states as evident from three distinct spots (spots #1 through 3) with spot #2 representing the predominant pool of myc-Pfn1 and an extremely weak fourth spot (#4) representing the most negatively charged form of the protein (Figure 16A). The most obvious FSK-dependent change in the 2D profile of myc-Pfn1 was a prominent increase in the intensity of spot #4 (Figure 16A) reflecting an acidic charge shift involving a small pool of Pfn1, a finding that is consistent with PKA's ability to phosphorylate Pfn1 in vitro. As spot #2 accounted for >95% of total pool of myc-Pfn1, we used the relative intensities of spot #2 at a very low exposure (that does not saturate the signal of this spot) between control and FSK-treatment groups as a correction factor for loading control in these experiments to quantify the fold-changes in the intensity of spot #4 in response to FSK. Using this correction factor, we estimated that FSK treatment led to approximately 9-fold (data summarized from 4 independent experiments) increase in the intensity of spot #4 (Figure 16B). In a set of follow-up experiments, we examined the isoelectric profile of myc-Pfn1 in FSK-stimulated HEK-293 cells with or without pharmacological inhibition of PKA by H89. As expected, H89 pretreatment significantly reduced the intensity of spot #4 (Figure 16C-D) further confirming that the most negatively charged pool of Pfn1 in FSK-treated condition is PKA-dependent. Overall, these cell-based experimental results are in agreement with PKA's effect on Pfn1 *in vitro*.

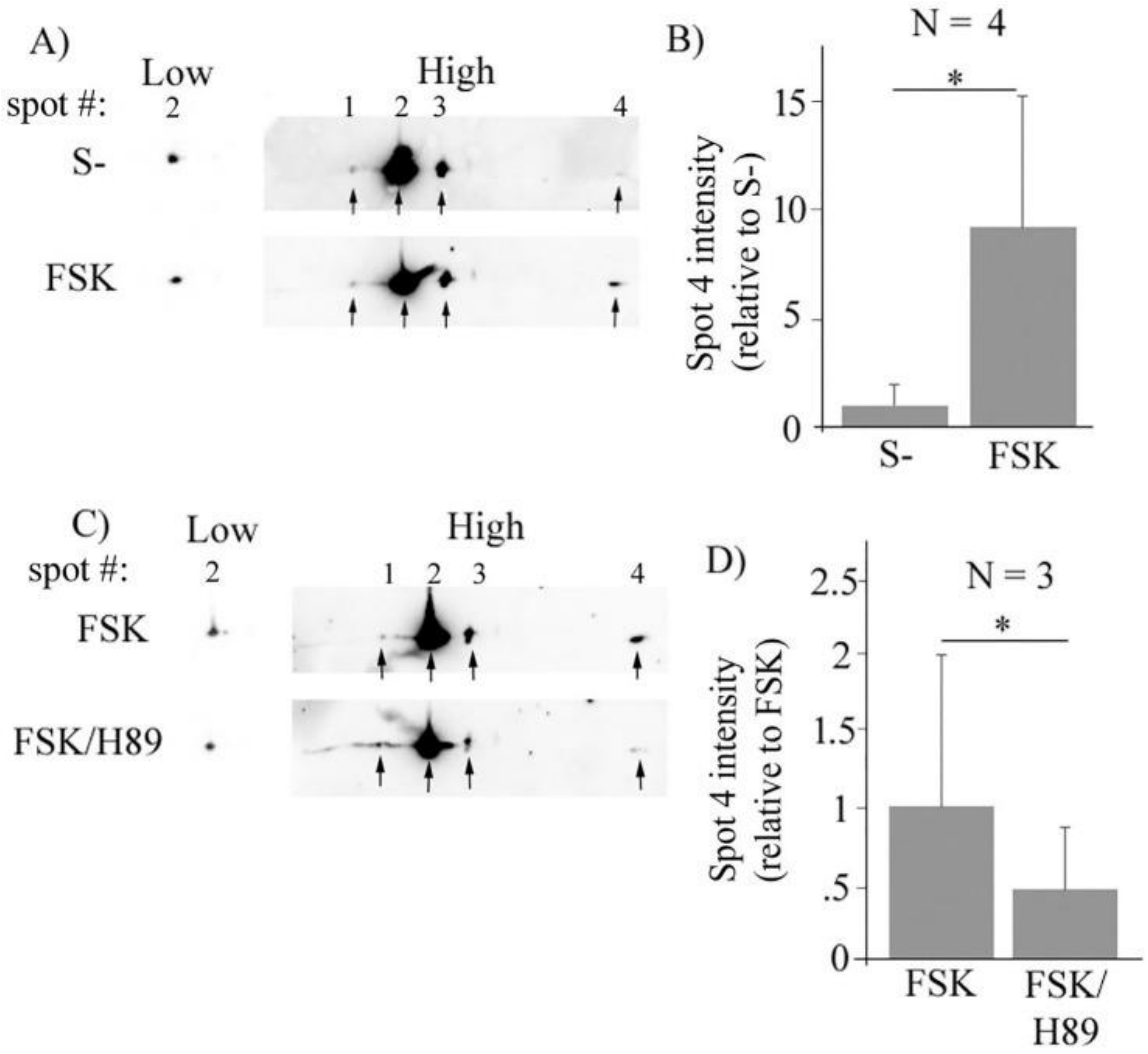

Figure 16. Pfn1 can be post-translationally modified in a PKA-dependent manner in HEK-293 cells. A) Lysates prepared from myc-Pfn1-expressing HEK-293 cells were resolved on 4–7 pH gradient IEF gels and then immunoblotted with anti-myc antibody to reveal the isoelectric profile of myc-Pfn1 in serum-starved (control: S-) vs FSK-stimulated conditions—two different exposure blots are shown. B) A bar graph summarizing the relative average intensity of the spot representing the most negatively charged form of myc-Pfn1 (spot #4) in control vs FSK-stimulated conditions. C-D) Isoelectric profiles of myc-Pfn1 in FSK-stimulated cells with or without H89 treatment (panel C), and the corresponding quantifications of the intensity of spot #4 (panel D). N denotes the number of independent experiments (*: $p<0.05$).

5.2.3 T89 phosphorylation affects the biochemical characteristics of Pfn1

Phosphopeptides of Pfn1 involving S56, S57, T89, S91, T92 have been previously found in global proteomic screens of mitotic cells, cancer and immortalized T cell lines, and endothelial cells suggesting that Pfn1 can be phosphorylated on these residues at least in some cell types under certain conditions (123,183,184). However, the functional significances of these post-translational modifications of Pfn1 are not known. We were particularly interested in the functional consequence of T89 phosphorylation since in a bound conformation with actin (PDB 2BTF), the backbone oxygen of T89 of Pfn1 makes an intermolecular hydrogen bond with Y166 of actin (Figure 17A-B) making T89 as a potentially interesting site for further exploration of possible regulation of the Pfn1:actin interaction. In the monomeric, unbound (i.e when not interacting with any other ligand) structure of Pfn1 (PDB 1PFL), the backbone oxygen of T89 forms an intramolecular hydrogen bond interaction (distance $\leq$ 3.0 Å) with the backbone nitrogen of F98 (Figure 17C). The T89:F98 hydrogen bond marks the transition between the loop defined by residues 89–98 and a beta sheet. Due to the geometry of the interactions, the intramolecular T89 (Pfn1):F98 (Pfn1) and intermolecular T89 (Pfn1):Y166 (actin) hydrogen bonds are mutually exclusive. Given the importance of the intramolecular T89:F98 interaction of Pfn1 in determining its interaction with actin, we asked whether phosphorylation of T89 could potentially affect the 98N-89O hydrogen bond. To address this question, we performed molecular dynamics simulations (MDS) on monomeric homology models of wild-type (WT)-Pfn1 with or without phosphorylated-T89, T89D-Pfn1 (T89 was replaced by an aspartic acid, a strategy that is commonly used to artificially mimic a phosphorylated state of an amino acid) or T89A (T89 was replaced by an alanine to simulate a corresponding non-phosphorylatable version). All simulations were started with a conformation where T89:F98 interaction was not

initially formed. We assessed the stability of the intramolecular 98N-89O hydrogen bond over the course of three independent 300-ns simulations. The time-dependent fluctuation of 98N-89O distance for each of the three simulations and a histogram summarizing the results of all three simulations for the four variants (WT, WT-phosphoT89, T89A and T89D) of Pfn1 are depicted in Figure 18. In all three simulations, the WT protein quickly established a stable intramolecular T89:F98 (distance ≤ 3.0 Å) bond. By contrast, the intramolecular hydrogen bond was not formed in any of the three THP89 (phosphorylated T89) simulations, suggesting that phosphorylation of T89 causes an extreme destabilization of the intramolecular T89:F98 interaction. Even though the histogram pattern of the T89D simulation was not exactly identical to that of THP89, in two out of three simulations T89D-Pfn1 also completely failed to establish the hydrogen bond throughout the course of the simulation suggesting that T89D-Pfn1 is a reasonable mimic for T89-phosphorylated Pfn1. Similarly, the histogram pattern of the T89A mutant, although not identical, was also fairly similar to that of the WT protein suggesting that this non-phosphorylatable mutant also stabilizes the interaction. The differences in histogram patterns between T89A and WT or THP89 and T89D simulations were not totally unexpected since aspartic acid and alanine are not structurally identical to phosphorylated and unphosphorylated threonine, respectively. In summary, these simulation results predicted that the intramolecular T89:F98 interaction of Pfn1 could be sensitive to the phosphorylation status of T89. Since T89 (Pfn1):F98 (Pfn1) and T89 (Pfn1):Y166 (actin) interactions are mutually exclusive, one possible consequence of destabilization of the T89:F98 interaction upon T89 phosphorylation is enhanced stability of the T89 (Pfn1):Y166 (actin) interaction when Pfn1 is in a complex with actin and, therefore, a potential stronger affinity of Pfn1 for actin.

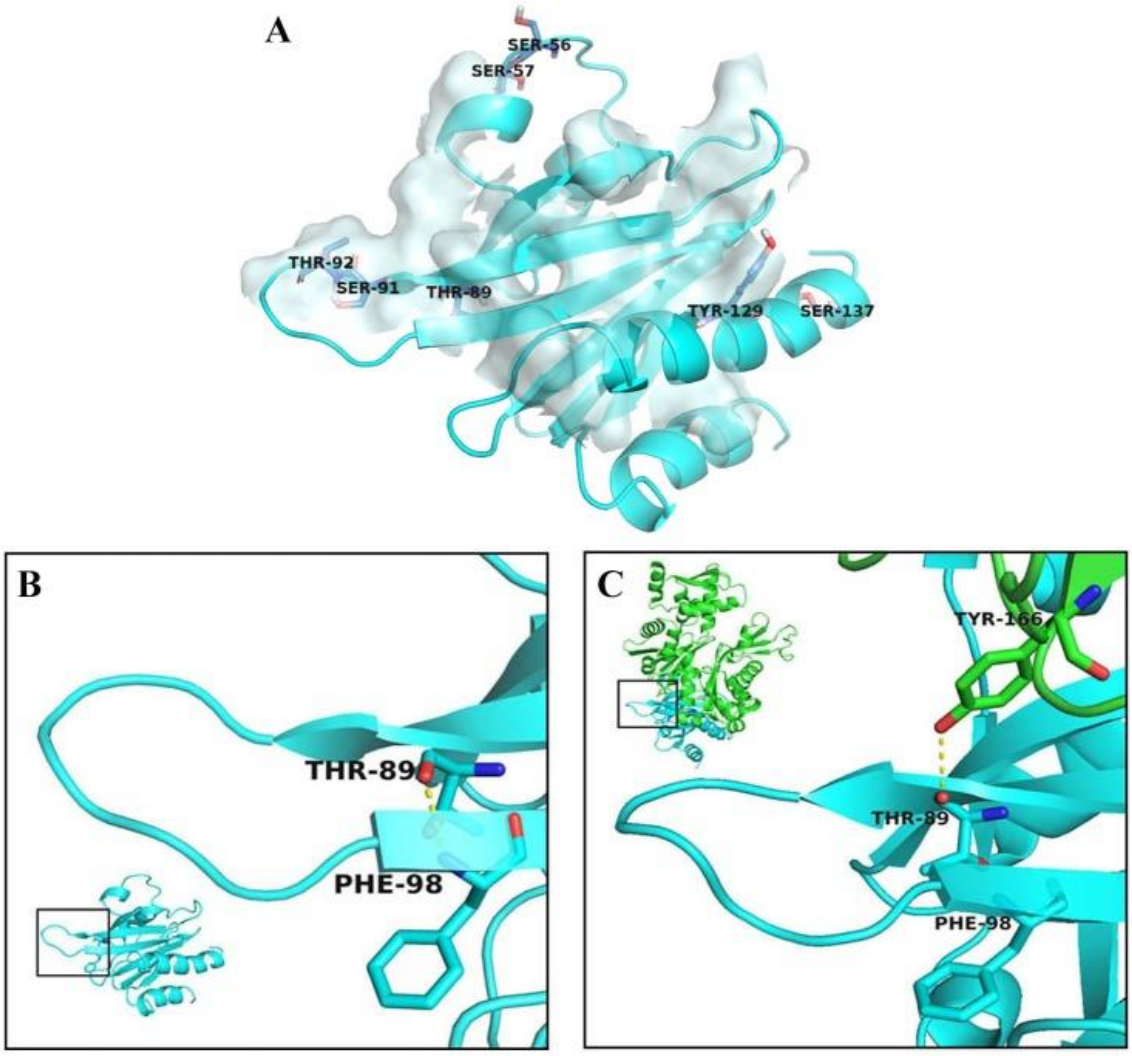

Figure 17. Molecular interactions of T89 of Pfn1. A) Actin-interacting surface of Pfn1 (Pfn1: blue; actin: grey); phosphorylatable residues of Pfn1 are indicated as sticks. B) In unbound Pfn1 (PDB 1PFL) T89 forms an intramolecular hydrogen bond with F98. C) In the Pfn1-actin complex (PDB 2BTF) an intermolecular hydrogen bond (dashed yellow line) is observed between T89 of Pfn1 (blue) and Y166 of actin (green). Figure courtesy of Dr. David Koes.

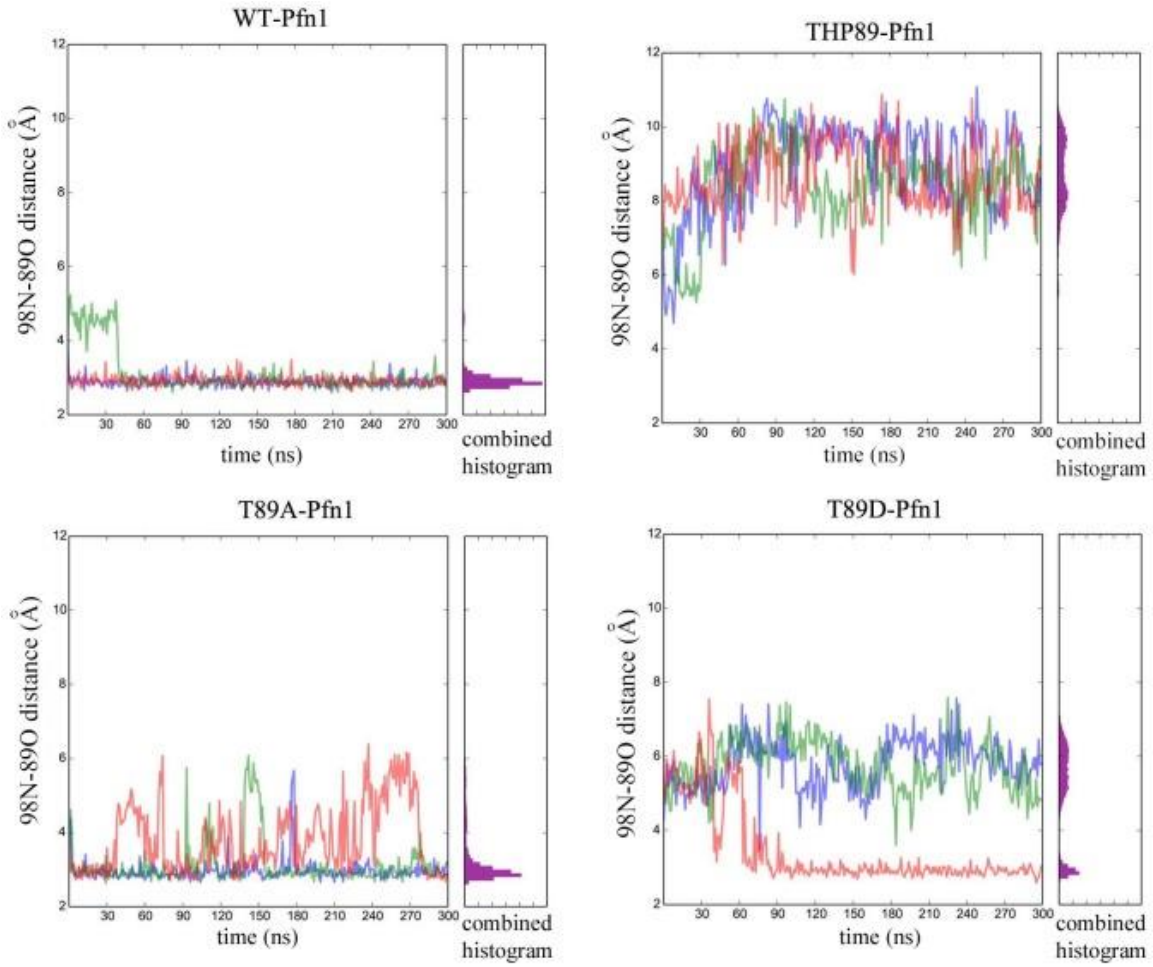

Figure 18. Molecular Dynamics Simulation predicting the effect of T89 phosphorylation on the stability of intramolecular 98N-89O bond. The stability of this intramolecular 98N-89O bond over the course of three 300ns molecular dynamics simulations of monomeric Pfn1 are shown for homology models based on the bound structure for WT, T89A, T89D and phosphorylated T89 (THP89) variants of Pfn1 (each color represents an individual simulation). The histograms alongside the line graphs summarize the results of all three simulations for each variant of Pfn1. Figure courtesy of Dr. David Koes.

We next performed GST-pull-down assays of bacterially expressed forms of either WT (control)- or various phosphomimetic Pfn1 using HEK-293 cell lysate to qualitatively assess the changes in Pfn1:actin binding conferred by T89D substitution. To our surprise, the pull-down assay failed for T89D-Pfn1 as this mutant protein was largely insoluble in non-denaturing lysis

buffer and therefore could not be extracted from the bacteria (data from Dr. William Veon, thesis title: PKA-mediated regulation of Profilin-1 implication in sprouting angiogenesis). T89D-Pfn1 was extractable from bacteria only under denaturing lysis buffer and in the presence of urea (Figure 19A), a condition that is unfortunately non-permissive for binding studies. The protein insolubility issue was specific to T89D substitution since phosphomimetic Pfn1 constructs involving all other PKA sites (S57, S91 and T92) were extractable in non-denaturing lysis buffer and showed ability to bind actin and VASP (a PLP ligand of Pfn1) similar to the extent of WT Pfn1, at least, on a qualitative scale (data from Dr. William Veon, thesis title: PKA-mediated regulation of Profilin-1 implication in sprouting angiogenesis). Even in mammalian HEK-293 cells, T89D-Pfn1, when transiently expressed as an EGFP-tagged protein, was barely extractable in non-denaturing lysis buffer and could only be extracted efficiently when both SDS and urea were present in the lysis buffer; WT- and T89A-Pfn1 were fully extractable in mild non-denaturing lysis buffer as expected (Figure 19B). Similarly, T89D-Pfn1 was hardly extractable in non-denaturing lysis buffer when expressed as a myc-tagged protein (Figure S 6). Therefore, protein insolubility of T89D-Pfn1 does not appear to be either epitope-tag- or cell-type (bacterial vs mammalian)-specific effect. Fluorescence microscopy of HEK-293 cells transfected with the various EGFP-Pfn1 constructs revealed that nearly all cells expressing EGFP-T89D-Pfn1 formed prominent protein aggregates of EGFP-Pfn1 whereas neither WT nor T89A overexpressors demonstrate EGFP-Pfn1 clustering, a result that is consistent with the insolubility characteristics of T89D-Pfn1 (Figure 19C). At the protein level, expression of EGFP-Pfn1-T89D was always found to be much lower than either of the other two exogenous (WT or T89A) forms of Pfn1 (Figure 19B). This was not due to differences in the levels of transfected DNA since mRNA levels of all three EGFP-fused Pfn1 constructs were comparable (Figure S 7). Note that

endogenous Pfn1 expression was not affected by overexpression of any of these ectopic Pfn1 constructs (Figure 19B). When we blocked new protein synthesis in HEK-293 cells by cycloheximide (CHX) treatment, both WT- and T89A-variants of EGFP-Pfn1 showed no detectable change in the protein level over a period of 8 hours but the expression level of T89D-Pfn1 declined substantially within 4 hours of CHX treatment (Figure 19D-E). These results demonstrate that T89D substitution accelerates the protein turnover of Pfn1. Folding of proteins into alternative three-dimensional conformation can lead to protein aggregation, insolubility and marking for proteolytic degradation. As T89D-Pfn1 exhibits all of these hallmarks, it indirectly suggests that T89D substitution causes a significant conformational change in Pfn1, an interpretation that is consistent with our in silico prediction of extreme destabilization of the intramolecular T89:F98 interaction upon T89 phosphorylation. Therefore, T89 appears to be a structurally important residue of Pfn1 that can be modified by phosphorylation.

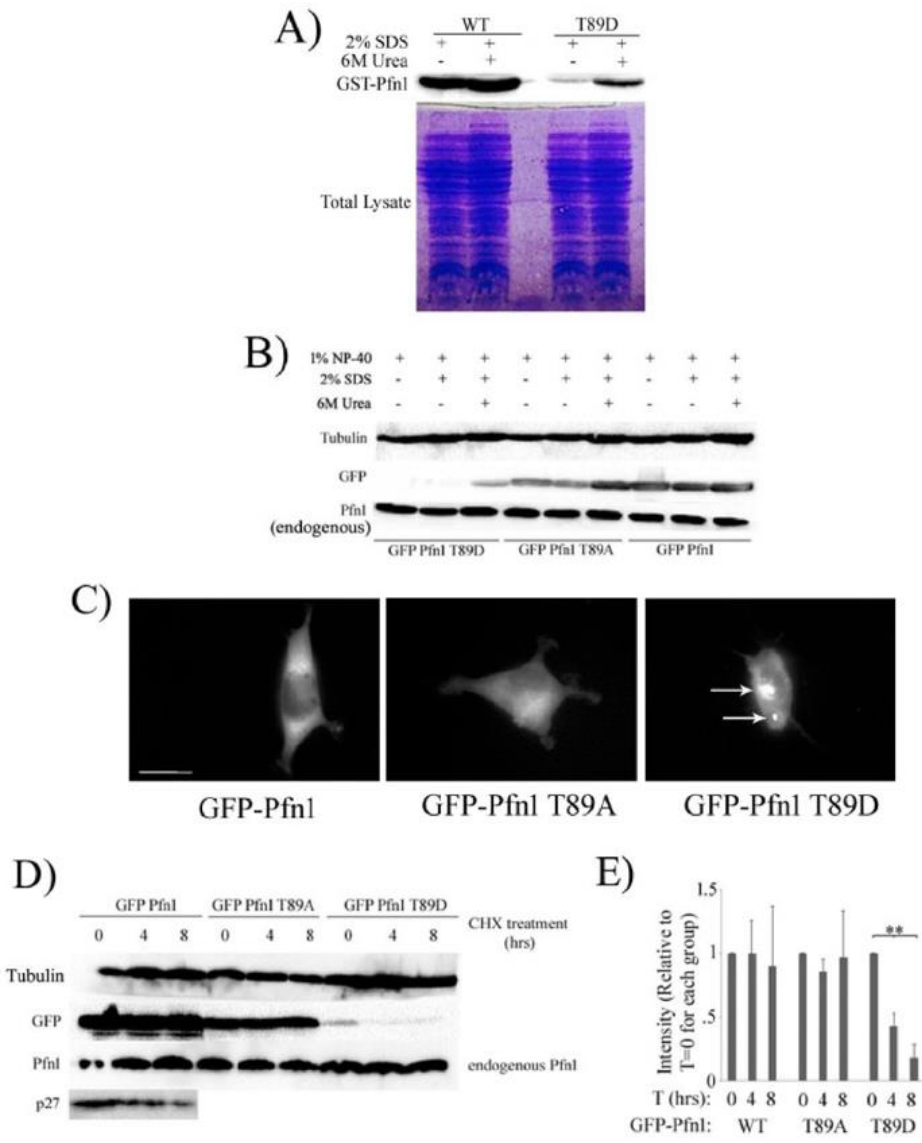

Figure 19. Effect of site-specific phosphorylation on biochemical characteristics of Pfn1. A) Bacteria expressing indicated GST-tagged Pfn1 constructs were lysed with either non-denaturing (containing 1% NP-40) or denaturing (containing 1% NP-40, 2% SDS for one buffer and the other with 6M urea in addition) extraction buffers. Bacterial lysates were immunoblotted with anti-Pfn1 antibody to demonstrate that T89D-Pfn1 is insoluble in non-denaturing lysis buffer. B) HEK-293 cells expressing indicated EGFP-fused Pfn1 constructs were lysed with either non-denaturing (containing 1% NP-40) or denaturing (containing 1% NP-40, 2% SDS for one buffer and the other with 6M urea in addition) extraction buffers. HEK-293 lysates were immunoblotted with anti-GFP antibody to demonstrate that GFP-T89D-Pfn1 is also insoluble in non-denaturing lysis buffer. Note that endogenous Pfn1 level is not affected by expression of any of the ectopic Pfn1 constructs and extractable completely in non-denaturing

lysis buffer. C) Fluorescence images of HEK-293 cells expressing indicated EGFP-fused Pfn1 constructs show that EGFP-Pfn1-T89D causes clustering of this fusion protein as indicated by the arrows. Scale bar represents 20 μm. D) HEK-293 cells expressing indicated EGFP-fused Pfn1 constructs were treated with CHX for up to 8 hours. Cell lysates prepared at different time-points after CHX addition were immunoblotted with the indicated antibodies. T89D-Pfn1 undergoes rapid protein degradation while WT- and T89A-Pfn1 are stable over that period of time, similar to the characteristic of endogenous Pfn1 (degradation of p27kip1, a cell-cycle protein that undergoes rapid turnover, validates CHX efficacy). Tubulin blot serves as the loading control. E) The bar graph summarizes quantification of the time-dependent changes in the expression of the indicated GFP-Pfn1 constructs following CHX treatment in HEK-293. Data was summarized from 3 independent experiments (** indicates $p < .01$).

Since a direct biochemical assessment of the effect of T89 phosphorylation on actin-binding of Pfn1 was not possible due to protein insolubility issues, we considered two indirect approaches. First, we performed the standard pyrene-actin polymerization assay to determine whether PKA-mediated phosphorylation has any effect on Pfn1's ability to inhibit actin polymerization. In the absence of PKA, Pfn1 inhibited actin polymerization by ~30% when added to actin at a 1:1 molar ratio. Unfortunately, pre-incubation with PKA (mimicking the in vitro kinase assay condition) made little to no difference in the overall effect of Pfn1 on the kinetics of actin polymerization (data not shown). This was not totally unexpected because if only a very small fraction of Pfn1 is modified on T89 by PKA, the resulting effect would be hard to detect in a bulk polymerization assay such as the pyrene-actin assay. It is possible that PKA-mediated phosphorylation on other residues may have a confounding effect masking the effect of T89 phosphorylation.

Therefore, as an alternative strategy, we investigated the effect of constitutive T89 phosphorylation of Pfn1 on actin polymerization in cells. First, we transiently overexpressed mCherry-actin along with either WT- or T89A- or T89D- variants of Pfn1 (all constructs were

EGFP-fused) in MDA-MB-231 (MDA-231) breast cancer cells. As in HEK-293 cells, T89D-Pfn1 a) expressed at a much lower level than either WT- or T89A-Pfn1 (Figure 20A), and b) formed prominent aggregates (Figure 20B) in MDA-231 cells. Interestingly, mCherry-actin was also found to be strikingly concentrated at T89D-Pfn1 clusters (Figure 20B). Clustering of mCherry-actin was not observed in cells overexpressing either WT or T89A-Pfn1. We considered two scenarios by which T89D-Pfn1 overexpression could induce actin clusters. One possibility is that T89D-Pfn1 directly binds to actin and co-clusters actin at the sites of their aggregation. As there is also experimental evidence of Pfn1's ability to oligomerize at least *in vitro* (185), an alternative possibility is that T89D-Pfn1 somehow oligomerizes with endogenous Pfn1 and in turn recruits actin bound to endogenous Pfn1. To determine whether T89D-Pfn1:actin co-clustering requires the action of endogenous Pfn1, we re-assessed T89D-Pfn1:actin co-clustering in MDA-231 cells when endogenous Pfn1 expression was selectively suppressed by siRNA transfection. Even in a near complete absence of endogenous Pfn1 expression, prominent co-clustering of mCherry actin and T89D-Pfn1 was observed (Figure 20C). These data suggest that in an overexpression setting (i.e in the presence of endogenous Pfn1), co-clustering of mCherry-actin and T89D-Pfn1 is most likely mediated by a direct interaction between T89D-Pfn1 and actin rather than involving an indirect action of endogenous Pfn1. In parallel experiments, we also found that overexpression of only T89D-Pfn1 but not WT- or T89A-Pfn1 has a significant impact on the average level of polymerized actin (as measured by rhodamine-phalloidin fluorescence on a cell-by-cell basis) in MDA-231 cells (Figure 21A-B; note that the overall expression of actin is not affected by T89D-Pfn1 overexpression (Figure S 8)). T89D-Pfn1 overexpression resulted in a robust 60% decrease in average F-actin content/cell when compared to the GFP control; there was no significant difference in average F-actin level

between either of WT- or T89A-Pfn1 overexpressor. Inhibitory action of T89D-Pfn1 on actin polymerization in cells, taken together with the actin clustering ability of T89D-Pfn1 even in the absence of endogenous Pfn1, is consistent with intact actin-binding of T89D-Pfn1 (or T89 phosphorylated Pfn1) as predicted by MDS. Despite the low expression level of T89D-Pfn1 compared to either WT—or T89A-Pfn1, a reduction in actin polymerization specifically in the setting of T89D-Pfn1 overexpression may suggest that T89D-Pfn1 has a dominant negative effect. This is clearly possible if T89D-Pfn1 has a stronger affinity for the actin monomer than endogenous Pfn1 (as predicted by MDS) and is thereby able to competitively inhibit the endogenous Pfn1:actin interaction.

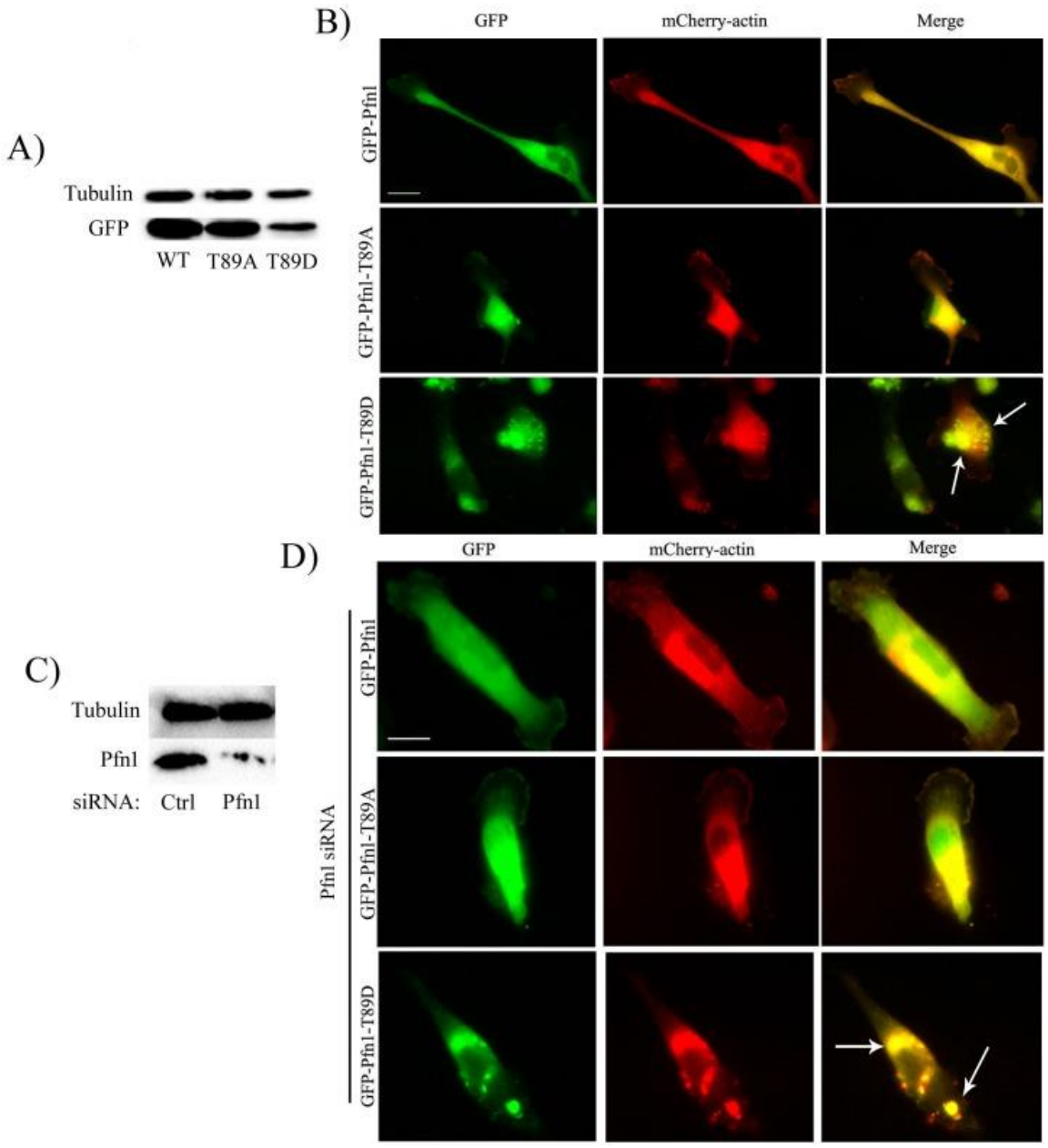

Figure 20. T89D-Pfn1 co-clusters with actin in cells. A) Lysates prepared from MDA-231 cells expressing indicated EGFP-fused Pfn1 constructs were immunoblotted with anti-GFP antibody to show the relative levels of various EGFP-Pfn1 constructs (tubulin blot serves as the loading control). B) Fluorescence images of MDA-231 cells expressing indicated EGFP-fused Pfn1 and mCherry-actin demonstrate mCherry-actin clustering at the sites of T89D-Pfn1 aggregates (arrows; Scale bar—20 μm). C) Fluorescence images of MDA-231 cells co-expressing mCherry-actin and EGFP-Pfn1-T89D, and treated with Pfn1 siRNA reveal mCherry-actin:T89D-Pfn1 co-clusters (arrows; Scale bar—20 μm). Pfn1 immunoblot alongside confirms near complete loss of endogenous Pfn1

expression in Pfn1-siRNA treated cells when compared against control siRNA transfected cells (tubulin blot—loading control).

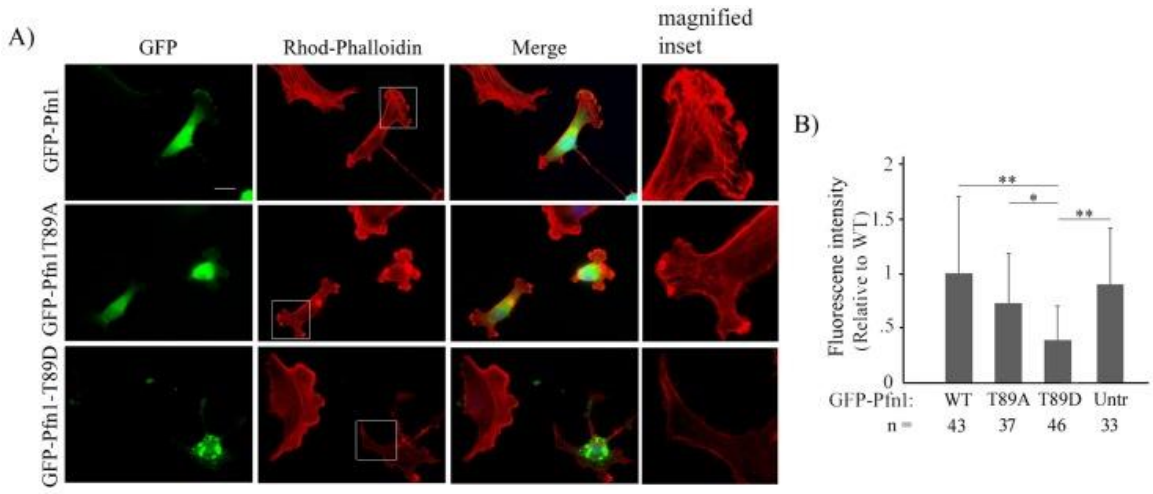

Figure 21. Overexpression of T89D-Pfn1 has a robust effect on actin cytoskeleton in MDA-231 cells. A) Fluorescence images of MDA-231 cells expressing indicated EGFP-fused Pfn1 constructs and stained with rhodamine-phallodin staining. Scale bar represents 20 μm. B) A bar graph summarizing the average rhodamine-phalloidin fluorescence intensity/cell for T89A-Pfn1 and T89D-Pfn1 expressors relative to that of WT-Pfn1 expressing and untransfected cells. 'N' indicates number of cells analyzed for each group pooled from 3 independent experiments (** indicates $p < .01$; * indicates $p < .05$).

5.2.4 T89 may be an *in vivo* modification site of Pfn1 in the basal state

We finally asked whether any subcellular pool of Pfn1 is post-translationally modified on T89 even under the basal condition. Unfortunately, we were unable to directly confirm T89 phosphorylation of Pfn1 by mass-spectrometry of immunoprecipitated myc-Pfn1 from HEK-293 cells. We speculated that this could be either due to a) a possibility of only a very negligible fraction of Pfn1 that is being modified at the T89 residue, and/or b) detergent insolubility of T89-

phosphorylated Pfn1 (as suggested by the biochemical characteristics of phosphomimetic T89D-Pfn1) thus precluding T89-phosphorylated Pfn1 from the immunoprecipitated sample. Therefore, we adopted an indirect approach where we expressed either WT- or non-phosphorylatable T89A forms of Pfn1 as myc-tagged proteins in HEK-293 cells and analyzed their post-translational modification patterns by two-dimensional gel electrophoresis (2D-GE). We reasoned that if any cellular pool of Pfn1 is phosphorylated on T89, rendering it non-phosphorylatable should result in a basic charge shift of the isoelectric profile of Pfn1 in 2D GE. We observed multiple charged states of myc-Pfn1 with the second spot representing the predominant pool of myc-Pfn1. Rendering T89 non-phosphorylatable by alanine substitution resulted in basic shift of a small population of myc-Pfn1 (Figure 22). As spot #2 accounts for >95% of total pool of myc-Pfn1, we used the relative intensities of spot #2 at a very low exposure (that does not saturate the signal of this spot) between WT- and T89A-Pfn1 IEFs as a correction factor for the loading control for the two groups. Using this correction factor, we estimated that T89A substitution led to an approximately 8.9-fold (mean of two independent experiments) increase in the ratio of intensity of spot #1 to that of spot #3 (a measure of net basic charge shift). This finding is consistent with the scenario that a small fraction of cellular Pfn1 could be post-translationally modified on the T89 residue in cells. Note that without direct mass-spectrometry-based evidence of T89 phosphorylation, we could not absolutely rule out an alternative interpretation that T89A substitution may render a certain pool of Pfn1 resistant to phosphorylation or other types of post-translational modification on sites other than T89.

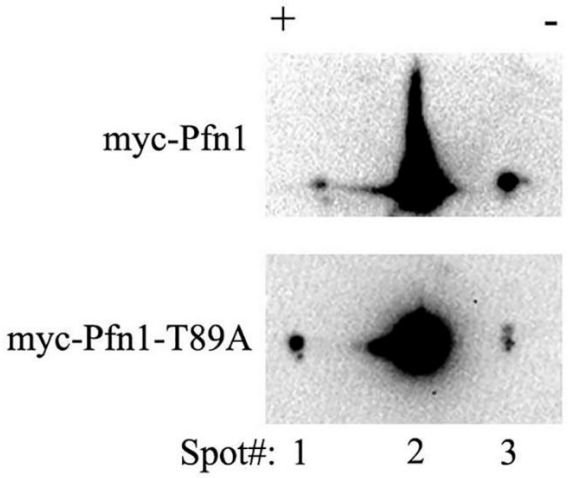

Figure 22. Effect of non-phosphorylatable amino-acid substitution at T89 on post-translational modification profile of Pfn1 in cells. 2D-GE of lysates from HEK-293 cells expressing either myc-Pfn1 or myc-Pfn1-T89A demonstrate that alanine substitution at T89 results in a basic shift of a small portion of myc-Pfn1.

5.3 DISCUSSION

It is well recognized that Pfn1 is a vital cog in the machinery that regulates actin polymerization in cells. Therefore, how Pfn1's interactions with actin and other major controllers of actin polymerization are regulated is a fundamentally important biological question in the context of actin-driven cellular events. There is emerging evidence that phosphorylation plays an important role in tuning Pfn1's ligand interactions. At present, only two phosphorylation events (Y128, S137) have been directly linked to functional alterations of Pfn1. This study demonstrates that Pfn1 can be directly phosphorylated by PKA, and accordingly, post-translationally modified in a PKA-dependent manner in cells. We identified at least three PKA phosphorylation sites (S56/S57, T89, S91/T92). As phosphopeptides of Pfn1 involving all of these residues were previously found in various proteomics screens (123,183,184), these phosphorylations appear to

be bona fide *in vivo* events. By MDS, we established similarities between the intramolecular changes caused by actual T89 phosphorylation and T89D substitution suggesting T89D-Pfn1 reasonably mimics a T89-phosphorylated state of Pfn1. We further showed that T89D-Pfn1 exhibits hallmarks of proteins in an alternative three-dimensional conformation including protein aggregation when expressed in cells, insolubility and marking for proteolytic degradation. Therefore, T89 appears to be a structurally critical residue of Pfn1 that is a target for phosphorylation leading to significant biochemical consequence.

Previous studies have mutated residues near and adjacent to T89, including R88 and K90, with no apparent impact on solubility (186,187). Recently, several Pfn1 mutations (C71G, M114T, E117G and G118V) have been linked to pathogenesis of familial Amyotrophic Lateral Sclerosis (ALS) (188). Except for E117G, the other three mutations were shown to result in protein aggregation and insolubility of Pfn1 in cells, very similar to the phenotypes exhibited by phosphomimetic mutation of the T89 residue demonstrated in the present study. Another phenotypic parallel between the ALS-linked mutations and the T89D mutation was the inhibitory effect on actin polymerization. ALS-linked mutations lie in close proximity to the actin-binding residues of Pfn1 while the backbone of the T89 residue directly interacts with Y166 of actin. As ALS-linked mutations still preserved a significant NP-40 soluble pool of Pfn1, a co-immunoprecipitation assay was feasible in that study to demonstrate that ALS-linked mutations result in reduced actin-binding of Pfn1. However, in our case, the insolubility issue of the T89D mutant was much more severe, precluding us from performing similar biochemical assays. In silico analyses predicted that phosphorylation of T89 could potentially result in an ‘actin-friendly’ conformation because the backbone oxygen of T89 is more accessible to Y166 of actin through destabilization of intramolecular T89:F98 interaction. T89D-Pfn1:actin co-clusters in

cells even in the near absence of endogenous Pfn1 expression is consistent with a direct interaction of T89D-Pfn1 and actin, as predicted by the *in silico* analyses.

Is our *in silico* prediction of the increased strength of Pfn1:actin binding conferred by T89 phosphorylation consistent with reduced level of actin polymerization in cells upon T89D-Pfn1 overexpression? Pfn1 has dual effects on actin cytoskeleton. Pfn1 can either inhibit actin polymerization (by sequestering G-actin, inhibiting spontaneous or Arp2/3-mediated actin nucleation) or promote barbed-end directed actin polymerization. Even for barbed-end elongation, Pfn1 must also dissociate from G-actin following shuttling of G-actin to the barbed ends. If T89 phosphorylation dramatically enhances Pfn1's affinity for actin to a point that dissociation of the Pfn1:actin complex is greatly inhibited, in an overexpression setting T89D-Pfn1 should not only competitively inhibit the endogenous Pfn1:actin interaction, but it could also act as a G-actin sequestering protein resulting in an overall inhibition of actin polymerization. There is, however, an alternative possibility that T89D-Pfn1 induces local actin polymerization at the sites of its aggregation and in turn make less G-actin available for actin polymerization elsewhere in the cell. We think this is unlikely since phalloidin staining did not reveal any F-actin clusters at the sites of T89D-Pfn1 aggregates. Although it remains to be seen whether activating the PKA pathway triggers T89 phosphorylation of Pfn1 in cells, if T89-phosphorylation of Pfn1 inhibits actin polymerization of Pfn1 as suggested by the F-actin phenotype of T89D-Pfn1 expressors in this study, it would be at least consistent with the recent finding of FSK-induced stellation of astrocytes in a Pfn-dependent manner (139).

Another interesting finding of this study was the faster protein turnover of Pfn1 conferred by the phosphomimetic mutation on the T89 residue. Although the structural basis for this observation is currently unclear, one simple explanation could be that T89D substitution affects

protein folding of Pfn1, and that the misfolded protein becomes a target for degradation. Previous proteomic studies have found evidence of ubiquitination of the adjacent residue K90 (189,190). Thus, it is possible that T89 phosphorylation induces a large structural change through destabilizing the beta sheet structure which increases the accessibility of K90 (or other ubiquitylable lysine residues) to ubiquitin-ligases and priming Pfn1 for degradation. If this is true, T89 phosphorylation could be a triggering event for local protein turnover of Pfn1.

In conclusion, we have identified T89 phosphorylation as a novel post-translational modification of Pfn1 which has important biochemical consequence on Pfn1. The actual biological significance of T89 phosphorylation still needs to be resolved in future studies. Although phosphorylation of other PKA sites identified herein (S57, S91/T92) residues did not show any obvious change in Pfn1's ability to co-precipitate actin and PLP ligand in a GST-pull down assay, without a quantitative binding assay, we cannot absolutely rule out subtle changes in ligand affinity of Pfn1 due to these mutations. Furthermore, whether phosphorylation of any these residues has any influence on other post-translational modifications or impacts other functionalities of Pfn1 (such as PPI binding), particularly if they occur simultaneously, need further investigation. Future studies should also examine whether PKA signaling influences actin dynamics and actin-dependent biological processes such as cell migration through phosphorylation of Pfn1.

6.0 CONCLUSIONS

Angiogenesis depends greatly on cell migration which in turn requires dynamic remodeling of the actin cytoskeleton. While angiogenesis is an important physiological process like in development or wound healing, angiogenesis can also contribute to pathological processes such as tumor growth or diabetic retinopathy. Current treatment for aberrant angiogenesis revolves around regulation of VEGF signaling, typically by anti-VEGF. For this dissertation, we set to demonstrate proof-of-concept that angiogenesis can be fundamentally regulated by pharmacologically targeting the MKL/SRF signaling pathway with small molecule inhibitors and its downstream targets, such as Pfn1. This hypothesis was supported by the myriad of studies previously performed by other groups demonstrating the genetic importance of the MKL/SRF signaling pathway in cell migration. A graphical abstract of the aims accomplished from this dissertation is shown in Figure 23. Work published in chapter 3 of this dissertation demonstrated that CCG-1423, a small molecule inhibitor of MKL activity, was able to abrogate EC migration and angiogenesis *in vitro, ex vivo,* and *in vivo (88).* We also demonstrated that MKL's regulation of cell migration is at least in part due to regulation of Pfn1 by an externalization mechanism (61). This raised the question whether regulation of Pfn1 alone is sufficient for regulation of angiogenesis. Work previously performed by the lab on EC *in vitro (121,122)* and *ex vivo* data (88) presented in this dissertation support the claim that regulation of Pfn1 alone is sufficient for regulation of angiogenesis and cell migration.

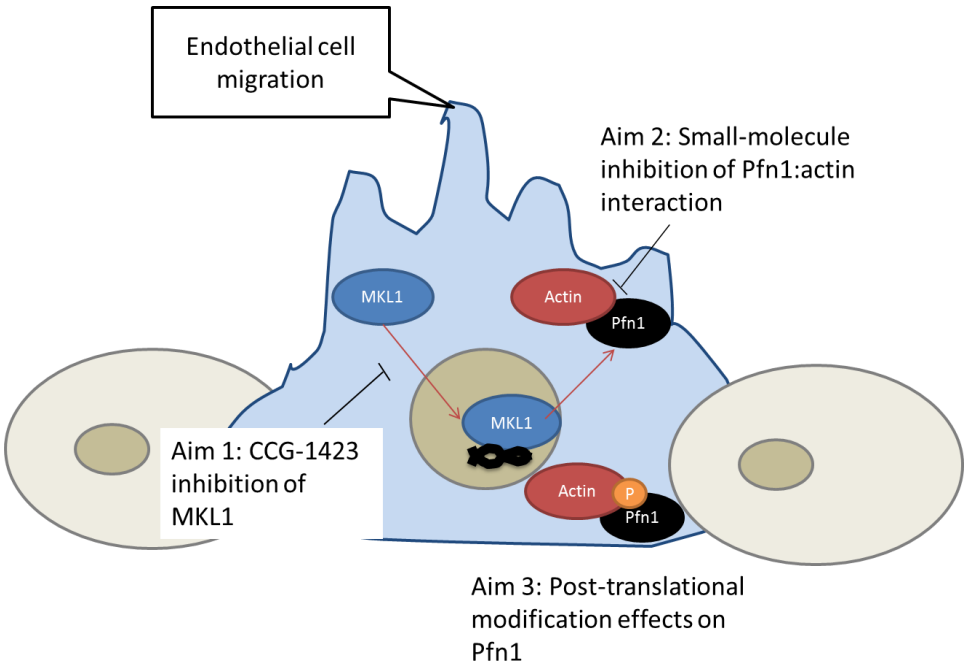

Figure 23. Graphical representation of aims accomplished from this dissertation. EC migration is partially dependent on *de novo* synthesis of new actin binding proteins by the MKL1 signaling pathway. Aim 1 sought to demonstrate proof-of-concept that small molecule inhibition of MKL1 signaling can inhibit EC migration and angiogenesis. Aim 2 demonstrated that downstream target of MKL1, Pfn1, can also be targeted by small molecule inhibition and also reduce EC migration and angiogenesis. Finally, Aim 3 explored the effects of post-translational modifications on Pfn1 and its effect on Pfn1 activity.

Since our data suggest that Pfn1 plays a vital role in cell migration and angiogenesis, we next sought to determine whether Pfn1 can be pharmacologically targeted by small molecule inhibitors. We screened for an inhibitor of Pfn1:actin interaction based on a report suggesting that Pfn1:actin interaction can regulate sprouting angiogenesis via an *ex vivo* animal model (123). Using a solved crystal structure of Pfn1:actin, we were able to screen and biochemically test 42 compounds, of which 2 compounds, C1 and C2, demonstrated an ability to inhibit Pfn1:actin interaction *in vitro*. With these compounds, we further demonstrated that cell migration, proliferation, and sprouting angiogenesis can be regulated with addition of C1 or C2

(191). Overall, this study demonstrated proof-of-concept that a downstream target of MKL/SRF can also be pharmacologically targeted in order to regulate angiogenesis.

In addition to small molecule inhibition of Pfn1:actin interaction, we also asked whether Pfn1 may be regulated by other post-translational means. Others have shown that post-translational modification of Pfn1 at various residues may impact Pfn1 binding activity (123,127,128,181). Using predictive software, we asked what is the likelihood of Pfn1 being regulated by various enzymes and found that PKA was predicted to modify Pfn1 at various residues. We biochemically demonstrated that PKA can indeed phosphorylate Pfn1 and identified a novel phosphorylation site on residue T89 on Pfn1. We further go to show that T89 phosphorylation on Pfn1 has profound impact on the protein by causing Pfn1 to aggregate with actin into insoluble components (192). This study demonstrated that there is potential for development of pharmacological inhibitors of Pfn1 targeting post-translational modifying regions as a strategy to regulate Pfn1 activity and its regulation of cell migration.

7.0 FUTURE DIRECTION

The past few decades of research on MKL primarily focused on its role as a key cofactor of SRF and a regulator of SRF-mediated gene transcription. This fact is strongly presented in the literature in various facets of cell biology including cell migration where there is overwhelming evidence of SRF-dependence for MKL-mediated regulation of cell migration. However, recent studies open a new area to MKL signaling and MKL's role in cell physiology by demonstrating that MKL is not just a cofactor for SRF, but is also able to initiate signaling on its own through its SAP domain. This further adds to the complexity of MKL signaling and regulation of cell migration and other cellular activities. Since major finding related to SAP-domain function of MKL have been reported in overexpression settings, it is worth revisiting the importance of the SAP-domain function of MKL in its endogenous expression level through knockdown-knockin experimental strategies, and in various *in vivo* contexts, whether physiological or pathological. Although many SAP-domain-responsive genes have been identified, the key MKL-targets that are responsible for its SAP-domain-dependent modulation of cell migration are yet to be determined. Another related interesting finding is that mechanosensitive gene expression is largely governed by the SAP-domain function of MKL at least in 4T1 breast cancer cells (107,111). However, we still do not know a) whether this is a universal feature that is generalizable across cell-types and if true, what is the underlying mechanism of ECM stiffness-mediated tuning of MKL function preferentially to its SAP-directed activity, and b) whether

there are isoform-specific differences in MKL response to mechanical milieu (at least a recent study by Hadden and colleagues showed increased nuclear localization of MKL1 but not MKL2 in stem cells in response to increasing substrate stiffness (193)).

Another general exciting area for future research is to unravel novel mechanisms of MKL-mediated control of cell migration. For example, our recent findings of cellular retention control of actin-cytoskeletal regulators such as profilin downstream of MKL function and overexpression of profilin reversing the effect of MKL knockdown on breast cancer cell migration (61) established a proof-of-principle of relevance of MKL/profilin connection in cell migration and therefore offers a potential new mechanistic avenue for MKL-mediated regulation of cell migration. However, the exact mechanism of profilin release in response to loss-of-function of MKL is yet to be discovered. Possibility of exosomal release of profilin will be an interesting avenue to pursue in the future. A recent study from Kapus laboratory has shown that MKL can regulate the expression of NAPDH oxidase (NOX), a key controller of the cellular redox state (194). Given that actin polymerization, activity of Rho-GTPases (such as Rac), surface integrin expression are sensitive to perturbations of the redox state (195,196), MKL could additionally impact cell migration through controlling the redox state of the cell. Finally, there is also evidence of microRNA regulation by MKL (197). Comprehensive whole-genome transcriptome analyses in the future may reveal novel non-coding RNAs regulated by MKL that are associated with cell motility control.

7.1 DETERMINE IF CCG-1423 INHIBITION OF MKL1/SRF SIGNALING PATHWAY AFFECTS OTHER ASPECTS OF CELL MIGRATION

This dissertation has furthered our understanding of MKL activity and EC migration/angiogenesis, however, there are still much that is not completely understood. This is due to the fact that MKL/SRF controls the expression of many genes including subunits of integrin, VE-cadherin, myosin, and others. We have shown that CCG-1423 inhibition of MKL/SRF also leads to reduction of other key promotors of actin dynamics like ArpC2, VASP, and Pfn1. Through our studies, we have only demonstrated that regulation of MKL/SRF signaling is at least partly due to Pfn1 by rescue experiment (61). In addition, the degree of inhibition on sprouting angiogenesis after Pfn1 knockout is lower than the result from CCG-1423 treatment, suggesting that there may be other mechanisms in play that contribute to the regulation of angiogenesis. Previous studies did not compare phenotypic changes between loss-of-function of MKL and the putative downstream genes. Future studies should investigate whether other aspects of migration, such as adhesion or contractility, are affected by CCG-1423 inhibition of MKL. This can in part be partially accomplished by comparing changes to EC phenotype by CCG-1423 inhibition of MKL and also loss-of-function of targeted downstream genes of MKL signaling.

7.2 ELUCIDATE THE MECHANISM BEHIND PFN1 EXTERNALIZATION BY MKL1 INHIBITION

Our lab has investigated the regulation of Pfn1 by MKL1 and found that Pfn1 is not transcriptionally or translationally regulated by the MKL1 signaling pathway (61). In fact, we showed that Pfn1 is externalized upon inhibition of MKL1 by either CCG-1423 or MKL1 knockdown. The exact mechanism behind this externalization is not yet understood. One possibility for increase in externalization is through exosome release of Pfn1 into the surrounding environment. One study has shown that Pfn1 is detected in exosomes released from dendritic cells (144). This can be examined by using exosome inhibitors such as amiloride and examining whether there are any changes to Pfn1 externalization upon inhibition of MKL signaling.

7.3 OPTIMIZE C1 AND C2 TO INCREASE PFN1:ACTIN INHIBITION

We demonstrated that our novel compounds C1 and C2 have anti-migratory, anti-proliferative, and anti-angiogenic actions albeit at high treatment concentrations (50-100 μM) (191). As such, these inhibitors are considered first-generation inhibitors (due to high concentration required for activity and inability to show inhibition of Pfn1/actin via cell-based assays such as immunoprecipitation). Further SAR analysis of the compounds should be performed in the future to identify important regions of the compound for optimal binding to Pfn1. In addition, we have only been able to show inhibition of Pfn1:actin biochemically and also by PLA. A more definitive proof of compound binding and inhibiting Pfn1 activity should be examined in the

future, possibly by NMR to show compound binding to Pfn1. NMR binding data will also show the exact binding mechanism of the compound to Pfn1 and allow for further optimization of the compound to increase binding affinity to Pfn1 and in turn, inhibition of Pfn1:actin binding.

7.4 INVESTIGATE WHETHER PHOSPHORYLATION OF ANY RESIDUES ON PFN1 HAS INFLUENCE ON FURTHER POST-TRANSLATIONAL MODIFICATION ON PFN1 OR ITS BINDING ACTIVITY

We demonstrated that phosphorylation of Pfn1 on T89 has profound impact on its activity and also increases Pfn1 turnover. This suggests that phosphorylation of Pfn1 at T89 may have affected the protein structure and allowed for ubiquitination sites to open up, such as K90 (or other lysine ubiquitination sites). Future studies should investigate how phosphorylation of Pfn1 at T89 or other sites impact the overall structure of Pfn1 by at least *in silico* modeling. Furthermore, our study on T89 phosphorylation only examined Pfn1:actin binding. Future studies should also investigate whether other binding partners of Pfn1 are affected upon T89 phosphorylation. In addition, effect of PKA phosphorylation of the other sites identified in our study (S56/S57, S91/T92) on Pfn1 binding to other ligands should be investigated and connected to impact on overall cell migration as well.

APPENDIX A

APPENDIX A - SUPPLEMENTAL FIGURES

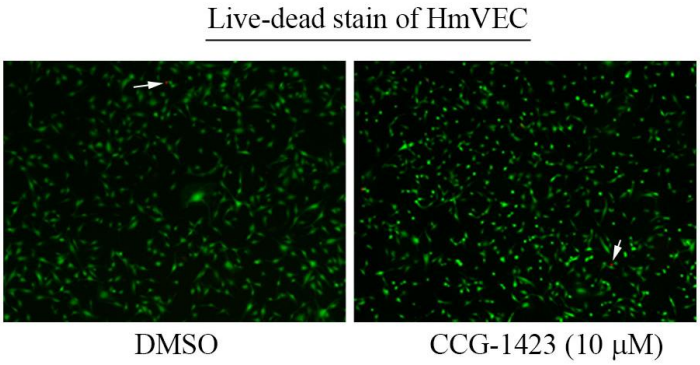

Figure S 1. Live/dead staining of HmVEC after treatment with either DMSO or CCG-1423 (10 μM). Green depicts live cells and red (arrow) shows dead cells.

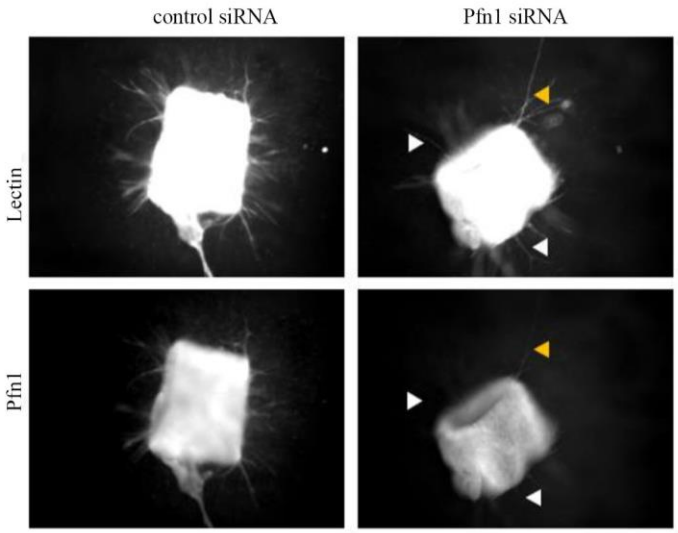

.

Figure S 2. Lectin and Pfn1 immunostaining of aortic rings treated with either control or Pfn1 siRNA (note that Pfn1-siRNA treated rings show an overall weaker staining Pfn1; white and yellow arrowheads depict sprouts with undetectable and intermediate levels of Pfn1).

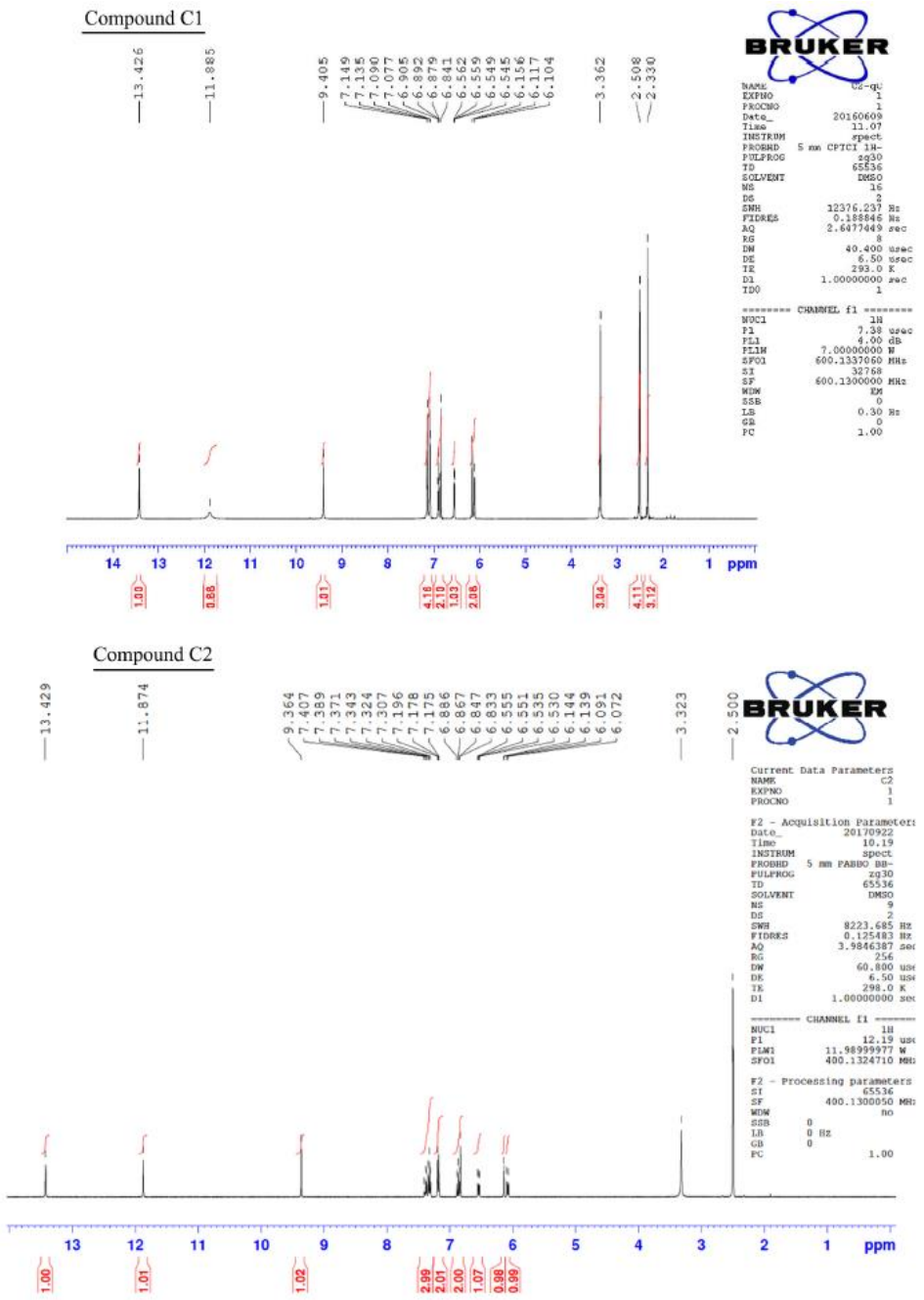

Figure S 3. 600 MHz ^{1}H NMR spectrum of compounds C1 and C2.

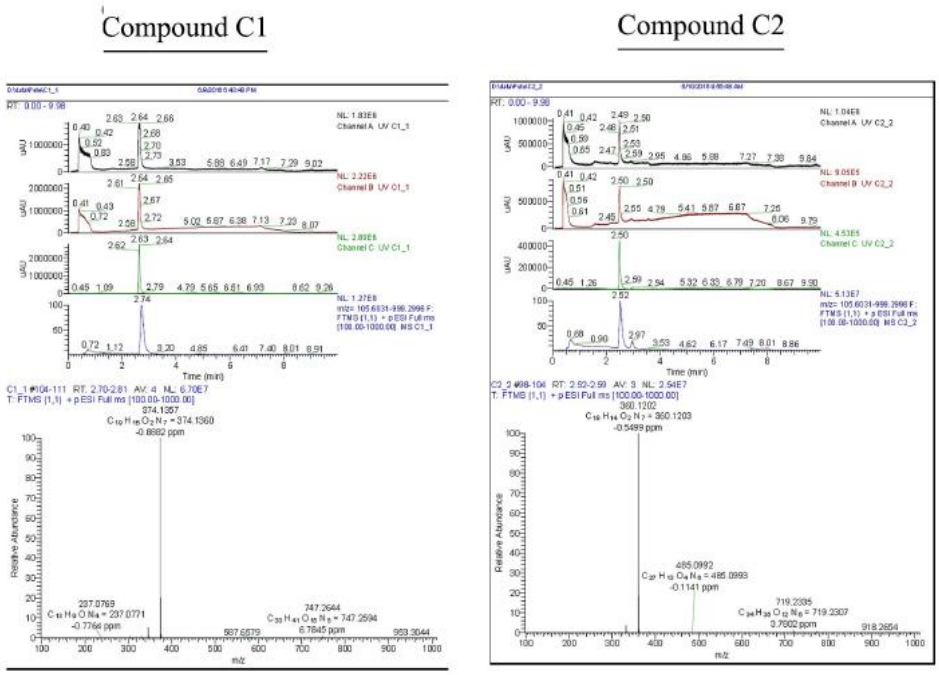

Figure S 4. LC-HRMS Data for Compounds C1 and C2. The high-resolution mass spectrum of C1 and C2 indicated the desired [M+H] mass of the respective molecular ions and was consistent with the structural assignment and >95% purity. HRMS data were obtained on a Thermo Scientific Exactive Orbitrap LC-MS (ESI positive ion mode) coupled to a Thermo Scientific Accela HPLC system using a 3.5 µm Waters XTerra C18 column (2.1 x 50 mm; 10 min gradient elution with MeCN/H_2O/MeOH containing 0.1% formic acid at a flow rate of 500 µL/min from 3:92:5 at 0-0.5 min to 93:2:5 at 4.0 min, back to 3:92:5 from 6.0 to 7.5 min).

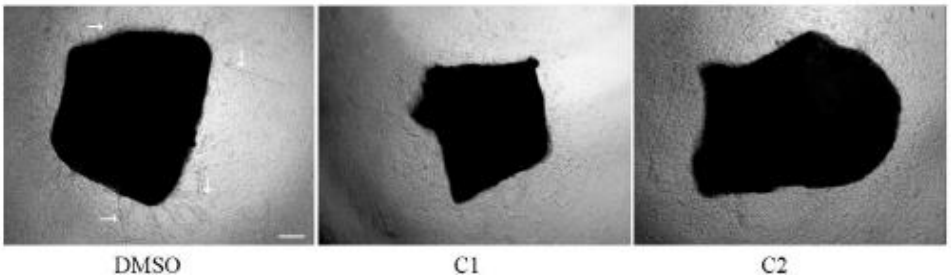

Figure S 5. Representative phase-contrast images of aortic rings subjected to either DMSO or compound (C1/C2) treatment. Arrows show endothelial sprouts (scale bar – 200 µm).

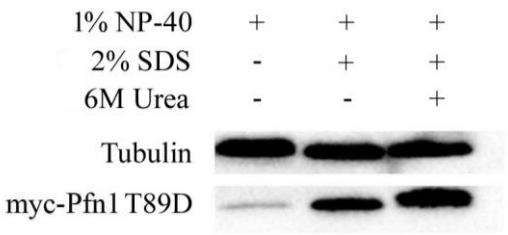

Figure S 6. HEK-293 cells expressing myc-tagged T89D-Pfn1were lysed with either non-denaturing (containing 1% NP-40) or denaturing (containing 1% NP-40, 2% SDS for one buffer and the other with 6M urea in addition) extraction buffers. Cell lysates were immunoblotted with anti-myc antibody to demonstrate that myc-tagged T89D-Pfn1 is insoluble in non-denaturing lysis buffer.

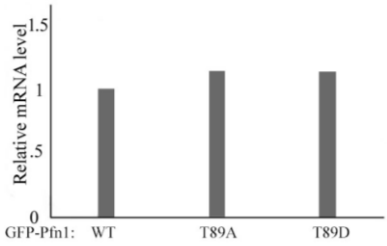

Figure S 7. Quantitative RT-PCR shows comparable mRNA levels of all three GFP-tagged Pfn1 constructs in HEK-293 cells.

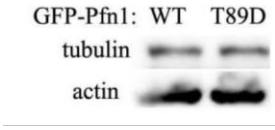

Figure S 8. Actin and tubulin (loading control) immunoblots of extracts prepared from MDA-231 cells expressing the indicated Pfn1 constructs as EGFP-tagged proteins.

APPENDIX B

APPENDIX B – PUBLICATIONS

Work from my graduate studies is represented in publications 6 – 10.

1. Ding, Z., **Gau, D.**, Deasy, B., Wells, A., and Roy, P. 2009. Both actin and polyproline interactions of profilin-1 are required for migration, invasion and capillary morphogenesis of vascular endothelial cells. Experimental Cell Research. 315(17):2963-73.
2. **Gau, D.**, Ding, Z., Baty, C., and Roy, P. 2011. Fluorescence resonance energy transfer (FRET)-based detection of Profilin-VASP interaction. Cellular and Molecular Bioengineering. 4(1):1-8.
3. Coumans, J., **Gau, D.**, Poljak, A., Wasinger, V., Roy, P., and Moens, P. Green fluorescent protein expression triggers proteome changes in breast cancer cells. Experimental Cell Research. 2014. 320(1):33-45.
4. Salvemini, I., **Gau, D.**, Reid, J., Bagatolli, L., Macmillan, A., and Moens, P. Low PIP(2) molar fractions induce nanometer size clustering in giant unilamellar vesicles. Chemistry and Physics of Lipids. 2014. 117:51-63.
5. Coumans, J., **Gau, D.**, Poljak, A., Wasinger, V., Roy, P., and Moens, P. Profilin-1 overexpression is associated with alterations in proteomic markers of cell proliferation, survival and motility of MDA-MB-231 breast cancer cells as revealed by proteomic analysis. OMICS: A Journal of Integrative Biology. 2014. 18(12):778-91.
6. **Gau, D.***, Lesnock, J.*, Hood, B., Bhargava, R., Sun, M., Darcy, K., Conrads, T., Edwards, R., Kelley, J., Krivak, T., and Roy, P. BRCA1 impacts ovarian cancer cell motility through regulating Profilin-1 expression. 2015. Cell Cycle. 14(12):1884-92. * designates co-first authors.
7. **Gau, D.***, Veon, W.*, Koes, D., Yates, N., Shroff, S., and Roy, P. Threonin 89 is an important residue of profilin-1 that is phosphorylatable by Protein Kinase A. 2016. PLoS One. https://doi.org/10.1371/journal.pone.0156313. * designates co-first authors.

8. Joy, M., **Gau, D.**, Castellucci, N., Prywes, R., and Roy, P. The myocardin-related transcription factor MKL co-regulates the cellular levels of two profilin isoforms. 2017. Journal of Biological Chemistry. 292(28):11777-11791.
9. **Gau, D.**, Veon, W., Capasso, T., Bottcher, R., Shroff, S., Roman, B., and Roy, P. Pharmacological intervention of MKL/SRF signaling by CCG-1423 impedes endothelial cell migration and angiogenesis. 2017. Angiogenesis. 20(4):663-672.
10. **Gau, D.**, Lewis, T., McDermott, L., Wipf, P., Koes, D., and Roy, P. Structure-based virtual screening identifies small molecule inhibitor of the Profilin1-actin interaction. 2018. Journal of Biological Chemistry. 293(7):2606-2616.

APPENDIX C – PRESENTATIONS

Work from my graduate studies is represented in listings 4 – 8.

1. Ding. Z, **Gau, D.**, Deasy, B., Wells, A., and Roy, P. Ligand interaction of profilin-1 in migration and capillary morphogenesis of vascular endothelial cells. Abstract for poster presentation. 2008. American Society for Cell Biology (ASCB) annual meeting.
2. **Gau, D.**, Ding, Z., Baty, C., and Roy, P. VASP-Pfn1 interaction negatively regulates breast cancer cell migration. Abstract for poster presentation. 2010. Biomedical Engineering Society and ASCB annual meeting.
3. **Gau, D.**, Salvemini, I., Reid, J., and Moens, P. Low PIP_2 molar fractions induce nanometer size clustering in giant unilamellar vesicles containing POPC. Abstract for podium talk. 2011. Australian Society for Biophysics annual meeting.
4. **Gau, D.**, Lesnock, J., Krivak, T., Edwards, R., and Roy, P. BRCA1 impacts cancer cell migration through modulating Pfn1. Abstract for poster presentation. 2014. AACR annual meeting.
5. **Gau, D.**, Veon, W., Guo, S., and Roy, P. Hyperactivation of Protein Kinase A inhibits endothelial cell migration and angiogenesis through phosphorylating and inhibiting actin-binding protein Profilin-1. Abstract for poster presentation. 2015. ASCB annual meeting.
6. **Gau, D.**, Veon, W., Capasso, T., Joy, M., Roman, B., Koes, D., and Roy, P. Small molecule-mediated inhibitions of transcriptional cofactor MKL and its downstream target profilin impedes endothelial cell migration and angiogenesis. 2016. ASCB annual meeting.
7. **Gau, D.**, Lewis, T., McDermott, L., Wipf, P., Koes, D., and Roy, P. Structure-based virtual screening identifies small molecule inhibitor of the Profilin1-actin interaction. 2017. ASCB annual meeting.
8. **Gau, D.**, Joy, M., Veon, W., Castellucci, N., Prywes, R., and Roy, P. Novel externalization of Pfn1 as a mechanism for MKL's regulation of cell migration and angiogenesis. 2017. ASCB annual meeting.

APPENDIX D – ACADEMIC AND PROFESSIONAL HONORS

Rotary Ambassadorial Scholarship, 2011

Whitaker Fellowship, 2011

Omicron Delta Kappa Senior of the Year, 2011

Valedictorian Speaker at Pitt Graduation, 2011

NSF Fellowship, 2012 – 2015

Pitt Chancellor Search Committee, 2013

Pitt Alumni Recruitment Volunteer of the Year, 2014

Cardiovascular Bioengineering Training Program, 2015 – 2017

Provost Development Fund, 2017 – 2018

BIBLIOGRAPHY

1. Carmeliet, P. (2000) Mechanisms of angiogenesis and arteriogenesis. *Nature medicine* **6**, 389-395

2. Risau, W., and Flamme, I. (1995) Vasculogenesis. *Annual review of cell and developmental biology* **11**, 73-91

3. Corliss, B. A., Azimi, M. S., Munson, J. M., Peirce, S. M., and Murfee, W. L. (2016) Macrophages: An Inflammatory Link Between Angiogenesis and Lymphangiogenesis. *Microcirculation* **23**, 95-121

4. Stockmann, C., Kirmse, S., Helfrich, I., Weidemann, A., Takeda, N., Doedens, A., and Johnson, R. S. (2011) A wound size-dependent effect of myeloid cell-derived vascular endothelial growth factor on wound healing. *The Journal of investigative dermatology* **131**, 797-801

5. Hellstrom, M., Phng, L. K., Hofmann, J. J., Wallgard, E., Coultas, L., Lindblom, P., Alva, J., Nilsson, A. K., Karlsson, L., Gaiano, N., Yoon, K., Rossant, J., Iruela-Arispe, M. L., Kalen, M., Gerhardt, H., and Betsholtz, C. (2007) Dll4 signalling through Notch1 regulates formation of tip cells during angiogenesis. *Nature* **445**, 776-780

6. Carmeliet, P. (2003) Angiogenesis in health and disease. *Nature medicine* **9**, 653-660

7. Ferrara, N., Gerber, H. P., and LeCouter, J. (2003) The biology of VEGF and its receptors. *Nature medicine* **9**, 669-676

8. Bauer, S. M., Bauer, R. J., and Velazquez, O. C. (2005) Angiogenesis, vasculogenesis, and induction of healing in chronic wounds. *Vascular and endovascular surgery* **39**, 293-306

9. Chrzanowska-Wodnicka, M., Kraus, A. E., Gale, D., White, G. C., 2nd, and Vansluys, J. (2008) Defective angiogenesis, endothelial migration, proliferation, and MAPK signaling in Rap1b-deficient mice. *Blood* **111**, 2647-2656

10. Brouty-Boye, D., and Zetter, B. R. (1980) Inhibition of cell motility by interferon. *Science* **208**, 516-518

11. Starzec, A., Vassy, R., Martin, A., Lecouvey, M., Di Benedetto, M., Crepin, M., and Perret, G. Y. (2006) Antiangiogenic and antitumor activities of peptide inhibiting the vascular endothelial growth factor binding to neuropilin-1. *Life sciences* **79**, 2370-2381

12. Xu, Y., Zhao, H., Zheng, Y., Gu, Q., Ma, J., and Xu, X. (2010) A novel antiangiogenic peptide derived from hepatocyte growth factor inhibits neovascularization in vitro and in vivo. *Molecular vision* **16**, 1982-1995

13. Connolly, J. O., Simpson, N., Hewlett, L., and Hall, A. (2002) Rac regulates endothelial morphogenesis and capillary assembly. *Molecular biology of the cell* **13**, 2474-2485

14. Park, H. J., Kong, D., Iruela-Arispe, L., Begley, U., Tang, D., and Galper, J. B. (2002) 3-hydroxy-3-methylglutaryl coenzyme A reductase inhibitors interfere with angiogenesis by inhibiting the geranylgeranylation of RhoA. *Circulation research* **91**, 143-150

15. Gerhardt, H., Golding, M., Fruttiger, M., Ruhrberg, C., Lundkvist, A., Abramsson, A., Jeltsch, M., Mitchell, C., Alitalo, K., Shima, D., and Betsholtz, C. (2003) VEGF guides angiogenic sprouting utilizing endothelial tip cell filopodia. *The Journal of cell biology* **161**, 1163-1177

16. Yamazaki, D., Suetsugu, S., Miki, H., Kataoka, Y., Nishikawa, S., Fujiwara, T., Yoshida, N., and Takenawa, T. (2003) WAVE2 is required for directed cell migration and cardiovascular development. *Nature* **424**, 452-456

17. van Nieuw Amerongen, G. P., Koolwijk, P., Versteilen, A., and van Hinsbergh, V. W. (2003) Involvement of RhoA/Rho kinase signaling in VEGF-induced endothelial cell migration and angiogenesis in vitro. *Arteriosclerosis, thrombosis, and vascular biology* **23**, 211-217

18. Franco, C. A., Mericskay, M., Parlakian, A., Gary-Bobo, G., Gao-Li, J., Paulin, D., Gustafsson, E., and Li, Z. (2008) Serum response factor is required for sprouting angiogenesis and vascular integrity. *Developmental cell* **15**, 448-461

19. Herbert, S. P., and Stainier, D. Y. (2011) Molecular control of endothelial cell behaviour during blood vessel morphogenesis. *Nature reviews. Molecular cell biology* **12**, 551-564

20. Le Clainche, C., and Carlier, M. F. (2008) Regulation of actin assembly associated with protrusion and adhesion in cell migration. *Physiological reviews* **88**, 489-513

21. Sheetz, M. P., Felsenfeld, D., Galbraith, C. G., and Choquet, D. (1999) Cell migration as a five-step cycle. *Biochemical Society symposium* **65**, 233-243

22. Small, J. V., Stradal, T., Vignal, E., and Rottner, K. (2002) The lamellipodium: where motility begins. *Trends in cell biology* **12**, 112-120

23. Bezanilla, M., Gladfelter, A. S., Kovar, D. R., and Lee, W. L. (2015) Cytoskeletal dynamics: a view from the membrane. *The Journal of cell biology* **209**, 329-337

24. Norman, C., Runswick, M., Pollock, R., and Treisman, R. (1988) Isolation and properties of cDNA clones encoding SRF, a transcription factor that binds to the c-fos serum response element. *Cell* **55**, 989-1003

25. Khachigian, L. M., and Collins, T. (1997) Inducible expression of Egr-1-dependent genes. A paradigm of transcriptional activation in vascular endothelium. *Circulation research* **81**, 457-461

26. Olson, E. N., and Nordheim, A. (2010) Linking actin dynamics and gene transcription to drive cellular motile functions. *Nature reviews. Molecular cell biology* **11**, 353-365

27. Sun, Q., Chen, G., Streb, J. W., Long, X., Yang, Y., Stoeckert, C. J., Jr., and Miano, J. M. (2006) Defining the mammalian CArGome. *Genome research* **16**, 197-207

28. Zinck, R., Hipskind, R. A., Pingoud, V., and Nordheim, A. (1993) c-fos transcriptional activation and repression correlate temporally with the phosphorylation status of TCF. *The EMBO journal* **12**, 2377-2387

29. Hill, C. S., Wynne, J., and Treisman, R. (1995) The Rho family GTPases RhoA, Rac1, and CDC42Hs regulate transcriptional activation by SRF. *Cell* **81**, 1159-1170

30. Miralles, F., Posern, G., Zaromytidou, A. I., and Treisman, R. (2003) Actin dynamics control SRF activity by regulation of its coactivator MAL. *Cell* **113**, 329-342

31. Wang, Z., Wang, D. Z., Hockemeyer, D., McAnally, J., Nordheim, A., and Olson, E. N. (2004) Myocardin and ternary complex factors compete for SRF to control smooth muscle gene expression. *Nature* **428**, 185-189

32. Ma, Z., Morris, S. W., Valentine, V., Li, M., Herbrick, J. A., Cui, X., Bouman, D., Li, Y., Mehta, P. K., Nizetic, D., Kaneko, Y., Chan, G. C., Chan, L. C., Squire, J., Scherer, S. W., and Hitzler, J. K. (2001) Fusion of two novel genes, RBM15 and MKL1, in the t(1;22)(p13;q13) of acute megakaryoblastic leukemia. *Nature genetics* **28**, 220-221

33. Buchwalter, G., Gross, C., and Wasylyk, B. (2004) Ets ternary complex transcription factors. *Gene* **324**, 1-14

34. Cen, B., Selvaraj, A., and Prywes, R. (2004) Myocardin/MKL family of SRF coactivators: key regulators of immediate early and muscle specific gene expression. *J Cell Biochem* **93**, 74-82

35. Pipes, G. C., Creemers, E. E., and Olson, E. N. (2006) The myocardin family of transcriptional coactivators: versatile regulators of cell growth, migration, and myogenesis. *Genes & development* **20**, 1545-1556

36. Posern, G., and Treisman, R. (2006) Actin' together: serum response factor, its cofactors and the link to signal transduction. *Trends in cell biology* **16**, 588-596

37. Gasparics, A., and Sebe, A. (2018) MRTFs- master regulators of EMT. *Developmental dynamics : an official publication of the American Association of Anatomists* **247**, 396-404

38. Hendzel, M. J. (2014) The F-act's of nuclear actin. *Current opinion in cell biology* **28**, 84-89

39. Miller, K. G. (2002) Extending the Arp2/3 complex and its regulation beyond the leading edge. *The Journal of cell biology* **156**, 591-593

40. Zaromytidou, A. I., Miralles, F., and Treisman, R. (2006) MAL and ternary complex factor use different mechanisms to contact a common surface on the serum response factor DNA-binding domain. *Molecular and cellular biology* **26**, 4134-4148

41. Imamura, M., Long, X., Nanda, V., and Miano, J. M. (2010) Expression and functional activity of four myocardin isoforms. *Gene* **464**, 1-10

42. Parmacek, M. S. (2007) Myocardin-related transcription factors: critical coactivators regulating cardiovascular development and adaptation. *Circulation research* **100**, 633-644

43. Vartiainen, M. K., Guettler, S., Larijani, B., and Treisman, R. (2007) Nuclear actin regulates dynamic subcellular localization and activity of the SRF cofactor MAL. *Science* **316**, 1749-1752

44. Posern, G., Miralles, F., Guettler, S., and Treisman, R. (2004) Mutant actins that stabilise F-actin use distinct mechanisms to activate the SRF coactivator MAL. *The EMBO journal* **23**, 3973-3983

45. Mouilleron, S., Guettler, S., Langer, C. A., Treisman, R., and McDonald, N. Q. (2008) Molecular basis for G-actin binding to RPEL motifs from the serum response factor coactivator MAL. *The EMBO journal* **27**, 3198-3208

46. Muehlich, S., Wang, R., Lee, S. M., Lewis, T. C., Dai, C., and Prywes, R. (2008) Serum-induced phosphorylation of the serum response factor coactivator MKL1 by the extracellular signal-regulated kinase 1/2 pathway inhibits its nuclear localization. *Molecular and cellular biology* **28**, 6302-6313

47. Cen, B., Selvaraj, A., Burgess, R. C., Hitzler, J. K., Ma, Z., Morris, S. W., and Prywes, R. (2003) Megakaryoblastic leukemia 1, a potent transcriptional coactivator for serum response factor (SRF), is required for serum induction of SRF target genes. *Molecular and cellular biology* **23**, 6597-6608

48. Sun, Y., Boyd, K., Xu, W., Ma, J., Jackson, C. W., Fu, A., Shillingford, J. M., Robinson, G. W., Hennighausen, L., Hitzler, J. K., Ma, Z., and Morris, S. W. (2006) Acute myeloid leukemia-associated Mkl1 (Mrtf-a) is a key regulator of mammary gland function. *Molecular and cellular biology* **26**, 5809-5826

49. Sotiropoulos, A., Gineitis, D., Copeland, J., and Treisman, R. (1999) Signal-regulated activation of serum response factor is mediated by changes in actin dynamics. *Cell* **98**, 159-169

50. Duggirala, A., Kimura, T. E., Sala-Newby, G. B., Johnson, J. L., Wu, Y. J., Newby, A. C., and Bond, M. (2015) cAMP-induced actin cytoskeleton remodelling inhibits MKL1-dependent expression of the chemotactic and pro-proliferative factor, CCN1. *Journal of molecular and cellular cardiology* **79**, 157-168

51. Wang, D., Chang, P. S., Wang, Z., Sutherland, L., Richardson, J. A., Small, E., Krieg, P. A., and Olson, E. N. (2001) Activation of cardiac gene expression by myocardin, a transcriptional cofactor for serum response factor. *Cell* **105**, 851-862

52. Guettler, S., Vartiainen, M. K., Miralles, F., Larijani, B., and Treisman, R. (2008) RPEL motifs link the serum response factor cofactor MAL but not myocardin to Rho signaling via actin binding. *Molecular and cellular biology* **28**, 732-742

53. Nakamura, S., Hayashi, K., Iwasaki, K., Fujioka, T., Egusa, H., Yatani, H., and Sobue, K. (2010) Nuclear import mechanism for myocardin family members and their correlation with vascular smooth muscle cell phenotype. *The Journal of biological chemistry* **285**, 37314-37323

54. Hayashi, K., and Morita, T. (2013) Differences in the nuclear export mechanism between myocardin and myocardin-related transcription factor A. *The Journal of biological chemistry* **288**, 5743-5755

55. Kokai, E., Beck, H., Weissbach, J., Arnold, F., Sinske, D., Sebert, U., Gaiselmann, G., Schmidt, V., Walther, P., Munch, J., Posern, G., and Knoll, B. (2014) Analysis of nuclear actin by overexpression of wild-type and actin mutant proteins. *Histochemistry and cell biology* **141**, 123-135

56. Baarlink, C., Wang, H., and Grosse, R. (2013) Nuclear actin network assembly by formins regulates the SRF coactivator MAL. *Science* **340**, 864-867

57. Plessner, M., Melak, M., Chinchilla, P., Baarlink, C., and Grosse, R. (2015) Nuclear F-actin formation and reorganization upon cell spreading. *J Biol Chem* **290**, 11209-11216

58. Lundquist, M. R., Storaska, A. J., Liu, T. C., Larsen, S. D., Evans, T., Neubig, R. R., and Jaffrey, S. R. (2014) Redox modification of nuclear actin by MICAL-2 regulates SRF signaling. *Cell* **156**, 563-576

59. Weissbach, J., Schikora, F., Weber, A., Kessels, M., and Posern, G. (2016) Myocardin-Related Transcription Factor A Activation by Competition with WH2 Domain Proteins for Actin Binding. *Molecular and cellular biology* **36**, 1526-1539

60. Kircher, P., Hermanns, C., Nossek, M., Drexler, M. K., Grosse, R., Fischer, M., Sarikas, A., Penkava, J., Lewis, T., Prywes, R., Gudermann, T., and Muehlich, S. (2015) Filamin

A interacts with the coactivator MKL1 to promote the activity of the transcription factor SRF and cell migration. *Science signaling* **8**, ra112

61. Joy, M., Gau, D., Castellucci, N., Prywes, R., and Roy, P. (2017) The myocardin-related transcription factor MKL co-regulates the cellular levels of two profilin isoforms. *The Journal of biological chemistry* **292**, 11777-11791

62. Somogyi, K., and Rorth, P. (2004) Evidence for tension-based regulation of Drosophila MAL and SRF during invasive cell migration. *Developmental cell* **7**, 85-93

63. Han, Z., Li, X., Wu, J., and Olson, E. N. (2004) A myocardin-related transcription factor regulates activity of serum response factor in Drosophila. *Proceedings of the National Academy of Sciences of the United States of America* **101**, 12567-12572

64. Arsenian, S., Weinhold, B., Oelgeschlager, M., Ruther, U., and Nordheim, A. (1998) Serum response factor is essential for mesoderm formation during mouse embryogenesis. *The EMBO journal* **17**, 6289-6299

65. Parlakian, A., Tuil, D., Hamard, G., Tavernier, G., Hentzen, D., Concordet, J. P., Paulin, D., Li, Z., and Daegelen, D. (2004) Targeted inactivation of serum response factor in the developing heart results in myocardial defects and embryonic lethality. *Molecular and cellular biology* **24**, 5281-5289

66. Sun, K., Battle, M. A., Misra, R. P., and Duncan, S. A. (2009) Hepatocyte expression of serum response factor is essential for liver function, hepatocyte proliferation and survival, and postnatal body growth in mice. *Hepatology* **49**, 1645-1654

67. Li, S., Czubryt, M. P., McAnally, J., Bassel-Duby, R., Richardson, J. A., Wiebel, F. F., Nordheim, A., and Olson, E. N. (2005) Requirement for serum response factor for skeletal muscle growth and maturation revealed by tissue-specific gene deletion in mice. *Proceedings of the National Academy of Sciences of the United States of America* **102**, 1082-1087

68. Stringer, J. L., Belaguli, N. S., Iyer, D., Schwartz, R. J., and Balasubramanyam, A. (2002) Developmental expression of serum response factor in the rat central nervous system. *Brain Res Dev Brain Res* **138**, 81-86

69. Li, S., Chang, S., Qi, X., Richardson, J. A., and Olson, E. N. (2006) Requirement of a myocardin-related transcription factor for development of mammary myoepithelial cells. *Molecular and cellular biology* **26**, 5797-5808

70. Oh, J., Richardson, J. A., and Olson, E. N. (2005) Requirement of myocardin-related transcription factor-B for remodeling of branchial arch arteries and smooth muscle differentiation. *Proceedings of the National Academy of Sciences of the United States of America* **102**, 15122-15127

71. Alberti, S., Krause, S. M., Kretz, O., Philippar, U., Lemberger, T., Casanova, E., Wiebel, F. F., Schwarz, H., Frotscher, M., Schutz, G., and Nordheim, A. (2005) Neuronal

migration in the murine rostral migratory stream requires serum response factor. *Proceedings of the National Academy of Sciences of the United States of America* **102**, 6148-6153

72. Knoll, B., Kretz, O., Fiedler, C., Alberti, S., Schutz, G., Frotscher, M., and Nordheim, A. (2006) Serum response factor controls neuronal circuit assembly in the hippocampus. *Nat Neurosci* **9**, 195-204

73. Mokalled, M. H., Johnson, A., Kim, Y., Oh, J., and Olson, E. N. (2010) Myocardin-related transcription factors regulate the Cdk5/Pctaire1 kinase cascade to control neurite outgrowth, neuronal migration and brain development. *Development* **137**, 2365-2374

74. Velasquez, L. S., Sutherland, L. B., Liu, Z., Grinnell, F., Kamm, K. E., Schneider, J. W., Olson, E. N., and Small, E. M. (2013) Activation of MRTF-A-dependent gene expression with a small molecule promotes myofibroblast differentiation and wound healing. *Proceedings of the National Academy of Sciences of the United States of America* **110**, 16850-16855

75. Trembley, M. A., Velasquez, L. S., de Mesy Bentley, K. L., and Small, E. M. (2015) Myocardin-related transcription factors control the motility of epicardium-derived cells and the maturation of coronary vessels. *Development* **142**, 21-30

76. Brandt, D. T., Baarlink, C., Kitzing, T. M., Kremmer, E., Ivaska, J., Nollau, P., and Grosse, R. (2009) SCAI acts as a suppressor of cancer cell invasion through the transcriptional control of beta1-integrin. *Nature cell biology* **11**, 557-568

77. Lei, H., Wu, D., Wang, J. Y., Li, L., Zhang, C. L., Feng, H., Fu, F. Y., and Wu, L. L. (2015) C1q/tumor necrosis factor-related protein-6 attenuates post-infarct cardiac fibrosis by targeting RhoA/MRTF-A pathway and inhibiting myofibroblast differentiation. *Basic research in cardiology* **110**, 35

78. Minami, T., Kuwahara, K., Nakagawa, Y., Takaoka, M., Kinoshita, H., Nakao, K., Kuwabara, Y., Yamada, Y., Yamada, C., Shibata, J., Usami, S., Yasuno, S., Nishikimi, T., Ueshima, K., Sata, M., Nakano, H., Seno, T., Kawahito, Y., Sobue, K., Kimura, A., Nagai, R., and Nakao, K. (2012) Reciprocal expression of MRTF-A and myocardin is crucial for pathological vascular remodelling in mice. *The EMBO journal* **31**, 4428-4440

79. Zabini, D., Granton, E., Hu, Y., Miranda, M. Z., Weichelt, U., Breuils Bonnet, S., Bonnet, S., Morrell, N. W., Connelly, K. A., Provencher, S., Ghanim, B., Klepetko, W., Olschewski, A., Kapus, A., and Kuebler, W. M. (2017) Loss of SMAD3 Promotes Vascular Remodeling in Pulmonary Arterial Hypertension via MRTF Disinhibition. *American journal of respiratory and critical care medicine*

80. Record, J., Malinova, D., Zenner, H. L., Plagnol, V., Nowak, K., Syed, F., Bouma, G., Curtis, J., Gilmour, K., Cale, C., Hackett, S., Charras, G., Moulding, D., Nejentsev, S., Thrasher, A. J., and Burns, S. O. (2015) Immunodeficiency and severe susceptibility to bacterial infection associated with a loss-of-function homozygous mutation of MKL1. *Blood* **126**, 1527-1535

81. Stapor, P., Wang, X., Goveia, J., Moens, S., and Carmeliet, P. (2014) Angiogenesis revisited - role and therapeutic potential of targeting endothelial metabolism. *Journal of cell science* **127**, 4331-4341

82. Franco, C. A., Blanc, J., Parlakian, A., Blanco, R., Aspalter, I. M., Kazakova, N., Diguet, N., Mylonas, E., Gao-Li, J., Vaahtokari, A., Penard-Lacronique, V., Fruttiger, M., Rosewell, I., Mericskay, M., Gerhardt, H., and Li, Z. (2013) SRF selectively controls tip cell invasive behavior in angiogenesis. *Development* **140**, 2321-2333

83. Franco, C. A., and Li, Z. (2009) SRF in angiogenesis: branching the vascular system. *Cell adhesion & migration* **3**, 264-267

84. Hinkel, R., Trenkwalder, T., Petersen, B., Husada, W., Gesenhues, F., Lee, S., Hannappel, E., Bock-Marquette, I., Theisen, D., Leitner, L., Boekstegers, P., Cierniewski, C., Muller, O. J., le Noble, F., Adams, R. H., Weinl, C., Nordheim, A., Reichart, B., Weber, C., Olson, E., Posern, G., Deindl, E., Niemann, H., and Kupatt, C. (2014) MRTF-A controls vessel growth and maturation by increasing the expression of CCN1 and CCN2. *Nature communications* **5**, 3970

85. Weinl, C., Riehle, H., Park, D., Stritt, C., Beck, S., Huber, G., Wolburg, H., Olson, E. N., Seeliger, M. W., Adams, R. H., and Nordheim, A. (2013) Endothelial SRF/MRTF ablation causes vascular disease phenotypes in murine retinae. *The Journal of clinical investigation* **123**, 2193-2206

86. Evelyn, C. R., Wade, S. M., Wang, Q., Wu, M., Iniguez-Lluhi, J. A., Merajver, S. D., and Neubig, R. R. (2007) CCG-1423: a small-molecule inhibitor of RhoA transcriptional signaling. *Molecular cancer therapeutics* **6**, 2249-2260

87. Hayashi, K., Watanabe, B., Nakagawa, Y., Minami, S., and Morita, T. (2014) RPEL proteins are the molecular targets for CCG-1423, an inhibitor of Rho signaling. *PloS one* **9**, e89016

88. Gau, D., Veon, W., Capasso, T. L., Bottcher, R., Shroff, S., Roman, B. L., and Roy, P. (2017) Pharmacological intervention of MKL/SRF signaling by CCG-1423 impedes endothelial cell migration and angiogenesis. *Angiogenesis* **20**, 663-672

89. Shu, X. Z., Zhang, L. N., Zhang, R., Zhang, C. J., He, H. P., Zhou, H., Wang, N., and Zhang, T. C. (2015) Histone acetyltransferase p300 promotes MRTF-A-mediates transactivation of VE-cadherin gene in human umbilical vein endothelial cells. *Gene* **563**, 17-23

90. Medjkane, S., Perez-Sanchez, C., Gaggioli, C., Sahai, E., and Treisman, R. (2009) Myocardin-related transcription factors and SRF are required for cytoskeletal dynamics and experimental metastasis. *Nature cell biology* **11**, 257-268

91. Zhang, R., Wang, N., Zhang, M., Zhang, L. N., Guo, Z. X., Luo, X. G., Zhou, H., He, H. P., and Zhang, T. C. (2015) Rho/MRTF-A-Induced Integrin Expression Regulates

Angiogenesis in Differentiated Multipotent Mesenchymal Stem Cells. *Stem cells international* **2015**, 534758

92. Evelyn, C. R., Bell, J. L., Ryu, J. G., Wade, S. M., Kocab, A., Harzdorf, N. L., Showalter, H. D., Neubig, R. R., and Larsen, S. D. (2010) Design, synthesis and prostate cancer cell-based studies of analogs of the Rho/MKL1 transcriptional pathway inhibitor, CCG-1423. *Bioorganic & medicinal chemistry letters* **20**, 665-672

93. Evelyn, C. R., Lisabeth, E. M., Wade, S. M., Haak, A. J., Johnson, C. N., Lawlor, E. R., and Neubig, R. R. (2016) Small-Molecule Inhibition of Rho/MKL/SRF Transcription in Prostate Cancer Cells: Modulation of Cell Cycle, ER Stress, and Metastasis Gene Networks. *Microarrays* **5**

94. Haak, A. J., Appleton, K. M., Lisabeth, E. M., Misek, S. A., Ji, Y., Wade, S. M., Bell, J. L., Rockwell, C. E., Airik, M., Krook, M. A., Larsen, S. D., Verhaegen, M., Lawlor, E. R., and Neubig, R. R. (2017) Pharmacological Inhibition of Myocardin-related Transcription Factor Pathway Blocks Lung Metastases of RhoC-Overexpressing Melanoma. *Molecular cancer therapeutics* **16**, 193-204

95. Watanabe, B., Minami, S., Ishida, H., Yoshioka, R., Nakagawa, Y., Morita, T., and Hayashi, K. (2015) Stereospecific Inhibitory Effects of CCG-1423 on the Cellular Events Mediated by Myocardin-Related Transcription Factor A. *PloS one* **10**, e0136242

96. Zhang, C., Luo, X., Liu, L., Guo, S., Zhao, W., Mu, A., Liu, Z., Wang, N., Zhou, H., and Zhang, T. (2013) Myocardin-related transcription factor A is up-regulated by 17beta-estradiol and promotes migration of MCF-7 breast cancer cells via transactivation of MYL9 and CYR61. *Acta biochimica et biophysica Sinica* **45**, 921-927

97. Luo, X. G., Zhang, C. L., Zhao, W. W., Liu, Z. P., Liu, L., Mu, A., Guo, S., Wang, N., Zhou, H., and Zhang, T. C. (2014) Histone methyltransferase SMYD3 promotes MRTF-A-mediated transactivation of MYL9 and migration of MCF-7 breast cancer cells. *Cancer letters* **344**, 129-137

98. Liao, X. H., Wang, N., Liu, L. Y., Zheng, L., Xing, W. J., Zhao, D. W., Sun, X. G., Hu, P., Dong, J., and Zhang, T. C. (2014) MRTF-A and STAT3 synergistically promote breast cancer cell migration. *Cellular signalling* **26**, 2370-2380

99. Xing, W. J., Liao, X. H., Wang, N., Zhao, D. W., Zheng, L., Zheng, D. L., Dong, J., and Zhang, T. C. (2015) MRTF-A and STAT3 promote MDA-MB-231 cell migration via hypermethylating BRSM1. *IUBMB life* **67**, 202-217

100. Xiang, Y., Liao, X. H., Yu, C. X., Yao, A., Qin, H., Li, J. P., Hu, P., Li, H., Guo, W., Gu, C. J., and Zhang, T. C. (2017) MiR-93-5p inhibits the EMT of breast cancer cells via targeting MKL-1 and STAT3. *Experimental cell research* **357**, 135-144

101. Xiang, Y., Liao, X. H., Yao, A., Qin, H., Fan, L. J., Li, J. P., Hu, P., Li, H., Guo, W., Li, J. Y., Gu, C. J., Bao, L. Y., and Zhang, T. C. (2017) MRTF-A-miR-206-WDR1 form

feedback loop to regulate breast cancer cell migration. *Experimental cell research* **359**, 394-404

102. Zhuang, C., Yuan, Y., Song, T., Wang, H., Huang, L., Luo, X., He, H., Huo, L., Zhou, H., Wang, N., and Zhang, T. (2017) miR-219a-5p inhibits breast cancer cell migration and epithelial-mesenchymal transition by targeting myocardin-related transcription factor A. *Acta biochimica et biophysica Sinica* **49**, 1112-1121

103. Subramaniam, V., Ace, O., Prud'homme, G. J., and Jothy, S. (2011) Tranilast treatment decreases cell growth, migration and inhibits colony formation of human breast cancer cells. *Experimental and molecular pathology* **90**, 116-122

104. Jurmeister, S., Baumann, M., Balwierz, A., Keklikoglou, I., Ward, A., Uhlmann, S., Zhang, J. D., Wiemann, S., and Sahin, O. (2012) MicroRNA-200c represses migration and invasion of breast cancer cells by targeting actin-regulatory proteins FHOD1 and PPM1F. *Molecular and cellular biology* **32**, 633-651

105. Zhang, W. L., Lv, W., Sun, S. Z., Wu, X. Z., and Zhang, J. H. (2015) miR-206 inhibits metastasis-relevant traits by degrading MRTF-A in anaplastic thyroid cancer. *International journal of oncology* **47**, 133-142

106. Peippo, M., Gardberg, M., Lamminen, T., Kaipio, K., Carpen, O., and Heuser, V. D. (2017) FHOD1 formin is upregulated in melanomas and modifies proliferation and tumor growth. *Experimental cell research* **350**, 267-278

107. Asparuhova, M. B., Secondini, C., Ruegg, C., and Chiquet-Ehrismann, R. (2015) Mechanism of irradiation-induced mammary cancer metastasis: A role for SAP-dependent Mkl1 signaling. *Molecular oncology* **9**, 1510-1527

108. Leitner, L., Shaposhnikov, D., Mengel, A., Descot, A., Julien, S., Hoffmann, R., and Posern, G. (2011) MAL/MRTF-A controls migration of non-invasive cells by upregulation of cytoskeleton-associated proteins. *Journal of cell science* **124**, 4318-4331

109. Kishi, T., Mayanagi, T., Iwabuchi, S., Akasaka, T., and Sobue, K. (2016) Myocardin-related transcription factor A (MRTF-A) activity-dependent cell adhesion is correlated to focal adhesion kinase (FAK) activity. *Oncotarget* **7**, 72113-72130

110. Smith, E. C., Thon, J. N., Devine, M. T., Lin, S., Schulz, V. P., Guo, Y., Massaro, S. A., Halene, S., Gallagher, P., Italiano, J. E., Jr., and Krause, D. S. (2012) MKL1 and MKL2 play redundant and crucial roles in megakaryocyte maturation and platelet formation. *Blood* **120**, 2317-2329

111. Gurbuz, I., Ferralli, J., Roloff, T., Chiquet-Ehrismann, R., and Asparuhova, M. B. (2014) SAP domain-dependent Mkl1 signaling stimulates proliferation and cell migration by induction of a distinct gene set indicative of poor prognosis in breast cancer patients. *Molecular cancer* **13**, 22

112. Carlsson, L., Nystrom, L. E., Sundkvist, I., Markey, F., and Lindberg, U. (1977) Actin polymerizability is influenced by profilin, a low molecular weight protein in non-muscle cells. *Journal of molecular biology* **115**, 465-483

113. Witke, W., Sutherland, J. D., Sharpe, A., Arai, M., and Kwiatkowski, D. J. (2001) Profilin I is essential for cell survival and cell division in early mouse development. *Proceedings of the National Academy of Sciences of the United States of America* **98**, 3832-3836

114. Reichstein, E., and Korn, E. D. (1979) Acanthamoeba Profilin - Protein of Low-Molecular Weight from Acanthamoeba-Castellanii That Inhibits Actin Nucleation. *Journal of Biological Chemistry* **254**, 6174-6179

115. Grumet, M., Loonsk, J., and Lin, S. (1980) Characterization of a Platelet Protein with Cytochalasin-Like Activity. *Journal of Cell Biology* **87**, A217-A217

116. Mockrin, S. C., and Korn, E. D. (1980) Acanthamoeba Profilin Interacts with G-Actin to Increase the Rate of Exchange of Actin-Bound Adenosine 5'-Triphosphate. *Biochemistry* **19**, 5359-5362

117. Pring, M., Weber, A., and Bubb, M. R. (1992) Profilin-actin complexes directly elongate actin filaments at the barbed end. *Biochemistry* **31**, 1827-1836

118. Pantaloni, D., and Carlier, M. F. (1993) How profilin promotes actin filament assembly in the presence of thymosin beta 4. *Cell* **75**, 1007-1014

119. Theriot, J. A., Rosenblatt, J., Portnoy, D. A., Goldschmidt-Clermont, P. J., and Mitchison, T. J. (1994) Involvement of profilin in the actin-based motility of L. monocytogenes in cells and in cell-free extracts. *Cell* **76**, 505-517

120. Buss, F., Temm-Grove, C., Henning, S., and Jockusch, B. M. (1992) Distribution of profilin in fibroblasts correlates with the presence of highly dynamic actin filaments. *Cell motility and the cytoskeleton* **22**, 51-61

121. Ding, Z., Lambrechts, A., Parepally, M., and Roy, P. (2006) Silencing profilin-1 inhibits endothelial cell proliferation, migration and cord morphogenesis. *Journal of cell science* **119**, 4127-4137

122. Ding, Z., Gau, D., Deasy, B., Wells, A., and Roy, P. (2009) Both actin and polyproline interactions of profilin-1 are required for migration, invasion and capillary morphogenesis of vascular endothelial cells. *Experimental cell research* **315**, 2963-2973

123. Fan, Y., Arif, A., Gong, Y., Jia, J., Eswarappa, S. M., Willard, B., Horowitz, A., Graham, L. M., Penn, M. S., and Fox, P. L. (2012) Stimulus-dependent phosphorylation of profilin-1 in angiogenesis. *Nature cell biology* **14**, 1046-1056

124. Bae, Y. H., Ding, Z., Das, T., Wells, A., Gertler, F., and Roy, P. (2010) Profilin1 regulates PI(3,4)P2 and lamellipodin accumulation at the leading edge thus influencing

motility of MDA-MB-231 cells. *Proceedings of the National Academy of Sciences of the United States of America* **107**, 21547-21552

125. Hansson, A., Skoglund, G., Lassing, I., Lindberg, U., and Ingelman-Sundberg, M. (1988) Protein kinase C-dependent phosphorylation of profilin is specifically stimulated by phosphatidylinositol bisphosphate (PIP2). *Biochemical and biophysical research communications* **150**, 526-531

126. Vemuri, B., and Singh, S. S. (2001) Protein kinase C isozyme-specific phosphorylation of profilin. *Cellular signalling* **13**, 433-439

127. Satish, K., Padma, B., Munugalavadla, V., Bhargavi, V., Radhika, K., Wasia, R., Sairam, M., and Singh, S. (2004) Phosphorylation of profilin regulates its interaction with actin and poly (L-proline). *Cell Signalling* **16**, 589-596

128. Rizwani, W., Fasim, A., Sharma, D., Reddy, D. J., Bin Omar, N. A., and Singh, S. S. (2014) S137 phosphorylation of profilin 1 is an important signaling event in breast cancer progression. *PloS one* **9**, e103868

129. Shao, J., Welch, W. J., Diprospero, N. A., and Diamond, M. I. (2008) Phosphorylation of profilin by ROCK1 regulates polyglutamine aggregation. *Molecular and cellular biology* **28**, 5196-5208

130. Bottcher, R. T., Wiesner, S., Braun, A., Wimmer, R., Berna, A., Elad, N., Medalia, O., Pfeifer, A., Aszodi, A., Costell, M., and Fassler, R. (2009) Profilin 1 is required for abscission during late cytokinesis of chondrocytes. *The EMBO journal* **28**, 1157-1169

131. Bae, Y. H., Ding, Z., Zou, L., Wells, A., Gertler, F., and Roy, P. (2009) Loss of profilin-1 expression enhances breast cancer cell motility by Ena/VASP proteins. *Journal of cellular physiology* **219**, 354-364

132. Maier, J. A., Martinez, C., Kasavajhala, K., Wickstrom, L., Hauser, K. E., and Simmerling, C. (2015) ff14SB: Improving the Accuracy of Protein Side Chain and Backbone Parameters from ff99SB. *Journal of chemical theory and computation* **11**, 3696-3713

133. Koes, D. R., Baumgartner, M. P., and Camacho, C. J. (2013) Lessons learned in empirical scoring with smina from the CSAR 2011 benchmarking exercise. *Journal of chemical information and modeling* **53**, 1893-1904

134. Trott, O., and Olson, A. J. (2010) AutoDock Vina: improving the speed and accuracy of docking with a new scoring function, efficient optimization, and multithreading. *J Comput Chem* **31**, 455-461

135. O'Boyle, N. M., Morley, C., and Hutchison, G. R. (2008) Pybel: a Python wrapper for the OpenBabel cheminformatics toolkit. *Chemistry Central journal* **2**, 5

136. Shevchenko, A., Tomas, H., Havlis, J., Olsen, J. V., and Mann, M. (2006) In-gel digestion for mass spectrometric characterization of proteins and proteomes. *Nature protocols* **1**, 2856-2860

137. D.A. Case, V. Babin, J. T., Berryman, R.M. Betz, Q. Cai, D.S. Cerutti, T.E. Cheatham, I., T.A. Darden, R.E. Duke, H. Gohlke, A.W. Goetz, S. Gusarov, N. Homeyer, P. Janowski, J. Kaus, I. Kolossváry, A. Kovalenko, T.S. Lee, S. LeGrand, T. Luchko, R. Luo, B. Madej, K.M. Merz, F. Paesani, D.R. Roe, A. Roitberg, C. Sagui, R. Salomon-Ferrer, G. Seabra, C.L. Simmerling, W. Smith, J. Swails, R.C. Walker, J. Wang, R.M. Wolf, X. Wu, and Kollman., P. A. (2014) AMBER 14. *University of California, San Francisco.*

138. Michaud-Agrawal, N., Denning, E. J., Woolf, T. B., and Beckstein, O. (2011) MDAnalysis: A toolkit for the analysis of molecular dynamics simulations. *J Comput Chem* **32**, 2319-2327

139. Schweinhuber, S. K., Messerschmidt, T., Hansch, R., Korte, M., and Rothkegel, M. (2015) Profilin isoforms modulate astrocytic morphology and the motility of astrocytic processes. *PloS one* **10**, e0117244

140. Wang, Z., Wang, D. Z., Pipes, G. C., and Olson, E. N. (2003) Myocardin is a master regulator of smooth muscle gene expression. *Proceedings of the National Academy of Sciences of the United States of America* **100**, 7129-7134

141. Choi, J., Dong, L., Ahn, J., Dao, D., Hammerschmidt, M., and Chen, J. N. (2007) FoxH1 negatively modulates flk1 gene expression and vascular formation in zebrafish. *Developmental biology* **304**, 735-744

142. Isogai, S., Lawson, N. D., Torrealday, S., Horiguchi, M., and Weinstein, B. M. (2003) Angiogenic network formation in the developing vertebrate trunk. *Development* **130**, 5281-5290

143. Pollard, T. D., and Borisy, G. G. (2003) Cellular motility driven by assembly and disassembly of actin filaments. *Cell* **112**, 453-465

144. Thery, C., Boussac, M., Veron, P., Ricciardi-Castagnoli, P., Raposo, G., Garin, J., and Amigorena, S. (2001) Proteomic analysis of dendritic cell-derived exosomes: a secreted subcellular compartment distinct from apoptotic vesicles. *Journal of immunology* **166**, 7309-7318

145. Gronborg, M., Kristiansen, T. Z., Iwahori, A., Chang, R., Reddy, R., Sato, N., Molina, H., Jensen, O. N., Hruban, R. H., Goggins, M. G., Maitra, A., and Pandey, A. (2006) Biomarker discovery from pancreatic cancer secretome using a differential proteomic approach. *Molecular & Cellular Proteomics* **5**, 157-171

146. Caglayan, E., Romeo, G. R., Kappert, K., Odenthal, M., Sudkamp, M., Body, S. C., Shernan, S. K., Hackbusch, D., Vantler, M., Kazlauskas, A., and Rosenkranz, S. (2010) Profilin-1 Is Expressed in Human Atherosclerotic Plaques and Induces Atherogenic Effects on Vascular Smooth Muscle Cells. *PloS one* **5**

147. Jella, K. K., Yu, L., Yue, Q., Friedman, D., Duke, B. J., and Alli, A. A. (2016) Exosomal GAPDH from Proximal Tubule Cells Regulate ENaC Activity. *PloS one* **11**

148. Hosseini-Beheshti, E., Pham, S., Adomat, H., Li, N., and Guns, E. S. T. (2012) Exosomes as Biomarker Enriched Microvesicles: Characterization of Exosomal Proteins Derived from a Panel of Prostate Cell Lines with Distinct AR Phenotypes. *Molecular & Cellular Proteomics* **11**, 863-885

149. Zou, L., Jaramillo, M., Whaley, D., Wells, A., Panchapakesa, V., Das, T., and Roy, P. (2007) Profilin-1 is a negative regulator of mammary carcinoma aggressiveness. *British journal of cancer* **97**, 1361-1371

150. Bergers, G., and Hanahan, D. (2008) Modes of resistance to anti-angiogenic therapy. *Nature reviews. Cancer* **8**, 592-603

151. Johnson, L. A., Rodansky, E. S., Haak, A. J., Larsen, S. D., Neubig, R. R., and Higgins, P. D. (2014) Novel Rho/MRTF/SRF inhibitors block matrix-stiffness and TGF-beta-induced fibrogenesis in human colonic myofibroblasts. *Inflammatory bowel diseases* **20**, 154-165

152. Jin, W., Goldfine, A. B., Boes, T., Henry, R. R., Ciaraldi, T. P., Kim, E. Y., Emecan, M., Fitzpatrick, C., Sen, A., Shah, A., Mun, E., Vokes, V., Schroeder, J., Tatro, E., Jimenez-Chillaron, J., and Patti, M. E. (2011) Increased SRF transcriptional activity in human and mouse skeletal muscle is a signature of insulin resistance. *The Journal of clinical investigation* **121**, 918-929

153. Esnault, C., Stewart, A., Gualdrini, F., East, P., Horswell, S., Matthews, N., and Treisman, R. (2014) Rho-actin signaling to the MRTF coactivators dominates the immediate transcriptional response to serum in fibroblasts. *Genes & development* **28**, 943-958

154. Ding, Z., Bae, Y. H., and Roy, P. (2012) Molecular insights on context-specific role of profilin-1 in cell migration. *Cell adhesion & migration* **6**, 442-449

155. Kullmann, J. A., Neumeyer, A., Gurniak, C. B., Friauf, E., Witke, W., and Rust, M. B. (2012) Profilin1 is required for glial cell adhesion and radial migration of cerebellar granule neurons. *EMBO reports* **13**, 75-82

156. Lambrechts, A., Jonckheere, V., Peleman, C., Polet, D., De Vos, W., Vandekerckhove, J., and Ampe, C. (2006) Profilin-I-ligand interactions influence various aspects of neuronal differentiation. *Journal of cell science* **119**, 1570-1578

157. Haugwitz, M., Noegel, A. A., Karakesisoglou, J., and Schleicher, M. (1994) Dictyostelium amoebae that lack G-actin-sequestering profilins show defects in F-actin content, cytokinesis, and development. *Cell* **79**, 303-314

158. Schutt, C. E., Myslik, J. C., Rozycki, M. D., Goonesekere, N. C., and Lindberg, U. (1993) The structure of crystalline profilin-beta-actin. *Nature* **365**, 810-816

159. Lawrence, H. R., Li, Z., Yip, M. L., Sung, S. S., Lawrence, N. J., McLaughlin, M. L., McManus, G. J., Zaworotko, M. J., Sebti, S. M., Chen, J., and Guida, W. C. (2009) Identification of a disruptor of the MDM2-p53 protein-protein interaction facilitated by high-throughput in silico docking. *Bioorganic & medicinal chemistry letters* **19**, 3756-3759

160. Mukherjee, P., Desai, P., Zhou, Y. D., and Avery, M. (2010) Targeting the BH3 domain mediated protein-protein interaction of Bcl-xL through virtual screening. *Journal of chemical information and modeling* **50**, 906-923

161. Chan, D. S., Lee, H. M., Yang, F., Che, C. M., Wong, C. C., Abagyan, R., Leung, C. H., and Ma, D. L. (2010) Structure-based discovery of natural-product-like TNF-alpha inhibitors. *Angewandte Chemie* **49**, 2860-2864

162. Koes, D. R., and Camacho, C. J. (2012) PocketQuery: protein-protein interaction inhibitor starting points from protein-protein interaction structure. *Nucleic Acids Res* **40**, W387-392

163. Ezezika, O. C., Younger, N. S., Lu, J., Kaiser, D. A., Corbin, Z. A., Nolen, B. J., Kovar, D. R., and Pollard, T. D. (2009) Incompatibility with formin Cdc12p prevents human profilin from substituting for fission yeast profilin: insights from crystal structures of fission yeast profilin. *The Journal of biological chemistry* **284**, 2088-2097

164. Koes, D. R., and Camacho, C. J. (2011) Pharmer: efficient and exact pharmacophore search. *Journal of chemical information and modeling* **51**, 1307-1314

165. Irwin, J. J., Sterling, T., Mysinger, M. M., Bolstad, E. S., and Coleman, R. G. (2012) ZINC: a free tool to discover chemistry for biology. *Journal of chemical information and modeling* **52**, 1757-1768

166. Gauvin, T. J., Fukui, J., Peterson, J. R., and Higgs, H. N. (2009) Isoform-selective chemical inhibition of mDia-mediated actin assembly. *Biochemistry* **48**, 9327-9329

167. Fan, Y., Potdar, A. A., Gong, Y., Eswarappa, S. M., Donnola, S., Lathia, J. D., Hambardzumyan, D., Rich, J. N., and Fox, P. L. (2014) Profilin-1 phosphorylation directs angiocrine expression and glioblastoma progression through HIF-1alpha accumulation. *Nature cell biology* **16**, 445-456

168. Moldovan, N. I., Milliken, E. E., Irani, K., Chen, J., Sohn, R. H., Finkel, T., and Goldschmidt-Clermont, P. J. (1997) Regulation of endothelial cell adhesion by profilin. *Current biology : CB* **7**, 24-30

169. Mouneimne, G., Hansen, S. D., Selfors, L. M., Petrak, L., Hickey, M. M., Gallegos, L. L., Simpson, K. J., Lim, J., Gertler, F. B., Hartwig, J. H., Mullins, R. D., and Brugge, J. S. (2012) Differential remodeling of actin cytoskeleton architecture by profilin isoforms leads to distinct effects on cell migration and invasion. *Cancer cell* **22**, 615-630

170. Finkel, T., Theriot, J. A., Dise, K. R., Tomaselli, G. F., and Goldschmidt-Clermont, P. J. (1994) Dynamic actin structures stabilized by profilin. *Proceedings of the National Academy of Sciences of the United States of America* **91**, 1510-1514

171. Rotty, J. D., Wu, C., Haynes, E. M., Suarez, C., Winkelman, J. D., Johnson, H. E., Haugh, J. M., Kovar, D. R., and Bear, J. E. (2015) Profilin-1 serves as a gatekeeper for actin assembly by Arp2/3-dependent and -independent pathways. *Developmental cell* **32**, 54-67

172. Schoors, S., De Bock, K., Cantelmo, A. R., Georgiadou, M., Ghesquiere, B., Cauwenberghs, S., Kuchnio, A., Wong, B. W., Quaegebeur, A., Goveia, J., Bifari, F., Wang, X., Blanco, R., Tembuyser, B., Cornelissen, I., Bouche, A., Vinckier, S., Diaz-Moralli, S., Gerhardt, H., Telang, S., Cascante, M., Chesney, J., Dewerchin, M., and Carmeliet, P. (2014) Partial and transient reduction of glycolysis by PFKFB3 blockade reduces pathological angiogenesis. *Cell metabolism* **19**, 37-48

173. Goveia, J., Stapor, P., and Carmeliet, P. (2014) Principles of targeting endothelial cell metabolism to treat angiogenesis and endothelial cell dysfunction in disease. *EMBO molecular medicine* **6**, 1105-1120

174. Carmeliet, P., and Jain, R. K. (2000) Angiogenesis in cancer and other diseases. *Nature* **407**, 249-257

175. Bugyi, B., and Carlier, M. F. (2010) Control of actin filament treadmilling in cell motility. *Annual review of biophysics* **39**, 449-470

176. Geese, M., Loureiro, J. J., Bear, J. E., Wehland, J., Gertler, F. B., and Sechi, A. S. (2002) Contribution of Ena/VASP proteins to intracellular motility of listeria requires phosphorylation and proline-rich core but not F-actin binding or multimerization. *Molecular biology of the cell* **13**, 2383-2396

177. Hansen, S. D., and Mullins, R. D. (2010) VASP is a processive actin polymerase that requires monomeric actin for barbed end association. *The Journal of cell biology* **191**, 571-584

178. Suetsugu, S., Miki, H., and Takenawa, T. (1998) The essential role of profilin in the assembly of actin for microspike formation. *The EMBO journal* **17**, 6516-6526

179. Suetsugu, S., Miki, H., and Takenawa, T. (1999) Distinct roles of profilin in cell morphological changes: microspikes, membrane ruffles, stress fibers, and cytokinesis. *FEBS letters* **457**, 470-474

180. Lassing, I., and Lindberg, U. (1985) Specific interaction between phosphatidylinositol 4,5-bisphosphate and profilactin. *Nature* **314**, 472-474

181. Kasina, S., Rizwani, W., Radhika, K. V., and Singh, S. S. (2005) Nitration of profilin effects its interaction with poly (L-proline) and actin. *Journal of biochemistry* **138**, 687-695

182. Kasina, S., Wasia, R., Fasim, A., Radhika, K. V., and Singh, S. S. (2006) Phorbol ester mediated activation of inducible nitric oxide synthase results in platelet profilin nitration. *Nitric oxide : biology and chemistry* **14**, 65-71

183. Hornbeck, P. V., Kornhauser, J. M., Tkachev, S., Zhang, B., Skrzypek, E., Murray, B., Latham, V., and Sullivan, M. (2012) PhosphoSitePlus: a comprehensive resource for investigating the structure and function of experimentally determined post-translational modifications in man and mouse. *Nucleic Acids Res* **40**, D261-270

184. Olsen, J. V., Vermeulen, M., Santamaria, A., Kumar, C., Miller, M. L., Jensen, L. J., Gnad, F., Cox, J., Jensen, T. S., Nigg, E. A., Brunak, S., and Mann, M. (2010) Quantitative phosphoproteomics reveals widespread full phosphorylation site occupancy during mitosis. *Science signaling* **3**, ra3

185. Korupolu, R. V., Achary, M. S., Aneesa, F., Sathish, K., Wasia, R., Sairam, M., Nagarajaram, H. A., and Singh, S. S. (2009) Profilin oligomerization and its effect on poly (L-proline) binding and phosphorylation. *International journal of biological macromolecules* **45**, 265-273

186. Bjorkegren, C., Rozycki, M., Schutt, C. E., Lindberg, U., and Karlsson, R. (1993) Mutagenesis of human profilin locates its poly(L-proline)-binding site to a hydrophobic patch of aromatic amino acids. *FEBS letters* **333**, 123-126

187. Skare, P., and Karlsson, R. (2002) Evidence for two interaction regions for phosphatidylinositol(4,5)-bisphosphate on mammalian profilin I. *FEBS letters* **522**, 119-124

188. Wu, C. H., Fallini, C., Ticozzi, N., Keagle, P. J., Sapp, P. C., Piotrowska, K., Lowe, P., Koppers, M., McKenna-Yasek, D., Baron, D. M., Kost, J. E., Gonzalez-Perez, P., Fox, A. D., Adams, J., Taroni, F., Tiloca, C., Leclerc, A. L., Chafe, S. C., Mangroo, D., Moore, M. J., Zitzewitz, J. A., Xu, Z. S., van den Berg, L. H., Glass, J. D., Siciliano, G., Cirulli, E. T., Goldstein, D. B., Salachas, F., Meininger, V., Rossoll, W., Ratti, A., Gellera, C., Bosco, D. A., Bassell, G. J., Silani, V., Drory, V. E., Brown, R. H., Jr., and Landers, J. E. (2012) Mutations in the profilin 1 gene cause familial amyotrophic lateral sclerosis. *Nature* **488**, 499-503

189. Kim, W., Bennett, E. J., Huttlin, E. L., Guo, A., Li, J., Possemato, A., Sowa, M. E., Rad, R., Rush, J., Comb, M. J., Harper, J. W., and Gygi, S. P. (2011) Systematic and quantitative assessment of the ubiquitin-modified proteome. *Molecular cell* **44**, 325-340

190. Wagner, S. A., Beli, P., Weinert, B. T., Nielsen, M. L., Cox, J., Mann, M., and Choudhary, C. (2011) A proteome-wide, quantitative survey of in vivo ubiquitylation sites reveals widespread regulatory roles. *Molecular & cellular proteomics : MCP* **10**, M111 013284

191. Gau, D., Lewis, T., McDermott, L., Wipf, P., Koes, D., and Roy, P. (2017) Structure-based virtual screening identifies small molecule inhibitor of the profilin1-actin interaction. *The Journal of biological chemistry*

192. Gau, D., Veon, W., Zeng, X., Yates, N., Shroff, S. G., Koes, D. R., and Roy, P. (2016) Threonine 89 Is an Important Residue of Profilin-1 That Is Phosphorylatable by Protein Kinase A. *PloS one* **11**, e0156313

193. Hadden, W. J., Young, J. L., Holle, A. W., McFetridge, M. L., Kim, D. Y., Wijesinghe, P., Taylor-Weiner, H., Wen, J. H., Lee, A. R., Bieback, K., Vo, B. N., Sampson, D. D., Kennedy, B. F., Spatz, J. P., Engler, A. J., and Choi, Y. S. (2017) Stem cell migration and mechanotransduction on linear stiffness gradient hydrogels. *Proceedings of the National Academy of Sciences of the United States of America* **114**, 5647-5652

194. Rozycki, M., Bialik, J. F., Speight, P., Dan, Q., Knudsen, T. E., Szeto, S. G., Yuen, D. A., Szaszi, K., Pedersen, S. F., and Kapus, A. (2016) Myocardin-related Transcription Factor Regulates Nox4 Protein Expression: LINKING CYTOSKELETAL ORGANIZATION TO REDOX STATE. *The Journal of biological chemistry* **291**, 227-243

195. Nimnual, A. S., Taylor, L. J., and Bar-Sagi, D. (2003) Redox-dependent downregulation of Rho by Rac. *Nature cell biology* **5**, 236-241

196. Yan, B., and Smith, J. W. (2000) A redox site involved in integrin activation. *The Journal of biological chemistry* **275**, 39964-39972

197. Song, Z., Liu, Z., Sun, J., Sun, F. L., Li, C. Z., Sun, J. Z., and Xu, L. Y. (2016) The MRTF-A/B function as oncogenes in pancreatic cancer. *Oncology reports* **35**, 127-138